Characterization, Spectroscopic and Kinetic Analyses of the Unexpected Gel Formed by Glycyl-Alanyl-Glycine (GAG) in an Ethanol/Water Mixture

A Thesis

Submitted to the Faculty

of

Drexel University

by

Stefanie Anne Farrell

in partial fulfillment of the

requirements for the degree

of

Master of Science in Chemistry

June 2016

Acknowledgements

I would like to thank my research advisor Dr. Reinhard Schweitzer-Stenner for his unending assistance with this thesis. He has challenged me continually since I began researching in his laboratory, and has never failed to encourage me to reach the best of my abilities. His dedication to his students is extremely rare and much appreciated.

In addition, I would like to thank various collaborators who assisted with the research presented in this thesis. Thank you to Dr. Nicolas Alvarez and his graduate student Mr. Zachary Hinton from the Drexel Department of Chemical and Biological Engineering for assistance with rheology and imaging, and many consultations regarding gel material. Thank you to Dr. Frank Ji and his recently graduated PhD student Dr. Joshua Smith from the Drexel Chemistry Department for assisting with microscope imaging and AFM. And thank you to Dr. Frank Ferrone from the Drexel Physics department for his discussions on kinetics topics.

The majority of this thesis involved collaboration with PhD candidate Mr. David DiGuiseppi from the Drexel Chemistry Department, who constantly brought forth a positive attitude and a smile no matter what came our way. I would like to thank him for his time and friendship throughout this process. Another special thanks extends to Dr. Siobhan Toal whom I had the pleasure to work with in my first years of research. She inspired me to pursue this path of research. Thank you also to the rest of the biospectroscopy group who I have had the pleasure to work with over the years.

Most of all, thank you to my family who brings forth unwavering support. Thank you to my mom, brother and grandparents for allowing me to pursue my dreams and for supporting my academic and personal endeavors.

Table of Contents

List of Tables

List of Figures

Abstract

Characterization, Spectroscopic and Kinetic Analyses of the Unexpected Gel Formedby Glycyl-Alanyl-Glycine (GAG) in an Ethanol/Water Mixture

Stefanie Anne Farrell

Reinhard Schweitzer-Stenner, Ph.D.

The introduction of a co-solvent system (55 mol% ethanol/45 mol% water) promoted the aggregation, fibrilization and subsequent gelation of the cationic tripeptide glycylanalylglycine (GAG). This is surprising because, unlike known gelators throughout the literature, GAG lacks hydrophobicity, extended chain length, alternating charges, and/or aromaticity. This tertiary system was extensively studied through the use of vibrational spectroscopies (FTIR, VCD), nuclear magnetic resonance spectroscopy (NMR), electronic spectroscopies (UVCD), microscope imaging (bright-field, AFM) and rheology. Conformational resampling from pPII to β-strand was observed with the addition of ethanol co-solvent, the result of ethanol penetrating into the hydration shell of the peptide. Significant enhancement of the amide I′ in the VCD spectrum with an increase in peptide concentration was attributed to the formation of helically twisted fibrils, which extended into a gel network. Bright-field and atomic force microscopy of the fibrils revealed dimensions of approximately 500 μm in length, 500 nm in height, and 7 μm in cross-section, dimensions characteristic of enormous size compared with those of other small peptide hydrogel fibrils, which exhibit on a sub-micrometer scale. The gelation of cationic GAG in 55 mol% ethanol/45 mol% water was broken down into a set of distinguishable kinetic processes which proceeded in the following order: aggregation into tapes and ribbons (10^{-1} min^{-1}), fibrilization as a cooperative process (10^{-2} min^{-1}),

initial gelation (10^{-2} min^{-1}), and subsequent further adjustments of the gelation process (10^{-4} min^{-1}). Understanding the kinetics of these processes has significant application for drug delivery and the synthesis of new biomaterials.

CHAPTER 1. INTRODUCTION

1.1 Defining a Gel

The term "gel" has an ambiguous definition since it has been used to refer to many different types of materials throughout the literature. Scientists have proposed that the definition of a gel should focus on the structural nature of the material. Bungenberg de Jong et al. defined gels as colloidal particles being penetrated and surrounded by a liquid solvent.[1] Flory et al. proposed a classification system that distinguished gels into categories including polymer networks formed through physical aggregation, ordered laminar structures and completely disordered covalent polymeric networks.[2] A more general definition has been proposed by Almdal et al.[3] after reviewing multiple existing definitions. They proposed that a gel must a) consist of two or more components, one of which is a liquid and b) be soft, solid, or solid-like materials. When the liquid is composed of mostly water, the gel can be referred to as a "hydrogel." Hydrogels have the potential to appear opaque or transparent depending on the macrostructure[4] and size of the solid or solid-like materials. Gels have been constructed from both synthetic and natural materials,[5] dependent on the desired application.

1.2 Biological gels: Fibrin and Gelatin Hydrogels

Hydrogels derived from natural materials are increasingly important for advancing the biomedical technology and biomaterial fields owing to their biocompatibility with living systems. Fibrin has been extensively studied for its applicability in controlled release of nanoparticles,[6,7] showing promise for tissue engineering and regeneration. Three-dimensional matrices of fibrin hydrogels have been

designed and manipulated to effect the storage and release properties of various particles.[7] Figure 1.1 shows microscope images of a fibrin hydrogel encapsulating growth factor particles to be delivered through a controlled release mechanism.

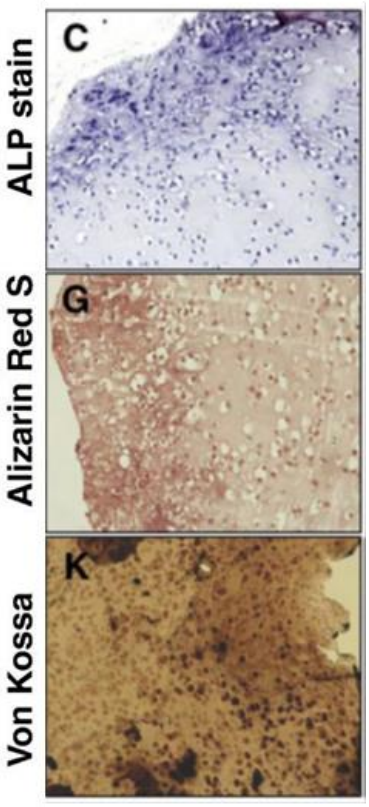

Figure 1.1. Fibrin hydrogel encapsulating human mesenchymal cells (hMSCs) with a BMP-2 growth factor to be delivered through a controlled release mechanism viewed under a microscope with several staining techniques. The cells are the small dots in the images. The image was taken from reference [6] and modified.

Gelatin is another common natural gel material used for investigating controlled release mechanisms. Tabata et al. studied controlled release by adjusting the concentration of gelatin and thus altering the extent of cross-linking throughout the gels.[8] Cross-linking agents have also been added to solutions to alter the adhesive properties of

gels that have the potential to repair damaged tissue.[9] In these natural gels, the entire structure is encapsulated by the solvent. A cross-linked, sample-spanning network creates a gelled matrix for carrying particles. The gel can be chemically or physically designed to achieve desired properties and ultimately perform specified functions.

1.3 Low Molecular Weight Hydrogels (LMWH) vs. Short Peptides

Hydrogels that arise from a self-aggregation (self-assembly) mechanism into a fibrous three-dimensional (3D) network are termed low molecular weight hydrogels (LMWH).[10] A general mechanism of the self-aggregation process is depicted in Figure 1.2, showing the development of monomers into oligomers, oligomers into fibril structures and bundles, then finally fibrils intertwining to form a cross-linking network. The interactions between fibers are strictly noncovalent and the connection can be characterized as a physical gel network.[11] The noncovalent interactions allow for thermoreversibility and control of the hydrogel and low minimal gelation concentrations.[10]

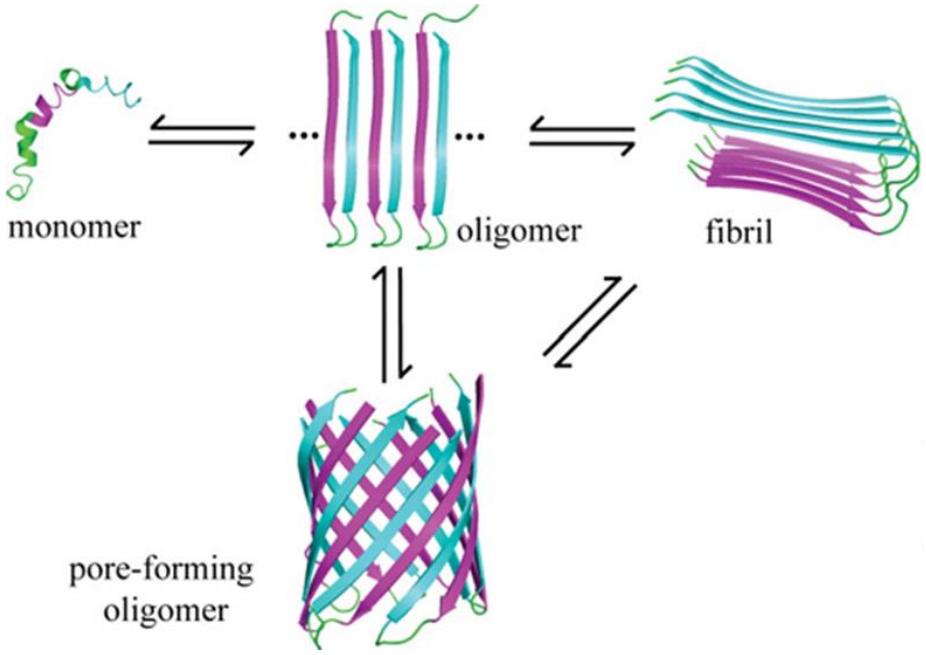

Figure 1.2. General mechanism of self-aggregation of monomers into oligomers, fibrils, and eventually cross-linked gel networks. Taken from reference [12] and modified.

Similar to other large natural gelators, LMWH are useful because they are highly biodegradable and biocompatible. The gels are environmentally responsive[13] and can be controlled by adjustments in pH[5], concentration[14] and temperature.[4]

This thesis focuses on a LMWH, specifically one formed by the aggregation of a short peptide. Short peptide gelators have become an increasingly attractive research topic, because they provide a low cost option that can suffice as a model for larger biological molecules. Although the benefits of applications of LMWH in biomaterials and biotechnology have been acknowledged, there are others necessary to note as well. Short peptides have been linked to neurodegenerative disorders such as Alzheimer's Parkinson's and Huntington's diseases[15,16,17,18] from self-assembly and self-aggregation into amyloid fibrils. Prevention tactics for these diseases could be developed as a

consequence of understanding the self-aggregation mechanisms associated with these peptides.

1.4 Aggregation of Peptides

Although self-aggregating peptides have been extensively studied in efforts to understand the onset of the above diseases,[15,16,17,18] it is still unclear what acts as the driving force for aggregation. It has been suggested that the peptide must have amphiphilic character, or even a series of alternating charges.[5] Other scientists have suggested that hydrophobicity[19,20] plays a crucial role and that π-stacking effects associated with aromaticity[21] may promote aggregation. A peptide without these characteristics would not be expected to aggregate.

Azriel et al. have shown that aromaticity can play a crucial role in the aggregation that promotes amyloid fibril formation.[21] These fibrils have been associated with the onset of diabetes mellitus (type II diabetes).[21,22] A 6-residue segment of the islet amyloid polypeptide (IAPP) was chosen for study because of its ability to create fibrils and maintain physical properties similar to those of the entire polypeptide. This segment called NFGAIL (asparagine-phenylalanine-glycine-alanine-isoleucine-leucine) had two serine residues added to the leucine end to improve solubility. In the study each amino acid of the fragmented chain was systematically replaced with an alanine residue to ensure some degree of hydrophobicity was maintained, and the new fragment was subject to aggregating conditions. Phenylalanine, with an aromatic ring as a side chain, was shown to be the most important residue in amyloid formation, whereas glycine only played a minor role.[21,22] Considering the results, the authors hypothesized that π-π interactions were the driving force for aggregation. They further tested their hypothesis

by synthesizing two aromatic dipeptides diphenylalanine and diphenylglycine. These were found to be the smallest amyloidogenic motifs that could self-aggregate to form tubular nanostructures and nano-spherical assemblies.[22,23,24] The results were significant for showing that a simple double-residue peptide could promote self-aggregation through π-π interactions without the presence of lengthy chains.

Other "dipeptide" amphiphiles have been studied to discern the requirements of effective self-aggregators and consequent hydrogelators. Mitra et al. investigated cationic amphiphiles by exchanging phenylalanine, proline, and tryptophan residues at the head group of an aliphatic chain.[4] They found that for each of the synthesized peptides self-aggregation was driven by strong intermolecular noncovalent interactions. ^{1}HNMR and 2D-NOESY experiments suggested the presence of hydrogen bonding, formation of hydrophobic domains, π-π stacking of aromatic rings and interaction between aromatic rings and the N-Hs of indoles and amides (N-H to π). In addition, a study by means of Fourier transformed infrared (FTIR) spectroscopy confirmed the existence of hydrogen bonding and van der Waals forces between an entangled network of fibrils within the gels. The authors attributed a combination of all these observed effects as the cause for aggregation, fibrilization and subsequent gelation processes.[4]

Further investigation of π-stacking effects as the predominant force driving aggregation and gelation processes included the study of low molecular weight hydrogelators in which the amino acid residues have a protecting group.[25,26] Smith et al. formed a hydrogel from an Fmoc-amino acid for which fluorenylmethoxycarbonyl (Fmoc) was used as the protecting group.[25] The resulting low molecular weight gelator, Fmoc-phenylalanine-phenylalanine (Fmoc-FF), was proposed to organize into a

cylindrical nanostructure with Fmoc-groups arranged in an anti-parallel π-stacking fashion. The authors concluded that a combination of the π-π stacking interaction between Fmoc-groups and the alignment of anti-parallel β-sheets governed the formation of both the fibril structures and the gel network.[25] Draper et al. also formed hydrogels from Fmoc-amino acids but with single residues.[26] As seen in Figure 1.3, Fmoc-groups attached to phenylalanine (F), tyrosine (Y), tryptophan (W), methionine (M), glycine (G), and isoleucine (I) residues formed gels after the addition of glucose-δ-lactone (GdL). This compound was used to uniformly control the pH change that induced gelation.

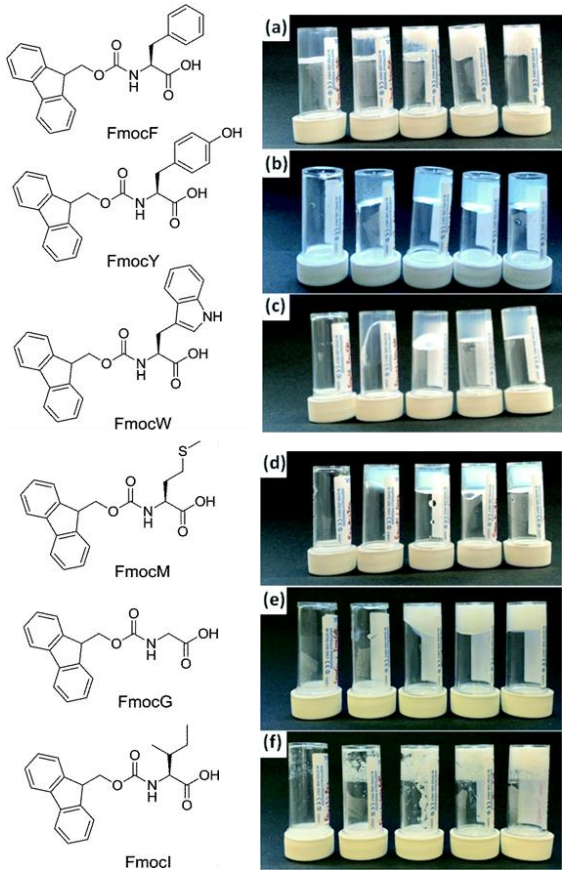

Figure 1.3. Fmoc-amino acid hydrogelator structure and corresponding photographs of gelation tests after the addition of 1, 2, 3, 4, and 5 $mgmL^{-1}$ glucono-δ-lactone taken 24 hours after gel formation. Taken from reference [26] and modified.

Notably, Fmoc-alanine (A), Fmoc-valine (V), and Fmoc-leucine (L) did not form hydrogels with any tested concentration of GdL. This suggested that Fmoc-groups had the potential to form hydrogels only when used as protecting groups on certain single peptide residues. Further analysis of the gels with x-ray diffraction allowed the authors to conclude that hydrogen bonding drove the self-aggregation into fibrillary structures of the gels,[26] contrary to the findings of Smith et al.[25] that π-stacking was responsible.

Other research groups synthesized peptides that aggregated without the use of agents to induce gelation. Schneider et al. synthesized a 20-residue peptide called MAX1 with alternating valine and lysine residues that formed a hydrogel under basic conditions.[5] The self-aggregation process followed one of two pathways where the peptide folded into a β-hairpin structure and eventually underwent subsequent gelation. Each β-hairpin was formed through hydrogen bonding interactions, and multiple β-hairpins could associate via hydrophobic interaction between the outer valine residues. This prompted the formation of an extended gel network.[27] The MAX1 peptide was unique because it could be manipulated reversibly in response to pH adjustments. Under basic conditions, the peptide folded into β-hairpin structures and formed a hydrogel. If the pH was reduced to acidic conditions, the β-hairpins were unstable and unfolded, preventing the gelation process. Subsequently returning the pH to basic conditions permitted folding and gelation, showing that the system was reversible and readily manipulated.[5] These findings confirmed that π-stacking interactions may promote, but are not required to induce self-aggregation and gelation of small peptides.

In 2011, a systematic screening strategy was developed by Frederix et al. to investigate the self-aggregating propensity of all possible dipeptide combinations.[28]

Assuming the molecular dynamics (MD) results agreed with experimental findings, the model had the potential to be a valuable predictive tool for quickly determining which dipeptides could self-aggregate. Any observed patterns in the data sets could provide information about the interactions driving the process. The simulation used a course-grain MARTINI water force field to model the interaction between 300 dipeptides in a confined cubic space. To interpret and compare results, Frederix et al. determined the aggregation propensity (AP) score, which they defined as the ratio of solvent-accessible surface area (SASA) initially over the final SASA. An AP score greater than two was considered to indicate a high degree of aggregation. Figure 1.4 shows the AP scores of the dipeptides arranged in a two-dimensional grid. The intensity of the red color indicated a higher AP score according to the scale at the right of the image.

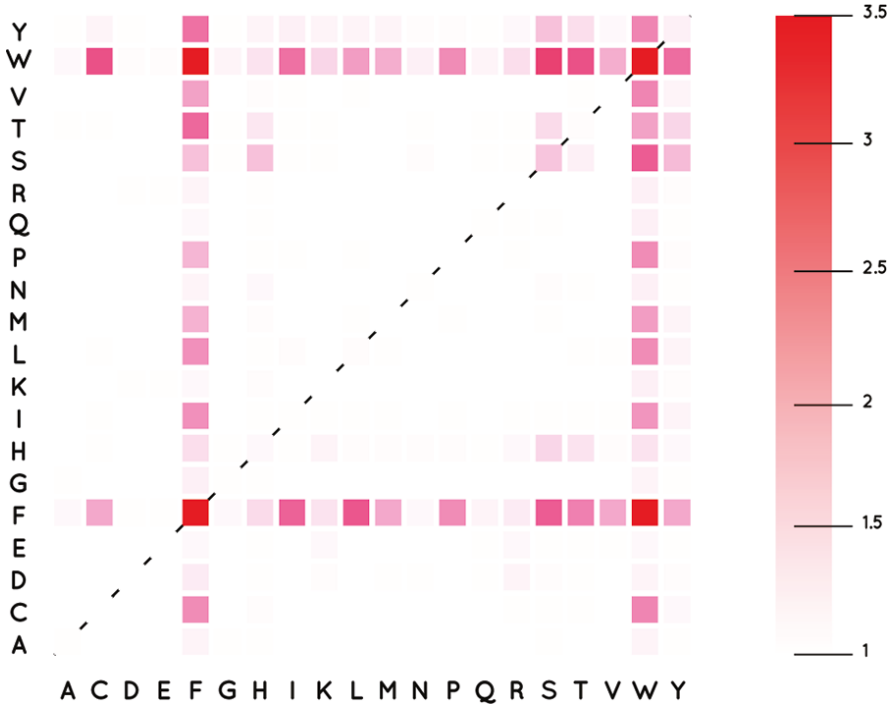

Figure 1.4. AP scores of dipeptides arranged in a two-dimensional grid. Taken from reference [28].

Phenylalanine (F) and tryptophan (W) residues clearly demonstrated a greater propensity to aggregate than did other residues. Most of the dipeptides had an AP score of approximately one (white), suggesting most were not predicted to aggregate under aqueous conditions. Comparing to experimental work throughout the literature, the model accurately predicted the ability (or lack of the ability) to aggregate for nine chosen dipeptides.[28] Although the model could not provide information about the details of the aggregation structures, it provided a sound, fast and reliable method for screening the ability of many dipeptides to aggregate.

The MD simulation used by Frederix et al. for screening dipeptides[28] was further extended to predict the ability of 8,000 tripeptide combinations to aggregate.[29] Initially, the same AP score from the dipeptide simulation was used to describe the tripeptides. Later a hydrophilic-corrected AP score (AP_H) was chosen to ensure a positive bias toward hydrophilic residues to address solubility limitations and ensure the monitoring of aggregation and gelation processes, not precipitation and crystallization. Figure 1.5 shows the normalized AP_H scores of the studied tripeptides with bar graphs along the bottom, grouping AP_H scores according to aromatic, hydrophilic, cationic, anionic, and small/hydrophobic side chain character of residues at the N-terminus, middle, or C-terminus positions.

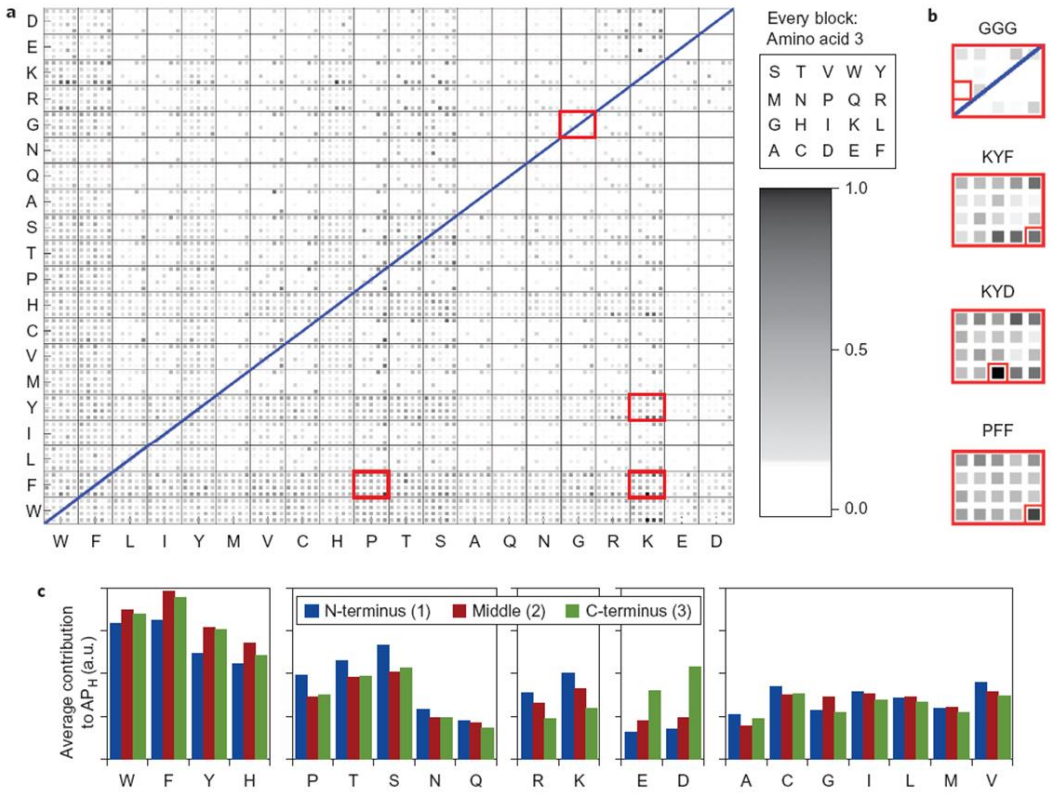

Figure 1.5. Normalized AP_H scores of the 8,000 tripeptides studied. The first two residues are determined by following the two-dimensional grid, then the third residue is determined using the coded box to the right of the figure. The intensity of the gray color corresponds to the AP_H score shown by the scale to the right of the figure. The bar graphs at the bottom of the figure show the average AP_H scores grouped according to aromatic, hydrophilic, cationic, anionic, and small/hydrophobic side chain character of residues at the N-terminus, middle, or C-terminus positions. Taken from reference [29].

The results of the simulation showed that 1) aromatic amino acids (phenylalanine (F), tyrosine (Y), and to lesser extent tryptophan (W)) were more favorable in the middle and C-terminal positions; 2) negatively charged amino acids (glutamic acid (E), aspartic acid (D)) were strongly favored in the C-terminal position; and 3) positively charged and hydrogen bond donating amino acids (lysine (K), arginine (R); serine (S), threonine (T)) promoted self-assembly in the N-terminal position.[29] The authors hypothesized that having positive and negative residues near the N- and C-termini, respectively, could

promote alignment by repulsion of similar charges and strong intermolecular salt bridge formation. The positioning of aromatic and negatively charged residues at the C-terminal position allowed for π-stacking interactions and amphiphilic character, respectively.[29] Most notably for this thesis, histidine (H) had the lowest contribution to AP_H score in the aromatic residues, and glycine (G) and alanine (A) had some of the lowest contributions to aggregation overall.

Various tripeptides were experimentally synthesized and characterized to indicate candidates for nanostructure formation and as well as check the validity of the model.[29] Several discrepancies between simulations and experimental observations included the following: SYF was insoluble in water whereas the simulations indicated solubility, RYF did not form a gel as predicted by simulation, and KYF hydrogel was not predicted to form fibrils after 1200 ns in the MD simulation. However, extended simulation time to 4800ns or an increase in concentration did lead to elongated fibrous nanostructures. The fibrils of the KYF hydrogel were determined to be stabilized through salt bridges, hydrogen bonding, and hydrophobic interactions. Despite some predicted inconsistences, overall the model provided useful design rules for new self-aggregating candidates and hydrogelators. The weak relationship between AP score and hydrophilicity proved that the ability to self-aggregate is not simply related to the hydrophobic character of the amino acid residues.[29]

1.5 Unexpected Aggregation of Short Peptides

The alanine-based peptide AAKA (Ac-$(AAKA)_4$-NH_2) was studied by Measey et al.[15] in 2010 and later by DiGuiseppi et al.[19] in 2016 for its interesting ability to form β-sheet like structures in spite of having protonated side chains. An alignment of four

positively charged residues would be expected to experience repulsion, thus preventing them from self-aggregation. Instead, when at a minimum peptide concentration of 10 mg/mL,[15] a hydrogen bonding network formed between the hydrophilic β-sheets, immobilizing water to form a hydrogel. AFM images revealed that stacks of β-sheet tapes were composed of fibrils 5-6 nm in thickness.[19] Spectroscopic methods such as VCD and FTIR were used to probe the interaction between β-sheets and the formation of the gel, respectively. This was a unique approach for using the intrinsic amide I′ intensity as a method for monitoring hydrogel formation.[19] These studies established that an amphiphilic, alanine-based, short peptide had the capability to undergo aggregation without aromaticity, extensive chain length, or alignment of alternating charged residues.

An even more surprising candidate for gelation is the three-residue peptide glycyl-histidyl-glycine (GHG). DiGuiseppi et al. discovered that zwitterionic GHG had the capability to form a hydrogel if the peptide concentration exceeded 25 mM in water at neutral pH.[30] Although the histidine residue is aromatic in character, it has not been considered to have high aggregation propensity. In support, the MD simulation scan of tripeptides performed by Frederix et al. revealed that histidine (H) had the lowest contribution to the hydrophilic-correct aggregation propensity (AP_H) score of the aromatic residues, and glycine (G) had some of the lowest contributions to aggregation overall.[29] A bright field microscope image showed extremely large fibrils on a sub-millimeter scale formed through aggregation of GHG peptides.[30] Enhancement of the amide I′ intensity in the VCD spectrum compared to monomeric GHG peptides in more acidic aqueous solution was attributed to the formation of the extended, helically twisted fibrils. The hydrogel was suggested to form an extended network through hydrogen

bonding interaction between the C-terminal groups and the imidazole NH group of the histidine residue.[30]

Another similar model GxG peptide was reported to form a gel at a certain peptide concentration with the use of a co-solvent system. Milorey et al. discovered that unblocked cationic glycyl-analyl-glycine (GAG) underwent gelation at a minimum peptide concentration of 200 mM in a solution of 55 mol% ethanol/45 mol% water.[14] The large crystalline fibrils shown in Figure 1.6 were determined to be on a sub-millimeter scale similar to those observed by GHG in water.[30]

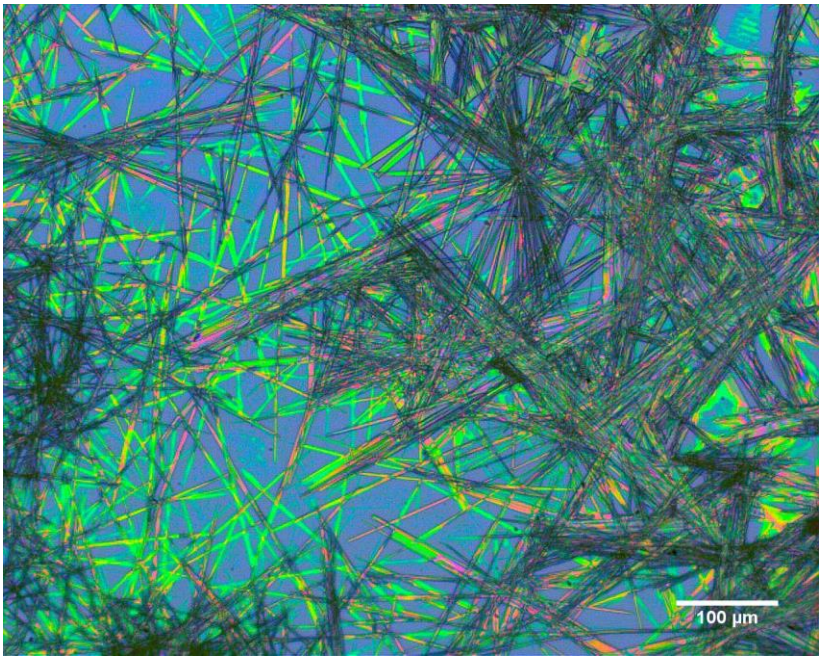

Figure 1.6. Bright field microscope image of 209 mM GAG in 55 mol% ethanol/45 mol% water co-solvent solution taken 24 hours after preparation. Taken from reference [14].

A similar enhancement of the amide I′ intensity in the VCD spectrum indicated the formation of an extended network of fibrils. A blue-shift of the amide I′ band in the

FTIR and VCD spectra suggested that ethanol promoted changes in the peptide's hydration shell.[14] The use of ethanol as a co-solvent stems from its interactions being between that of a "good" solvent and a "bad" one. It is well-known throughout the literature that ethanol disrupts the tetrahedral network formed by water as an effect of its comparatively limited ability to hydrogen bond.[31] Ethanol-water mixtures are seemingly miscible in all proportions to the eye, but the interaction between the molecules is much more complicated. In an attempt to elucidate the interactions between the ternary mixture of peptide/ethanol/water, this thesis will focus its analysis on the unexpected hydrogel formed by GAG in 55 mol% ethanol/ 45 mol% water despite the lack of aromaticity, long aliphatic chains, charged residues, or high hydrophobic character of the amino acid residues therein.

1.6 Research Goals and Aims

As mentioned in this introduction, investigation of the aggregation and gelation properties and kinetics of a short peptide in a co-solvent system can provide information about local interactions through use of a model system. The surprising ability of GAG to form a hydrogel in 55 mol% ethanol/45 mol% water suggests that the rules and driving forces of aggregation and gelation are not as straight-forward and predictable as previously thought. Short peptide LMWHs are inexpensive, biodegradable, and biocompatible with living systems. Most importantly, this system potentially could advance biomaterials and biotechnology and provide valuable information for mechanisms of self-assembly associated with neurodegenerative diseases. There were two major questions that were addressed in the work described in this thesis.

1. What role does the ethanol co-solvent play in the GAG hydrogel formation?

2. What are the time scales of local aggregation, fibrilization, and gelation relative to one another?

The first question was answered with vibrational spectroscopic techniques such as infrared (IR), and vibrational circular dichroism (VCD). These were used to monitor changes in the peptide structural propensity as the ethanol content of the system was increased. The second question was answered using IR, VCD, electronic circular dichroism (ECD) spectroscopies along with microscope imaging and rheology. Together the techniques provided a holistic view of the various kinetic processes taking place leading to formation of the hydrogel. Appropriate models selected from the literature were used to fit the experimental data, and the resulting time constants were compared.

1.7 References

1. Bungenberg de Jong, H. A Survey of the Study Objects in this Volume. *Colloid. Polym. Sci.* **1949,** *2*, 1-18.

2. Flory, P. Introductory Lecture. *Faraday Discuss.* **1974,** *57*, 7-18.

3. Almdal, K.; Dyre, J.; Hvidt, S.; Kramer, O. Towards a Phenomenological Definition of the Term 'Gel'. *Polym. Gels Networks.* **1993,** *1* (1), 5-17.

4. Mitra, R. N.; Das, D.; Roy, S.; Das, P. K. Structure and Properties of Low Molecular Weight Amphiphilic Peptide Hydrogelators. *J. Phys. Chem. B.* **2007,** *111* (51), 14107-14113.

5. Schneider, J. P.; Pochan, D. J.; Ozbas, B.; Rajagopal, K.; Pakstis, L.; Kretsinger, J. Responsive Hydrogels from the Intramolecular Folding and Self-assembly of a Designed Peptide. *J. Am. Chem. Soc.* **2002,** *124* (50), 15030-15037.

6. Park, K.-H.; Kim, H.; Moon, S.; Na, K. Bone Morphogenic Protein-2 (BMP-2) Loaded Nanoparticles Mixed with Human Mesenchymal Stem Cell in Fibrin Hydrogel for Bone Tissue Engineering. *J. Biosci. Bioeng.* **2009,** *108* (6), 530-537.

7. Hall, H. Modified Fibrin Hydrogel Matrices: Both, 3D-Scaffolds and Local and Controlled Release Systems to Stimulate Angiogenesis. *Curr. Pharm. Des.* **2007,** *13* (35), 3597-3607.

8. Tabata, Y.; Hijikata, S.; Ikada, Y. Enhanced Vascularization and Tissue Granulation by Basic Fibroblast Growth Factor Impregnated in Gelatin Hydrogels. *J. Controlled Release* **1994,** *31* (2), 189-199.

9. Sung, H. W.; Huang, D. M.; Chang, W. H.; Huang, R. N.; Hsu, J. C. Evaluation of Gelatin Hydrogel Crosslinked with Various Crosslinking Agents as Bioadhesives: In Vitro Study. *J. Biomed. Mater. Res.* **1999,** *46* (4), 520-530.

10. de Loos, M.; Feringa, B. L.; van Esch, J. H. Design and Application of Self-Assembled Low Molecular Weight Hydrogels. *Eur. J. Org. Chem.* **2005,** *2005* (17), 3615-3631.

11. Tomasini, C.; Castellucci, N. Peptides and Peptidomimetics That Behave as Low Molecular Weight Gelators. *Chem. Soc. Rev.* **2013,** *42* (1), 156-172.

12. Cerf, E.; Sarroukh, R.; Tamamizu-Kato, S.; Breydo, L.; Derclaye, S.; Dufrêne, Y. F.; Narayanaswami, V.; Goormaghtigh, E.; Ruysschaert, J.-M.; Raussens, V. Antiparallel β-sheet: a Signature Structure of the Oligomeric Amyloid β-Peptide. *Biochem. J.* **2009,** *421* (3), 415-423.

13. Peppas, N. A.; Huang, Y.-S.; Torres-Lugo, M.; Ward, J. H.; Zhang, J. Physicochemical Foundations and Structural Design of Hydrogels in Medicine and Biology. *Annu. Rev. Biomed. Eng.* **2000,** *2*, 9-29.

14. Milorey, B.; Farrell, S.; Toal, S. E.; Schweitzer-Stenner, R. Demixing of Water and Ethanol Causes Conformational Redistribution and Gelation of the Cationic GAG Tripeptide. *Chem. Commun. (Camb)* **2015,** *51* (92), 16498-501.

15. Measey, T. J.; Schweitzer-Stenner, R.; Sa, V.; Kornev, K. Anomalous Conformational Instability and Hydrogel Formation of a Cationic Class of Self-Assembling Oligopeptides. *Macromol.* **2010,** *43*, 7800-7806.

16. Measey, T. J.; Schweitzer-Stenner, R. Vibrational Circular Dichroism as a Probe of Fibrillogenesis: The Origin of the Anomalous Intensity Enhancement of Amyloid-like Fibrils. *J. Am. Chem. Soc.* **2011,** *133*, 1066-1076.

17. Knowles, T. P.; Waudby, C. A.; Devlin, G. L.; Cohen, S. I.; Aguzzi, A.; Vendruscolo, M.; Terentjev, E. M.; Welland, M. E.; Dobson, C. M. An Analytical Solution to the Kinetics of Breakable Filament Assembly. *Science* **2009,** *326* (5959), 1533-1537.

18. Chen, S.; Ferrone, F. A.; Wetzel, R. Huntington's Disease Age-of-Onset Linked to Polyglutamine Aggregation Nucleation. *Proc. Nat. Acad. Sci.* **2002,** *99* (18), 11884-11889.

19. DiGuiseppi, D.; Krauss, J.; Toal, S.; Schweitzer-Stenner, R. Unexpected Hydrogelation of a Cationic Amphiphilic Alanine Based Peptide in Water at Low Ionic Strenth Probed by IR and VCD Spectroscopy. Submitted to *Macromol.*, **2015**.

20. Singh, V.; Rai, R. K.; Arora, A.; Sinha, N.; Thakur, A. K. Therapeutic Implication of L-Phenylalanine Aggregation Mechanism and Its Modulation by D-Phenylalanine in Phenylketonuria. *Sci. Rep.* **2014,** *4*.

21. Azriel, R.; Gazit, E. Analysis of the Minimal Amyloid-Forming Fragment of the Islet Amyloid Polypeptide: An Experimental Support for the Key Role of the Phenylalanine Residue in Amyloid Formation. *J. Biol. Chem.* **2001,** *276* (36), 34156-61.

22. Gazit, E. Self Assembly of Short Aromatic Peptide into Amyloid Fibrils and Related Nanostructures. *Prion* **2007,** *1*, 32-35.

23. Reches, M.; Gazit, E. Formation of Closed-Cage Nanostructures By Self-Assembly of Aromatic Dipeptides. *Nano Lett.* **2004,** *4* (4), 581-585.

24. Reches, M.; Gazit, E. Casting Metal Nanowires within Discrete Self-Assembled Peptide Nanotubes. *Science* **2003,** *300*, 625.

25. Smith, A. M.; Williams, R. J.; Tang, C.; Coppo, P.; Collins, R. F.; Turner, M. L.; Saiani, A.; Ulijn, R. V. Fmoc-Diphenylalanine Self Assembles to a Hydrogel via a Novel Architecture Based on π–π Interlocked β-Sheets. *Adv. Mater.* **2008,** *20* (1), 37-41.

26. Draper, E. R.; Morris, K. L.; Little, M. A.; Raeburn, J.; Colquhoun, C.; Cross, E. R.; McDonald, T. O.; Serpell, L. C.; Adams, D. J. Hydrogels Formed from Fmoc Amino Acids. *Cryst. Eng. Comm.* **2015,** *17* (42), 8047-8057.

27. Veerman, C.; Rajagopal, K.; Palla, C. S.; Pochan, D. J.; Schneider, J. P.; Frust, E. M. Gelation Kinetics of β-Hairpin Peptide Hydrogel Networks. *Macromol.* **2006,** *39*, 6608-6614.

28. Frederix, P. W.; Ulijn, R. V.; Hunt, N. T.; Tuttle, T. Virtual Screening for Dipeptide Aggregation: Toward Predictive Tools for Peptide Self-Assembly. *J. Phys. Chem. Lett.* **2011,** *2* (19), 2380-2384.

29. Frederix, P. W.; Scott, G. G.; Abul-Haija, Y. M.; Kalafatovic, D.; Pappas, C. G.; Javid, N.; Hunt, N. T.; Ulijn, R. V.; Tuttle, T. Exploring the Sequence Space for (Tri-)Peptide Self-Assembly to Design and Discover New Hydrogels. *Nat. Chem.* **2015,** *7* (1), 30-7.

30. DiGuiseppi, D.; Schweitzer-Stenner, R. Probing conformational propensities of histidine in different protonation states of the unblocked glycyl-histidyl-glycine peptide by vibrational and NMR spectroscopy. *J. Raman Spectrosc.* **2016,** *in press*.

31. Yoshida, K.; Yamaguchi, T.; Kovalenko, A.; Hirata, F. Structure of Tert-Butyl Alcohol-Water Mixtures Studied by the RISM Theory. *J. Phys. Chem. B.* **2002,** *106* (19), 5042-5049.

CHAPTER 2. CHARACTERIZATION OF GEL STATIONARY STATE

Taken in part from:
Milorey, B.; Farrell, S.; Toal, S.; Schweitzer-Stenner, R. Demixing of Water and Ethanol Causes Conformational Redistribution and Gelation of the GAG Tripeptide. *Chemical Communications,* **2015**, 51, 16498-16501.

2.1 Abstract

The aggregation and fibrilization processes leading to the gelation of the cationic peptide GAG in 55 mol% ethanol/45 mol% water cause changes in the infrared (FTIR/IR), vibrational circular dichroism (VCD) and ultra-violet electronic circular dichroism (UVCD) spectra. Ethanol enters the peptide's hydration shell, resulting in a blueshift of the amide I′ in the FTIR and VCD spectra. The VCD spectrum of the amide I′ shows significant enhancement with an increase in peptide concentration, attributed to the formation of an extended network of helically twisted fibrils. An observed change in the UVCD spectrum was hypothesized to reflect local aggregation from many combined crosslinking fibrils instead of traditional secondary structure. The opaque hydrogel formed by cationic GAG in 55 mol% ethanol/45 mol% water was characterized with bright-field and atomic force microscopy. Fibrils were determined to be approximately 500 μm in length, 500 nm in height, and 7 μm in cross-section, comparable in size to fibrils formed by GHG in water.[1] The fibrils are massive in size compared to those of other Fmoc-peptide hydrogels found in the literature.[2,3]

2.2 Introduction

The tripeptide GAG is one of the model GxG peptides that allows for study of the central amino acid residue, alanine. Hagarman et al. found that the tripeptide exhibits a strong propensity for polyproline II (pPII) conformation in water through NMR and

vibrational spectroscopy studies.[4] These results were in agreement with many literature sources suggesting that alanine is most stabilized in the pPII conformation when solvated by water.[5,6,7] Interactions between solvent and peptide become increasingly complicated when this preferred aqueous solvation is disrupted with a co-solvent such as ethanol. Toal et al. found that even with a small addition of ethanol (1.6 mol%, 5% v/v), the propensity of the backbone configuration of the peptide resamples.[8] Milorey et al. observed a shift in conformational sampling from pPII to β-strand at 17 mol% ethanol (40% v/v).[9] A higher concentration of ethanol (55 mol%, 80% v/v) induces significant changes to the peptide backbone conformation resulting in the formation of a viscous hydrogel.[9] This gelation process was initiated through aggregation and fibrilization of the peptide following the alteration of peptide-solvent interactions.

The aggregation and fibrilization of cationic peptide GAG in 55 mol% ethanol/ 45 mol% water causes changes in the infrared (FTIR/IR), vibrational circular dichroism (VCD) and ultra-violet electronic circular dichroism (UVCD) spectra. These processes drive the formation of a gel, which can be examined more closely with microscopic imaging. This chapter aims to compare spectroscopic differences in the sol and gel phases of cationic GAG in 55 mol% ethanol/ 45 mol% water. Imaging techniques will then be used to analyze and propose estimated dimensions of the crystalline fibrils within the gel.

2.3 Experimental

Materials. The tripeptide, L-glycyl-L-alanyl-L-glycine (GAG) was purchased from Bachem Biosciences Inc. (King of Prussia, PA) with > 98% purity and was not further purified for any experiments. Ethanol (200 proof, Pharmco-Aaper, Brookfield, CT) was used to create a 55 mol% ethanol/45 mol% water solution. The 0.2 M peptide

solution was prepared in the co-solvent solution and the pH of the solution was adjusted to about 1.5-2.0 by adding HCl (ACS grade, Ricca Chemical Company, Arlington, TX). The mixture was allowed to set for twenty four hours at room temperature prior to microscope imaging. Deuterated solvents were used for the vibrational spectroscopy measurements.

Bright-Field Microscopy. The image was taken with an Olympus Model BX51 Microscope equipped with a PixeLINK PL-A662 camera. A 20 x objective lens was used to provide a total magnification of 200 x.

Atomic Force Microscopy (AFM). Images were taken using a Multi-Mode Scanning Probe Microscope (SPM) System (Nanoscope IIId; Veeco Metrology, Inc., Plainview, NY). A portion of the sample was placed onto a 500 micron silica wafer plate and allowed to sit for ten minutes. Veeco model FESP cantilevers and tips (2.5-3.5 μm in thickness, 200-250 μm in length, 23-33 μm in width) were used in tapping mode to take phase, amplitude, and height images with a force constant ranging from 1-5 N/m and a drive frequency of 60-100 kHz. The images were taken with a scanning rate of 0.500 Hz with 512 samples per line. Images and profiles were processed using WSxM 4.0 software.

Vibrational Spectroscopy. FTIR and VCD spectra of ethanol/water with GAG peptide were simultaneously recorded at a temperature of nearly 25 ^{o}C using a Chiral IR^{TM} Fourier Transform VCD spectrometer from BioTools with a spectral resolution of 8 cm^{-1}. Approximately 3600 scans were collected of each sample. The sample was loaded into a 56.5-μm CaF_2 Biocell (BioTools). Background of the solvent without peptide was subtracted from the spectra and then baseline-corrected using Multifit.

2.4 Results and Discussion

Figure 2.1 shows the infrared spectrum of cationic GAG in various concentrations of ethanol co-solvent. The amide I′ region (1600-1700 cm^{-1}) clearly is a superposition of two bands, the first at lower energy corresponding to the C-terminal amide I′ (1646 cm^{-1}) and the second at higher energy corresponding to the N-terminal amide I′ (1670 cm^{-1}). In D_2O, the amide I′ mode is predominantly C-terminal but with increasing ethanol content the C-terminal amide I′ band shifts towards the N-terminal band position, forming a single, broad band.[9,10]

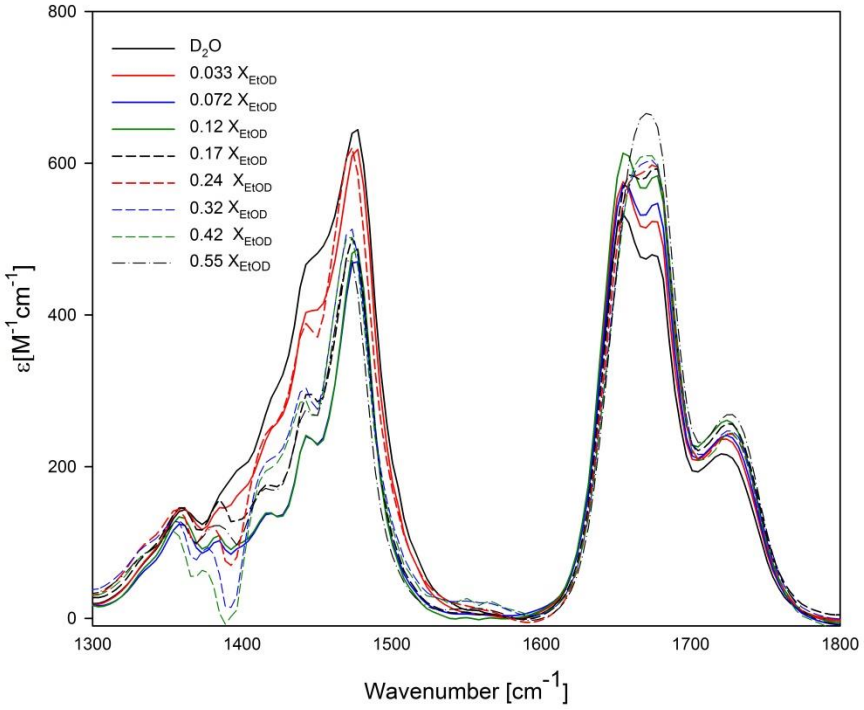

Figure 2.1. IR spectra of the 1300-1800 cm^{-1} region of 200 mM cationic GAG dissolved in the indicated ethanol/water mixture. The numbers reflect the molar fractions of ethanol in the mixture. The bands between 1300 and 1500 cm^{-1} result mostly from CH_2 and CH_3 deformation modes. The most intense band in this region is assignable to a mixture of amide II′ and CH_3 out-plane antisymmetric bending modes. The 1600-1700 cm^{-1} region contains the amide I′ band profile. The band at ca. 1700 cm^{-1} is assignable to the C-terminal C=O stretching mode. Taken from reference [9].

The observed peak shift to lower wavenumber with increasing ethanol content provides information about the strength of hydrogen bonding and the polarity of the solvent. Ethanol penetrates into the peptide's hydration shell, disrupting the strong hydrogen bonding network and lessening the polarity of the solvent in the hydration shell. This increased the probability of aggregation by removing water from the peptide hydration shell, and consequently set the stage for gelation.

A blueshift of the amide I′ band was similarly observed in the VCD spectrum with increasing ethanol content, as shown in Figure 2.2. The signal showed a quantitative shift to higher energy and also became more negatively biased. Together the IR and VCD data indicated structural redistribution of the peptide's central amino acid residue and substantial changes in the hydration shell. Together with NMR data reported by Milorey et al. these spectral changes reflect a conformational shift from pPII to β-strand-like conformations as the hydrogen bonding network of hydration water becomes perturbed by the ethanol co-solvent.[9]

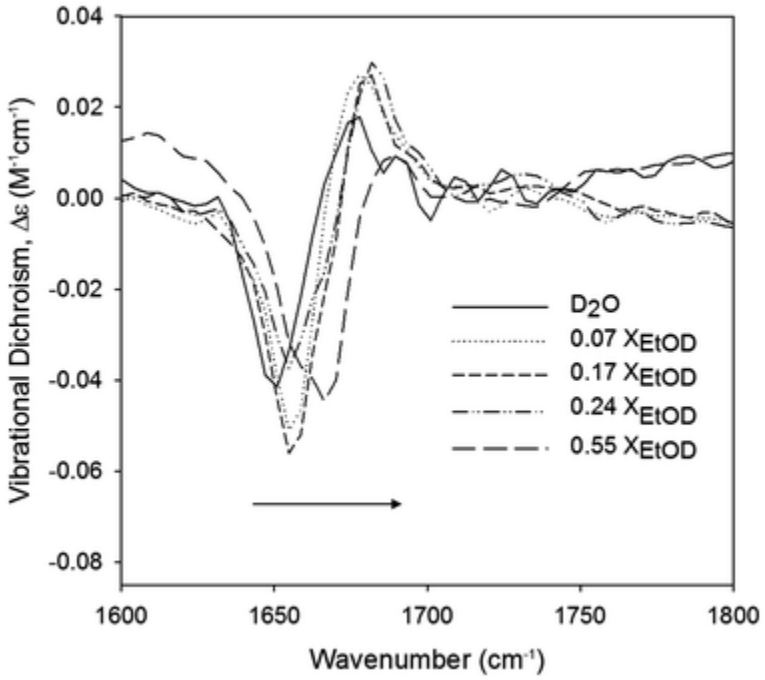

Figure 2.2. VCD of the amide I' region of cationic GAG recorded for the indicated D_2O/ethan(ol)-d/mixtures. Taken from reference [9].

In addition to the changes observed with increasing ethanol content, the VCD signal of the amide I′ also exhibited spectral changes with an adjustment of peptide concentration. Figure 2.3 shows that at higher peptide concentration (208.8 and 209.5 mM), the signal changes from a negative couplet to a W-shape (-+-) and increases by an order of magnitude from that observed at lower peptide concentration (195.2 mM). Similar qualitative enlargement has been attributed to helically twisted β-sheet amyloid-like fibrils,[11,12] and in this case could be used to monitor the formation of fibrils that, as shown below, extend into a cross-linked gel network.

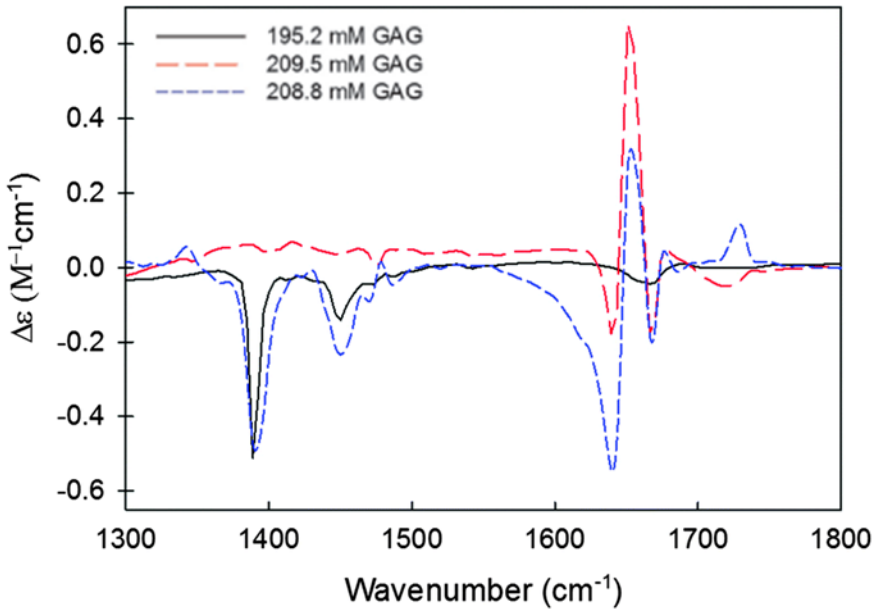

Figure 2.3. Amide I' IR (upper panel) and VCD (lower panel) band profile of cationic GAG dissolved in a 55/45 mol% mixture of ethan(ol)-d and water. The concentrations of GAG are indicated in the figure. Taken from reference [9] and modified.

Structural rearrangements induced changes in the ultra-violet circular dichroism (UVCD) spectrum as well, which traditionally monitors secondary structure compositions of peptides and proteins. The cationic tripeptide GAG at 5mM concentration in water exhibits a classical pPII signal with a positive maximum around 215 nm ($n \rightarrow \pi^*$ transition) and a negative maximum around 195 nm ($\pi \rightarrow \pi^*$ transition). The intensity of both maxima decreased with an increase in temperature, similar to what was observed by Toal et al. for cationic trialanine.[8] When ethanol was added as a co-solvent, the CD signal was comparable at 5 mM concentration with similar temperature dependence over a broad range of ethanol concentrations (0-55 mol%, 0-80% v/v) (Figure 2.4A). At higher peptide concentration (55 mol%, 80% v/v), the signal changed drastically, coinciding with the formation of a viscous hydrogel (Figure 2.4B).[9] As temperature increased, the

positive maximum at 215 nm converted into a negative maximum centered around 225 nm.

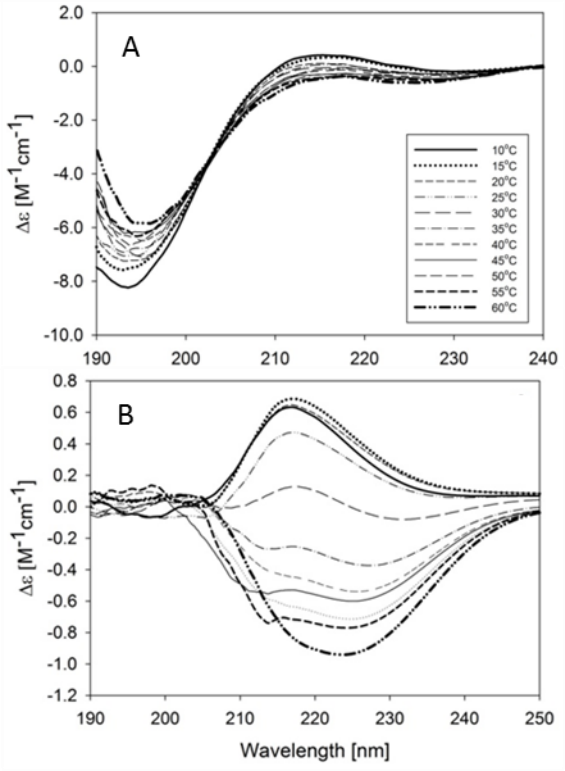

Figure 2.4. UVCD spectrum of A) 5 mM GAG in 55 mol% ethanol/45 mol% water and B) 220 mM GAG in 55 mol% ethanol/45 mol% water. For the 220 mM solution, the absorbance exceeded the instrumental detection limit at wavelengths below 210 nm. Taken from reference [9] and modified.

We have found that an observed change in the UVCD spectra does not always coincide with a change in the VCD spectrum, contrary to expectations. Chapter 4 of this thesis explains this discrepancy in more detail. The UVCD traditionally shows secondary structure, but in this case of a gelling peptide the picture becomes more complicated. It is possible that the signal reflects local aggregation from many cross-linked fibrils, so the

observed spectra can no longer be described in terms of mixtures of canonical secondary structures.

Bright-field microscopy and atomic force microscopy were used to image a sample of the GAG hydrogel 24 hours after preparation to characterize the fibrils formed after gelation. The time was chosen to ensure a stabilized gel with fully formed fibrils. The bright-field microscope images in Figure 2.5 show overlapping crystalline fibrils,[9] yielding a network appearance. The extended fibrils of the GAG hydrogel seemed to form nucleation centers, then spanned outwards forming a star-like cluster of rigid rods. The solvent is visible in images B and D, but was not present in other images due to some evaporation of the solvent with high ethanol content over time. The fibrils were on a sub-millimeter scale, similar to what was observed by DiGuiseppi et al. for 102 mM GHG in water.[1]

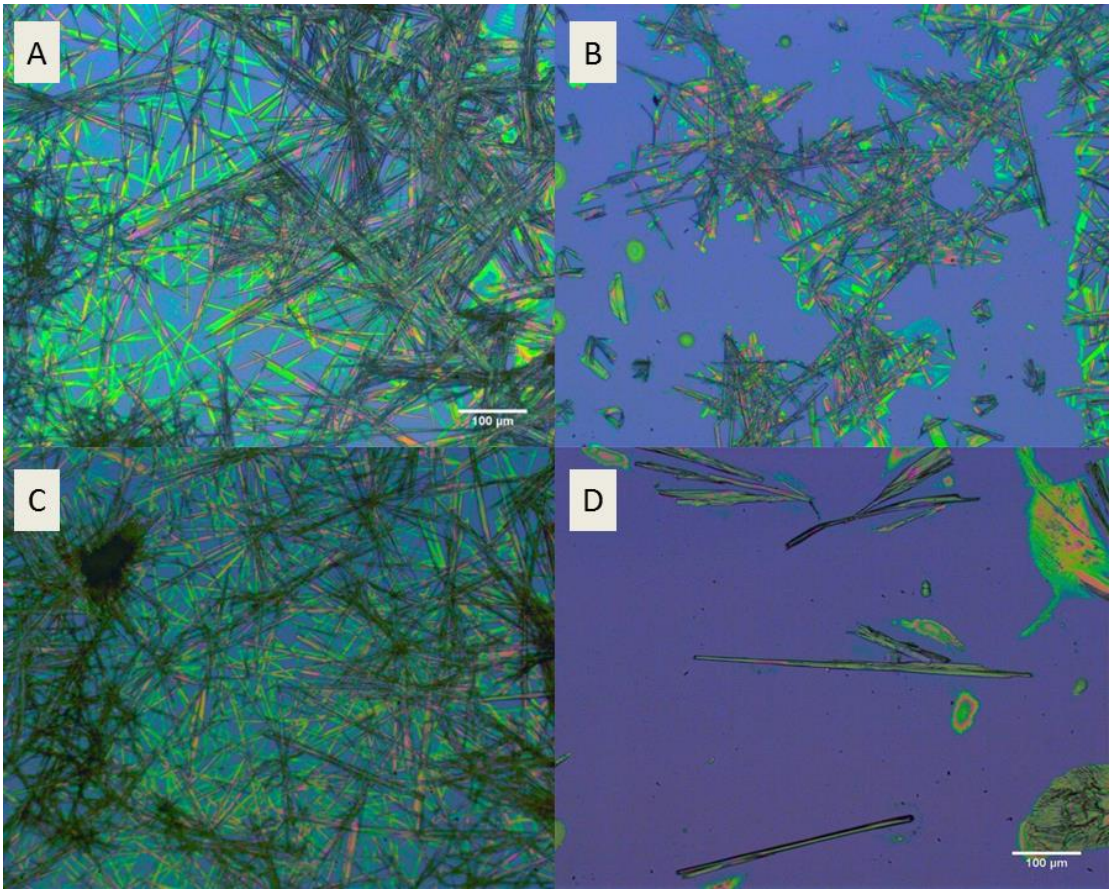

Figure 2.5. Bright-field microscope images of 208 mM GAG in 55 mol% ethanol/45 mol% water.

Mitra et al. investigated various low molecular weight peptide amphiphilic hydrogels with tryptophan and phenylalanine residues by means of scanning electron microscopy, transmission electron microscopy, bright-field microscopy and fluorescence microscopy.[13] They found that opaque gels were primarily fibrillous in nature.[13] Fibrils are likely to provide surfaces that refract light and give the opaque appearance. Other amorphous gels were transparent and clear without these fibril surfaces.[13] The fibrils and clusters formed by GAG create many surfaces for scattering and refracting light, probably giving the gel its opaque white color.

The fibrils of the GAG gel were examined more closely with AFM. Figure 2.5D shows a bright-field image of the centered lone fibril which was used to take height, amplitude and phase images with AFM. The length of the fibril was approximately 500 μm. The height image and corresponding profile in Figures 2.6A and 2.6B respectively showed that the fibril had a cross-section of about 7 μm, and a height of about 500 nm.

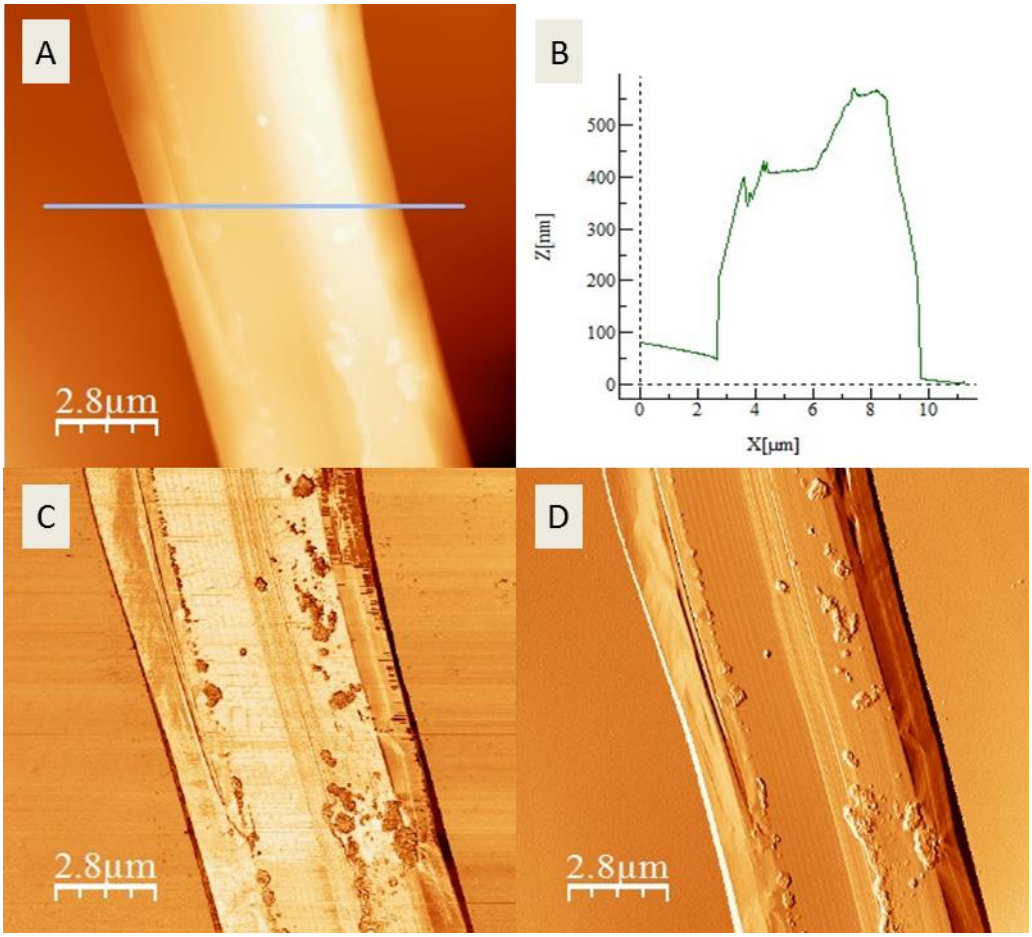

Figure 2.6. AFM images of a sample of 208 mM GAG in 55 mol% ethanol/45 mol% water: A) height image, B) height profile, C) amplitude image, D) phase image.

The amplitude image in Figure 2.6C appears to have a fibril divided into sections that run the length of the fibril, where the brightest portions indicate greatest amplitude.

The central regions of the fibril were brightest, agreeing with the shapes seen in the other images. The fibril was typically rod-like shaped and cylindrical, although not perfectly symmetrical. Phase imaging showed that on the central right side of the fibril there was a protruding edge (Figure 2.6D). This corresponded to the jagged height profile in Figure 2.6B.

AFM imaging has been performed on other short peptides from the literature. Figure 2.6 shows two images of hydrogels formed from Fmoc-valine-aspartic acid (Fmoc-VD) and a mixture of Fmoc-phenylalanine-phenylalanine (Fmoc-FF) and Fmoc-arginine-glycine-aspartic acid (Fmoc-RGD) on a micrometer scale.

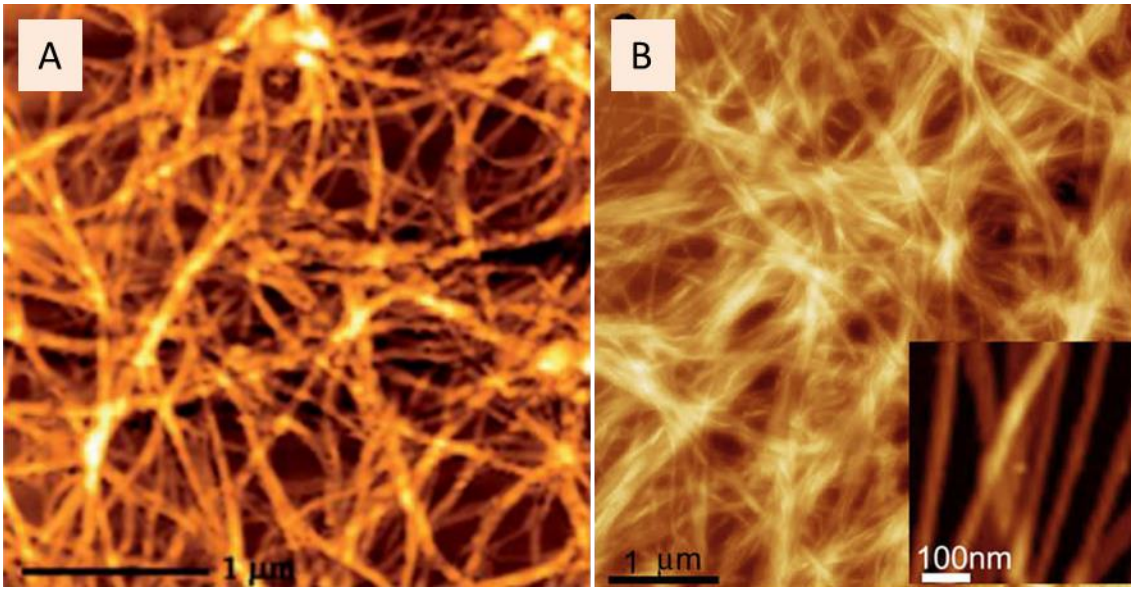

Figure 2.7. AFM images of A) Fmoc-VD and B) mixture of Fmoc-FF/Fmoc-RGD peptide hydrogels. Taken from references [2] and [3], respectively.

Both images show an entangled network of fibrils on a micrometer scale. Adhikari et al. described the fibrils of Fmoc-VD as a uniform three-dimensional nanofibrillar network

that forms a supramolecular structure.[2] Zhou et al. used the term 'flat ribbons' for the fibrils of the Fmoc-FF/Fmoc-RGD hydrogel which had a range of heterogeneous widths.[3] Both dramatically contrast with the fibrils formed by the GAG hydrogel in size and appearance. The part of the fibril of the GAG hydrogel shown in Figure 2.6 is gigantic in comparison to the nanoscale fibers of the other peptide gels in Figure 2.7. The fibers of GAG seem to be layered on top of one another as opposed to forming a supramolecular entwined structure of one long chain. High crystalline character of the fibrils contrasts with the flexible structures seen from the other short peptide hydrogels.

2.5 Conclusion

Changes in the infrared (FTIR/IR), vibrational circular dichroism (VCD) and ultra-violet electronic circular dichroism (UVCD) spectra have been observed as the result of the aggregation and fibrilization of cationic peptide GAG in 55 mol% ethanol/ 45 mol% water, eventually leading to formation of a hydrogel. A blueshift observed in the FTIR and VCD spectra provided evidence of ethanol entering the peptide's hydration shell, causing conformational shift from that of pPII to β-strand. This increased the probability of aggregation by removing water, setting the stage for gelation. A significant enhancement in the VCD spectrum with an increase in peptide concentration was attributed to the formation of an extended network of helically twisted fibrils. An observed change in the UVCD spectrum was hypothesized to reflect local aggregation from many combined cross-linked fibrils instead of traditional secondary structure.

The opaque hydrogel formed by cationic GAG in 55 mol% ethanol/45 mol% water was characterized using bright-field and atomic force microscopy. It is possible that the opaque character of the hydrogel occurs from scattering and refraction of light

between the surfaces of the crystalline fibrils. Fibrils were determined to be approximately 500 μm in length, 500 nm in hieght, and 7 μm in cross-section, comparable in size to fibrils formed by GHG in water.[1] Star-like clusters of crystalline fibrils overlap to form an extensive network that encases the solvent. The fibrils are massive in size compared to those of other Fmoc-peptide hydrogels found in the literature.[2,3]

2.6 Acknowledgements

We would like to thank Professor Haifeng Ji for allowing us to use his bright-field microscope and former graduate student Dr. Joshua Smith for assistance with using both bright-field and atomic force microscopes and creating profiles.

2.7 References

1. DiGuiseppi, D.; Schweitzer-Stenner, R. Probing Conformational Propensities of Histidine in Different Protonation States of the Unblocked Glycyl-Histidyl-Glycine Peptide by Vibrational and NMR Spectroscopy. *J. Raman Spectrosc.* **2016,** *in press*.

2. Adhikari, B.; Banerjee, A. Short-Peptide-Based Hydrogel: A Template for the In Situ Synthesis of Fluorescent Silver Nanoclusters by Using Sunlight. *Chem. Eur. J.* **2010,** *16* (46), 13698-13705.

3. Zhou, M.; Smith, A. M.; Das, A. K.; Hodson, N. W.; Collins, R. F.; Ulijn, R. V.; Gough, J. E. Self-Assembled Peptide-Based Hydrogels as Scaffolds for Anchorage-Dependent Cells. *Biomater.* **2009,** *30* (13), 2523-2530.

4. Hagarman, A.; Measey, T. J.; Mathieu, D.; Schwalbe, H.; Schweitzer-Stenner, R. Intrinsic Propensities of Amino Acid Residues in GxG Peptides Inferred from Amide I' Band Profiles and NMR Scalar Coupling Constants. *J. Am. Chem. Soc.* **2010,** *132* (2), 540-51.

5. Toal, S.; Meral, D.; Verbaro, D.; Urbanc, B.; Schweitzer-Stenner, R. pH-Independence of Trialanine and the Effects of Termini Blocking in Short Peptides: A Combined Vibrational, NMR, UVCD, and Molecular Dynamics Study. *J. Phys. Chem. B.* **2013,** *117* (14), 3689-706.

6. Toal, S. E.; Verbaro, D. J.; Schweitzer-Stenner, R. Role of Enthalpy-Entropy Compensation Interactions in Determining the Conformational Propensities of Amino Acid Residues in Unfolded Peptides. *J. Phys. Chem. B.* **2014,** *118* (5), 1309-18.

7. Garcia-Pietro, F. F.; Galván, I. F.; Aguliar, M. A.; Martin, M. E. Study on the Conformational Equilibrium of the Alanine Dipeptide in Water Solution by Using the Averaged Solvent Electrostatic Potential from Molecular Dynamics Methodology. *J. Chem. Phys.* **2011,** *135*, 194502.

8. Toal, S.; Omidi, A.; Schweitzer-Stenner, R. Conformational Changes of Trialanine Induced by Direct Interactions between Alanine Residues and Alcohols in Binary Mixtures of Water with Glycerol and Ethanol. *J. Am. Chem. Soc.* **2011,** *133*, 12728.

9. Milorey, B.; Farrell, S.; Toal, S.; Schweitzer-Stenner, R. Demixing of Water and Ethanol Causes Conformational Redistribution and Gelation of the GAG Tripeptide. *Chem. Commun.* **2015,** 51, 16498-16501.

10. Farrell, S.; DiGuiseppi, D.; Alvarez, N.; Schweitzer-Stenner, R. The Interplay of Aggregation, Polymerization and Gelation of an Unexpected Low Molecular Weight Gelator: Glycylanalylglycine in Ethanol/water. Submitted to *Soft Matt.,* **2016**.

11. Measey, T. J.; Schweitzer-Stenner, R. Vibrational Circular Dichroism as a Probe of Fibrillogenesis: The Origin of the Anomalous Intensity Enhancement of Amyloid-like Fibrils. *J. Am. Chem. Soc.* **2011,** *133*, 1066-1076.

12. Ma, S.; Cao, X.; Mak, M.; Sadik, A.; Walkner, C.; Freedman, T. B.; Lednev, I. K.; Dukor, R. K.; Nafie, L. A., Vibrational Circular Dichroism Shows Unusual Sensitivity to Protein Fibril Formation and Development in Solution. *J. Am. Chem. Soc.* **2007,** *129*, 12364-12365.

13. Mitra, R. N.; Das, D.; Roy, S.; Das, P. K., Structure and Properties of Low Molecular Weight Amphiphilic Peptide Hydrogelators. *J. Phys. Chem. B.* **2007,** *111* (51), 14107-14113.

CHAPTER 3. DEMIXING OF WATER AND ETHANOL CAUSES CONFORMATIONAL REDISTRIBUTION AND GELATION OF THE CATIONIC GAG TRIPEPTIDE

Reproduced from :
Milorey, B.; Farrell, S.; Toal, S.; Schweitzer-Stenner, R. Demixing of Water and Ethanol Causes Conformational Redistribution and Gelation of the GAG Tripeptide. *Chemical Communications*, **2015**, 51, 16498-16501.

3.1 Abstract

The cationic tripeptide GAG undergoes three conformational changes in binary mixtures of water and ethanol. At 17 mol% of ethanol conformational sampling is shifted from pPII towards β-strands. A more pronounced shift in the same direction occurs at 40 mol%. At ca. 55 mol% of ethanol and above a peptide concentration of ca. 0.2 M the ternary peptide–water–ethanol mixture forms a hydrogel which is comprised of unusually large crystalline like non-β sheet fibrils forming a sample spanning matrix.

3.2 Introduction

The random coil model suggests that amino acid residues in unfoldable peptides sample the entire sterically and electrostatically allowed space of the Ramachandran plot.[1,2] However, results from recent examinations of short peptides in water and of coil libraries suggest that conformational distributions deviate from random coil prediction.[3,4,5] For alanine, they suggest a very high fraction (i.e. 0.72) of polyproline II (pPII)-like conformations in both unblocked GAG and the canonical alanine dipeptide in aqueous solution[6,7] and an even higher value for trialanine (0.84–0.9).[7,8] Multiple lines of experimental evidence suggest that pPII is enthalpically stabilized by peptide/protein–water interactions,[9,10,11,12,13] but the role of hydration has thus far been investigated

mostly by computational means.[14,15,16,17,18] Here, we assess the influence of the solvent on the conformational distribution of cationic GAG by utilizing ethanol as amphiphilic co-solvent.[19,20,21] Such co-solvents can interact with an unfolded peptide (and proteins) indirectly by affecting backbone hydration and directly by interacting with functional backbone groups and side chains alike.[22,23,24,25,26,27] In the peptide concentration regime chosen for this study, ethanol can be expected to function as a crowding agent reagent for the peptide[28] since it produces a much larger excluded volume effect than water (the volume fraction reaches 0.8 at the highest chosen ethanol concentration). We investigated GAG in different ethanol–water mixtures by combining ^{1}H-NMR, IR, vibrational and far UV circular dichroism (VCD and UVCD) spectroscopy. IR spectra of the solvent mixture were used to obtain reorganizations of the bulk liquid and corresponding deviations from ideal behavior.

3.3 Experimental

Materials. The tripeptide, L-glycyl-L-alanyl-L-glycine (GAG) was purchased from Bachem Biosciences Inc. (King of Prussia, PA) with > 98% purity and was not further purified for any experiments. The deuterated solvents, D_2O and ethan(ol)-d (EtOD), were used for vibrational spectroscopy studies. EtOD is the deuterated ethyl alcohol, with the alcoholic hydrogen replaced by deuterium. The EtOD was purchased from Sigma with a purity of > 98%.

Methods

Solution preparation. Solutions of cationic GAG were prepared by dissolving the peptide in a mixture of ethanol and DI-water at mole fractions of ethanol ranging from 0 to 0.552, which corresponds to 0 to 80% (v/v). The pH of each solution was adjusted to

about 1.5-2.0 by adding HCl. For NMR studies, solutions with a peptide concentration of approximately 100 mM were made by dissolving the solid GAG in a H_2O/D_2O mixture of 9 parts H_2O to one part D_2O containing 0.1% trimethylsilane (TMS). Solutions with a mole fraction of ethanol greater than 0.12 were pipetted into a double-chamber NMR tube, which became necessary in order to mix solvents without affecting the deuterium-detecting lock signal of the NMR. The inside chamber held D_2O containing 0.1% TMS used as an internal standard. Vibrational studies (FTIR and VCD) required a peptide concentration of 200 mM and the use of deuterated solvents D_2O and EtOD to avoid any spectral overlap of amide I with the broad band assignable HOH bending vibrations. The use of deuterated ethanol prevents the contamination of binary mixtures with H_2O and HOD owing to an H⇔D exchange of hydroxyl proton. The prepared solutions were pipetted into a CaF_2 demountable cell with a path length of 56-μm from BioTools (Jupiter, FL). For UVCD studies, 5 mM GAG was prepared from a 200 mM stock solution.

^{1}H-NMR. Temperature dependent ^{1}H-NMR spectra were recorded for all GAG samples using a Varian 500 MHz FT-NMR with a 5 mm HCN triple resonance probe at Drexel University. The v.6.1 Varian software was used for processing of all spectra, and the pre-saturation mode (presat) was used to suppress the strong signals of solvents. The sample was set at a spin of 20 Hz, and spectra were collected starting at 25 ^oC while increasing by 5 ^{o} for each measurement with the maximum temperature of 55 ^oC. At each temperature, the sample was given approximately two minutes to equilibrate. Either 16 or 32 scans were collected for each spectrum, with higher temperature and mole fraction of ethanol causing the need for 32 scans. The fid files were opened in MestReC software,

which was used for the Fourier transform and phase correction, then exported as text files. The amide proton three-bond J-coupling $^{3}J(H^{N}H^{\alpha})$) was determined using the technique described by Toal et al.[27]

Vibrational Spectroscopy. FTIR and VCD spectra of ethanol/water with and without GAG peptide were simultaneously recorded at a temperature of nearly 25 ^{o}C using a Chiral IR^{TM} Fourier Transform VCD spectrometer from BioTools with a spectral resolution of 8 cm^{-1}. Approximately 3600 scans were collected for each sample. Background and baseline corrections were performed as described earlier.[29]

Ultra-Violet Circular Dichroism (UVCD) Spectroscopy. Temperature dependent UVCD spectra were measured on a Jasco J-180 spectropolarimeter (model J-810-150S) purged with N_2. The temperatures ranged from 10-60 ^{o}C in 5 degree increments using a Peltier controller (model PTC-423S). A delay time of 150 s was used to ensure adjustment at each temperature. The sample was loaded into a 100 μm cell from International Crystral Laboratories. Spectra were measured from 180-300 nm using a data pitch of 0.05 nm, a scan speed of 500 nm/min, a response time of 1.0 s, and a bandwidth of 5 nm. The spectra were corrected using appropriate background subtraction, and ten accumulations were averaged at each temperature.

Bright-Field Microscopy. The image was taken using an Olympus Model BX51 Microscope equipped with a PixeLINK PL-A662 camera. A 20 x objective lens was used to provide a total magnification of 200 x.

3.4 Results and Discussion

Figure 3.1 depicts the $^{3}J(H^{N}H^{\alpha})$ coupling constant of the N-terminal alanine proton as a function of ethanol mole fraction, χ_{ET}, measured at the indicated temperatures. This observable is an indicator of the average φ-angle of the conformational manifold sampled by the alanine residue.[30,31,32] The data reveal a highly non-linear and non-monotonic relationship between $^{3}J(H^{N}H^{\alpha})$ and χ_{ET}. Three regions of the plot are noteworthy. At very low χ_{ET} (0.01–0.02) a rather sharp maximum appears which grows with increasing temperature (region 1). A small but sharp increase of $^{3}J(H^{N}H^{\alpha})$ by ca. 0.1 Hz occurs between χ_{ET} values of 0.12 and 0.15 (region 2). At ca. 0.4 (region 3), the data indicate a more pronounced increase of the coupling constant by ca. 0.22 Hz.

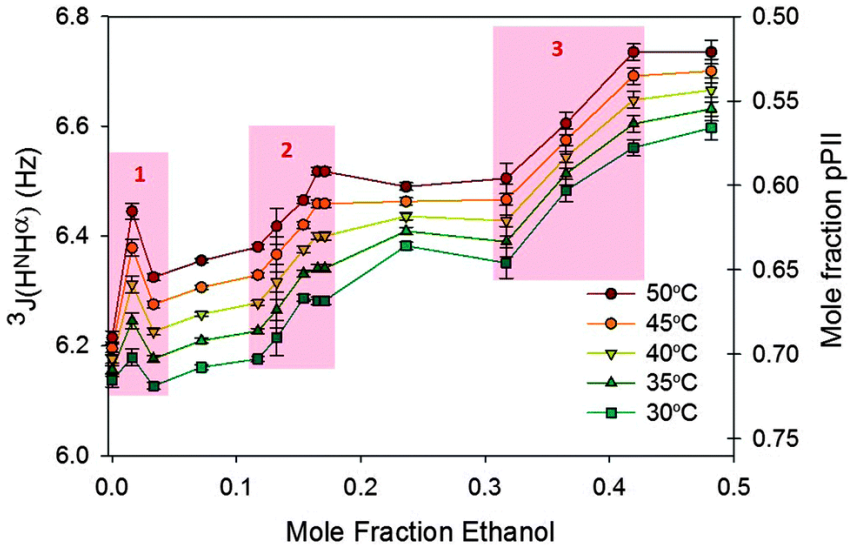

Figure 3.1. $^{3}J(H^{N}H^{\alpha})$ of the N-terminal amide proton of cationic GAG in different water/ethanol mixtures determined from ^{1}H-NMR spectra taken at the indicated temperatures. Three notable regions are highlighted and labelled accordingly.

The observed changes of the $^{3}J(H^{N}H^{\alpha})$ are not attributable to any type of peptide aggregation that one might suspect to occur at the rather high peptide concentration (0.1

M) chosen for our experiment in order to optimize the signal to noise, a necessity for measurements at higher temperatures. As shown in Figures A3.1 and A3.2 (Appendix), $^{3}J(H^{N}H^{\alpha})$ of GAG in pure water and in ethanol/water mixtures of 14/86 mol% (region 2) and 48/52 mol% (past region 3) are within their statistical uncertainties independent of the peptide concentration between 10 and 100 mM. This suggests the absence of any structural change in this region. To ensure that peptides did not aggregate even at 10 mM, we measured the UVCD spectra of 10 mM GAG in a solution with χ_{ET} = 0.48 as a function of temperature. The spectra in Figure A3.3 (Appendix) are clearly indicative of a monomeric pPII/β-strand mixture with the β-content increasing with rising temperatures.[13]

The increases of $^{3}J(H^{N}H^{\alpha})$ with χ_{ET} can be indicative of a population redistribution from pPII to β-strand or of a shift of the pPII distribution towards more negative values of φ.[6] Based on arguments presented in the Appendix (Figure A3.4 and text) we think that the observed changes of the coupling constant are predominantly caused by conformational redistribution. Thus, we map our $^{3}J(H^{N}H^{\alpha})$ onto the mole fraction of pPII as depicted in Figure 3.1. The data suggest that the pPII content of the alanine distribution is reduced to 78% of its value in water at χ_{ET} of ca. 0.5 and room temperature.

In order to explore whether the obtained conformational redistribution of GAG reflects changes of the solvent organization, we measured and analyzed the FTIR spectra of several mixtures of ethanol/D_2O mixtures in the region between 1100 and 1500 cm^{-1}. It is known that the co-solvent system of water and ethanol is known to be not ideal and that the formation of micro-domains of ethanol can start at rather low mole fractions of

this binary mixture.[25,33] The spectra shown in Figure A3.5 (Appendix) contain several bands assignable to CH bending type modes of the co-solvent's hydrophobic tail.[34] Aggregation of ethanol in the mixture should lead to a change of these modes' intrinsic oscillator strengths and thus to a departure from Beer–Lambert's law. We decomposed all these spectra into a set of Gaussian bands by using our program Multifit.[35] The same set of spectral parameters was used for fits to all spectra. Figure 3.2 shows the obtained integrated intensities of selected bands plotted as a function of χ_{ET}. The concentration dependence of the intensities of the bands at 1136 and 1451 cm^{-1} start to deviate from linearity at ca. 0.17, which coincides with the increase of $^{3}J(H^{N}H^{\alpha})$ in region 2 of Figure 3.1. Interestingly, another band at 1332 cm^{-1} appears only at an ethanol concentration of ca. 30 mol% and increases steadily with increasing ethanol concentration. Only the intensity of the 1418 cm^{-1} seems to be unaffected by any changes in region 2 in that its increase with increasing ethanol fraction remains linear. All these observations suggest that the underlying structural redistribution of the peptide probed by $^{3}J(H^{N}H^{\alpha})$ in region 2 correlates with the demixing of the two co-solvents caused by the formation of ethanol clusters due to hydrophobic interactions.[36] At the relatively high peptide concentration used for our experiments, such clusters are very likely to penetrate the hydration shell of the peptide. As shown in Figure A3.6 (Appendix), these changes of peptide solvation lead to a blue-shift of the amide I' band profile in the IR spectrum. The corresponding VCD (Figure 3.3) signals exhibit the same behavior. The blue-shift reflects a weakening of hydrogen bonding between peptide and water and/or a partial replacement of peptide–water with peptide–ethanol hydrogen bonds.[37,38,39]

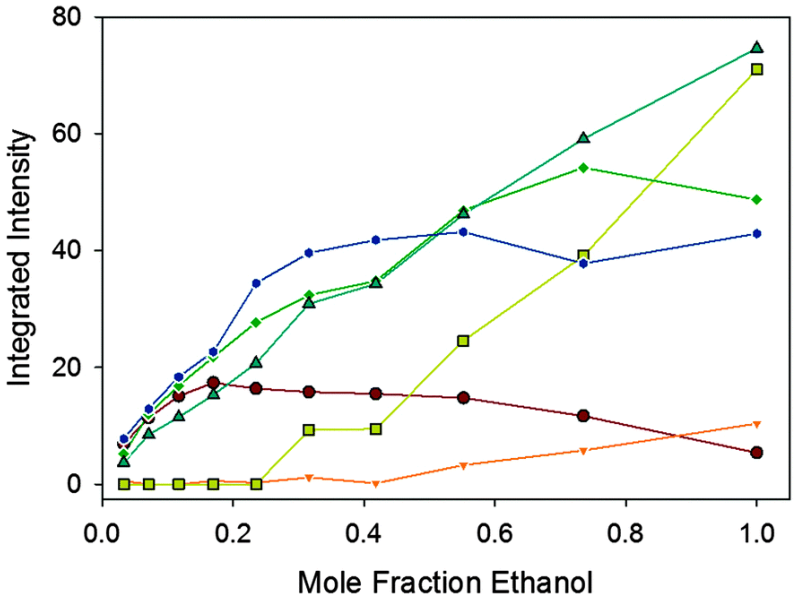

Figure 3.2. Integrated intensities of bands in the 1100–1500 cm^{-1} region of water/ethanol mixtures plotted as a function of ethanol mole fraction (red ●: 1136 cm^{-1}, orange ▼: 1274 cm^{-1}, yellow ■: 1332 cm^{-1}, green ◆: 1392 cm^{-1}, teal ▲: 1418 cm^{-1}, blue ●: 1451 cm^{-1}). Solid lines are provided as a guide to the viewer.

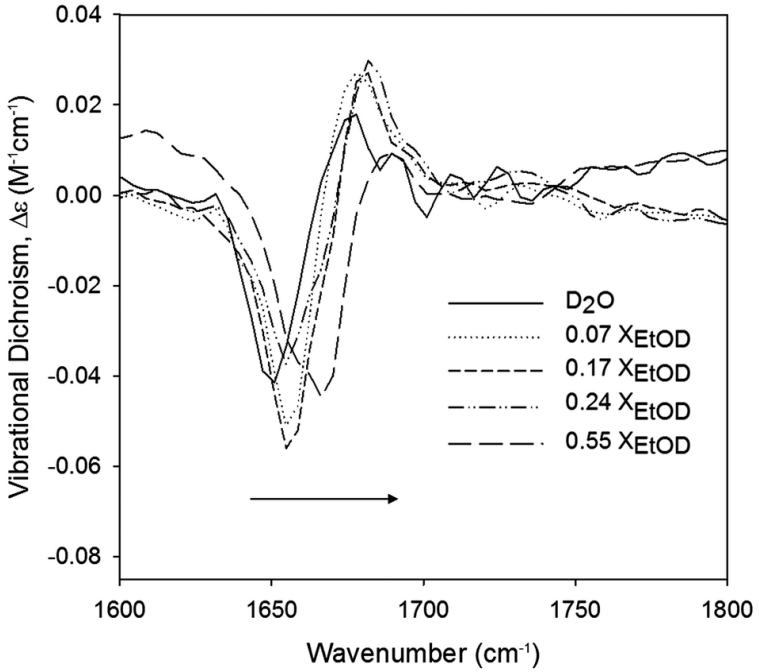

Figure 3.3. VCD of the Amide I' region of cationic GAG recorded for the indicated D_2O/ethan(ol)-d/mixtures.

The data in Figure 3.2 do indicate further changes of the ethanol/water mixtures in region 3 of the $^{3}J(H^{N}H^{\alpha})$-plot in Figure 3.1. The band at 1332 cm^{-1} suddenly increases its intensity relatively sharply. Another band at 1274 cm^{-1} starts to gain intensity and increases linearly with increasing ethanol concentration. On the contrary, the intensities of bands at 1274 cm^{-1} and 1392 cm^{-1} reach saturation and become nearly ethanol independent above χ_{ET} of ca. 0.5. Concomitant changes in the peptide spectrum are also noteworthy. As shown in Figure A3.5 (Appendix), the amide I' profile exhibits a further blue-shift of the low-wavenumber band (predominantly assignable to the C-terminal amide I').[40] It merges with the high-wavenumber band (N-terminal amide I') into a single broad band. The VCD blue-shifts as well (Figure 3.3) and becomes more negatively biased.

Taken together, our spectroscopic data provide evidence for the notion that a reorganization (demixing) of the solvent probed by deviations from Beer–Lambert's law induces changes in the peptides hydration shell (dehydration due to enrichment with ethanol, probed by amide I'), which involve a redistribution of the peptide's backbone conformations from pPII towards β-strand. These findings underscore the notion that backbone hydration is the key stabilizing factor for pPII, in agreement with many theoretical predictions.[14,15,16,17,18,19] Furthermore, they reflect that changes of the bulk solvent configuration are transduced to the peptide's hydration shell.

There is a large volume of literature on both binary alcohol/water and ternary (bio)polymer/alcohol water mixtures, which cannot be comprehensively considered in this chapter. Microphase separation leading to excess molar and apparent modal volumes owing to interactions between the aliphatic groups of the alcohol co-solvent has been

suggested for region 1.[25] For cationic trialanine, Toal et al. found evidence for hydrophobic peptide–ethanol interactions at very low ethanol concentrations.[27] With regard to region 2, a combined MD/NMR study on the [val5]angiotensin peptide in χ_{ET} = 0.14 ethanol/water yielded of a much higher population of β-strand-like structures of the peptide's residues than one would expect from their intrinsic propensities in water.[6] Results of his MD simulations suggest a preferential binding of ethanol in the hydration shell, which involves predominantly hydrophobic interactions.[41]

In the remainder of this chapter we focus on more drastic changes of the investigated ternary mixture for which the changes in region 3 serve as a precursor. They are reflected by the spectral changes in the IR and VCD spectra of three only slightly different concentrations of GAG in a 55/45 mol% mixture ethan(ol)-d and water (i.e. 195.2, 208.8 and 209.5 mM GAG). The IR amide I' bands of the samples are very similar and representative of peptides in region 3. However, the corresponding VCD spectra show dramatic changes (Figure 3.4). At 195.2 mM we observed an abnormal enhancement of the otherwise nearly negligible rotational strength of the CH_3 symmetric bending mode of alanine at ca. 1390 cm^{-1}. Spectra measured at 208.8 and 209.5 mM GAG, depict a dramatic increase of the amide I' signal, which now exhibits a − + − W shape (+ and − indicate the sign of maxima). The strength of the signal exceeds that observed in the spectra measured at lower χ_{ET} (Figure 3.3) by more than an order of magnitude. Such amide I' enhancements are assignable to peptide self-aggregation into fibrilar structures.[42,43] A major change of the peptide's conformation and state is also indicated by the UVCD-spectra of the peptide (Figure A3.3, Appendix).

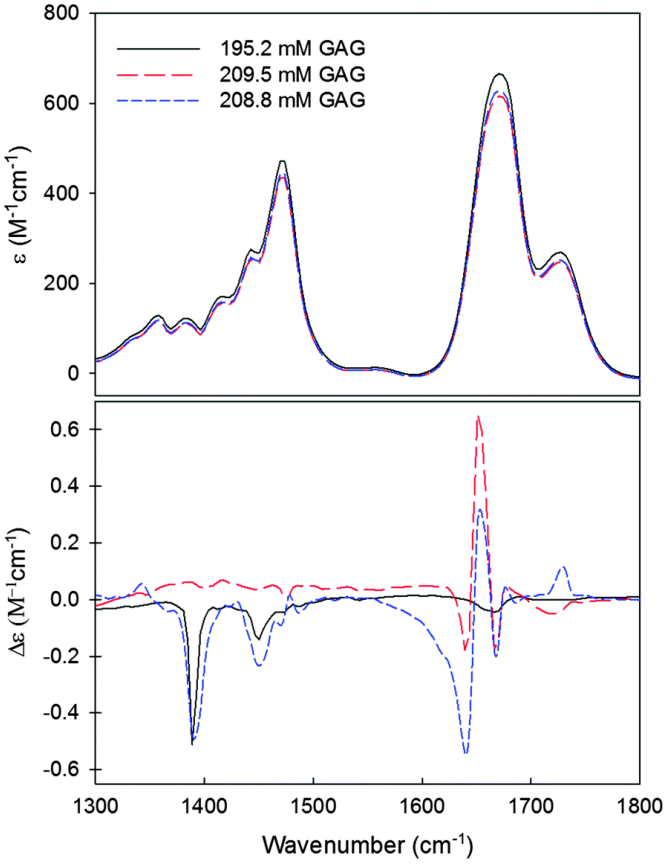

Figure 3.4. Amide I' IR (upper panel) and VCD (lower panel) band profile of cationic GAG dissolved in a 55/45 mol% mixture of ethan(ol)-d and water. The concentrations of GAG are indicated in the figure. The spectrum of the lowest peptide concentration (195 mM, shown as the black line) has an amide I' signal intensity of the same magnitude as the spectra in Figure 3.3.

The above data clearly indicate peptide/solvent demixing and a self-assembly of the peptide into a supramolecular structure. Indeed, we found that the peptide/ethanol/water mixture with the 209.5 mM peptide concentration formed a hydrogel after a few minutes. The bright-field microscope image in Figure 3.5 exhibits a cellular structure that resembles a classical sample-spanning network of fibrils found for many hydrogels formed by organic and biological compounds.[44] However, the sub-millimeter length scale of our rather crystalline fibrils is peculiar. Normally, gel forming

webs show the same structure on a sub-micrometer scale.[45, 46,47,48] While the gelation of (bio)polymers in water is a well-known phenomenon, the co-solvent induced gelation of such a small (low molecular weight) peptide that does not exhibit the hydrophobicity of the phenylalanine peptides[49] or peptides with other aromatic side chains or end groups,[50] has not yet been reported. The position of the amide I' band in Figure 3.4 (upper panel) does not suggest any formation of β-sheet-like arrangement, but the rather intense VCD signal is indicative of some long range, possibly helical, order.[43] Interestingly, region 3 corresponds to a mixing range where some solutes (e.g. poly(n-isopropylacrylamide)) are not dissolvable in ethanol/water,[51] even though they can be dissolved in either of the two co-solvents. In our case the solute forms a gel rather than precipitates.

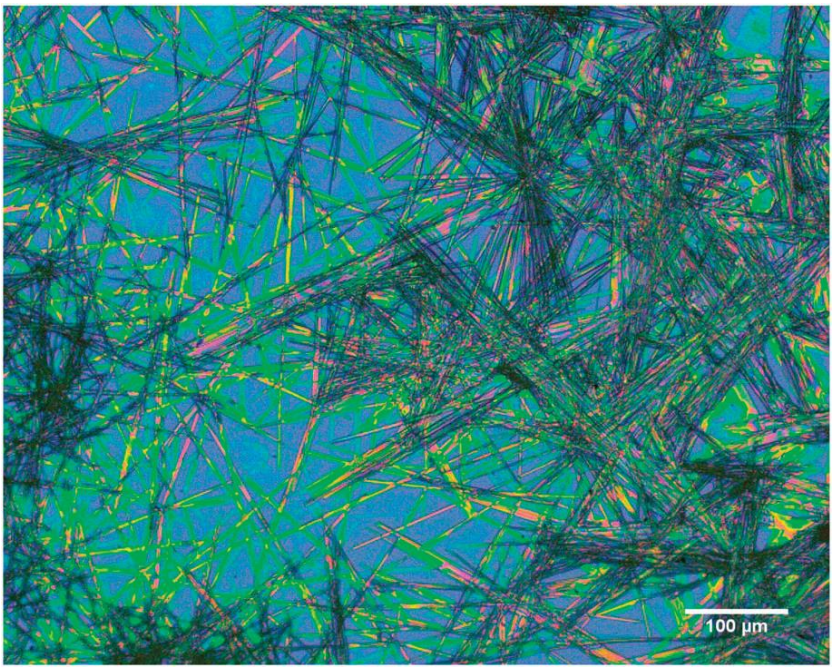

Figure 3.5. Bright field microscope image of the gel formed by a ternary GAG/water/ethanol mixture with a peptide concentration of 208.9 mM in 55 mol% ethanol.

It is noteworthy in this context that GAG together with long polyalanine stretches appear as repeating motifs in silk proteins[52] which to a major extent determine their capability to aggregate into fibers, films and gels. The alanine rich sequences can adopt rather crystalline structures as GAG does in ethanol/water mixtures.[53]

3.5 Conclusion

Taken together, the present study demonstrates that unblocked GAG can be utilized as an indicator of reorganization processes in water–ethanol mixtures. This sensitivity stems firstly from the capability of ethanol to substantially increase the sampling of the extended β-strand conformation at the expense of the peptide's pPII propensity and secondly from desolvation induced demixing of the peptide from the solvent and the subsequent gel formation. The properties of the gel, its dependence on peptide concentration and temperature and it suitability for biotechnological application will be the subject of future investigations.

3.6 Acknowledgements

We like to thank Prof. Haifeng Ji for allowing us to use his bright-field microscope for taking Figure 3.5 and his graduate student Joshua Smith for assistance with the instrument.

3.7 References

1. Ramachandran, G. N.; Ramachandran, C.; Sasisekharan, V. Stereochemistry of Polypeptide Chain Configurations. *J. Mol. Biol.* **1963,** *7*, 95-99.

2. Flory, P. J. *Statistical Mechanics of Chain Molecules*. Wiley & Sons: New York, 1969; p 30-31.

3. Toal, S. E.; Schweitzer-Stenner, R. Local Order in the Unfolded State: Conformational Biases and Nearest Neighbor Interactions. *Biomol.* **2014,** *4*, 725-773.

4. DeBartolo, J.; Jha, A.; Freed, K., F.; Sosnick, T. R. Local Backbone Preferences and Nearest Neighbor Effects in the Unfolded and Native States. In *Proteins and Peptides. Folding, Misfolding and Unfolding.*, Schweitzer-Stenner, R., Ed. Wiley & Sons: Chichester, 2012; pp 79-98.

5. Shi, Z.; Olson, C. A.; Rose, G. D.; Baldwin, R. L.; Kallenbach, N. R. Polyproline II Structure in a Sequence of Seven Alanine Residues. *Proc. Natl. Acad. Sci. USA* **2002,** *99*, 9190-9195.

6. Hagarman, A.; Measey, T. J.; Mathieu, D.; Schwalbe, H.; Schweitzer-Stenner, R. Intrinsic Propensities of Amino Acid Residues in GxG Peptides Inferred from Amide I' Band Profiles and NMR Scalar Coupling Constants. *J. Am. Chem. Soc.* **2010,** *132* (2), 540-51.

7. Toal, S.; Meral, D.; Verbaro, D.; Urbanc, B.; Schweitzer-Stenner, R. pH-Independence of Trialanine and the Effects of Termini Blocking in Short Peptides: A Combined Vibrational, NMR, UVCD, and Molecular Dynamics Study. *J. Phys. Chem. B.* **2013,** *117* (14), 3689-3706.

8. Graf, J.; Nguyen, P. H.; Stock, G.; Schwalbe, H. Structure and Dynamics of the Homologous Series of Alanine Peptides: A Joint Molecular Dynamics/NMR Study. *J. Am. Chem. Soc.* **2007,** *129* (5), 1179-89.

9. Toal, S. E.; Verbaro, D. J.; Schweitzer-Stenner, R. Role of Enthalpy–Entropy Compensation Interactions in Determining the Conformational Propensities of Amino Acid Residues in Unfolded Peptides. *J. Phys. Chem. B.* **2014,** *118* (5), 1309-1318.

10. Toal, S. E.; Kubatova, N.; Richter, C.; Linhard, V.; Schwalbe, H.; Schweitzer-Stenner, R. Randomizing the Unfolded State of Peptides (and Proteins) by Nearest Neighbor Interactions between Unlike Residues. *Chem. Eur. J.* **2015,** *21*, 5173-5192.

11. Eker, F.; Griebenow, K.; Schweitzer-Stenner, R. Stable conformations of tripeptides in aqueous solution studied by UV circular dichroism spectroscopy. *J. Am. Chem. Soc.* **2003,** *125* (27), 8178-85.

12. Shi, Z.; Shen, K.; Liu, Z.; Kallenbach, N. R. Conformation in the Backbone in Unfolded Proteins. *Chem. Rev.* **2006,** *106*, 1877-1897.

13. Eker, F.; Cao, X.; Nafie, L.; Huang, Q.; Griebenow, K.; Schweitzer-Stenner, R. The Structure of Alanine Based Tripeptides in Water and Dimethyl Sulfoxide Probed by Vibrational Spectroscopy. *J. Phys. Chem. B.* **2003,** *107*, 358-365.

14. Gnanakaran, S.; Garcia, A. E. Validation of an All-Atom Protein Force Field: From Dipeptides to larger Peptides. *J. Phys. Chem. B.* **2003,** *107*, 12555-12557.

15. Garcia, A. E. Characterization of Non-Alpha Conformations in Ala Peptides. *Polym.* **2004,** *120*, 885-890.

16. Avbelj, F. Solvation and Electrostatics as Determined of Local Structural Order in Unfolded Peptides and Proteins. In *Protein and Peptide Folding, Misfolding and Non-Folding*, Schweitzer-Stenner, R., Ed. John Wiley & Sons,: Hobocken, 2012; pp 131-158.

17. Fleming, P. J.; Fitzkee, N. C.; Mezei, M.; Srinivasan, R.; Rose, G. D. A Novel Method Reveals that Solvent Water Favors Polyproline II Over β-Strand Conformation on Peptides and Unfolded Proteins: Conditional Hydrophobic Accessible Surfact Areas (CHASA). *Prot. Sci.* **2005,** *14*, 111-118.

18. Drozdov, A. N.; Grossfield, A.; Pappu, R. V. Role of Solvent in Determining Conformational Preferences of Alanine Dipeptide in Water. *J. Am. Chem. Soc.* **2004,** *126* (8), 2574-2581.

19. Liu, Z.; Chen, K.; Ng, A.; Shi, Z.; Woody, R. W.; Kallenbach, N. R. Solvent Dependence of PII Conformation in Model Alanine Peptides. *J. Am. Chem. Soc.* **2004,** *126* (46), 15141-15150.

20. Johnson, M. E.; Malardier-Jugroot, C.; Head-Gordon, T. Effects of Co-Solvents on Peptide Hydration Water Structure and Dynamics. *Phys. Chem. Chem. Phys.* **2010,** *12* (2), 393-405.

21. Maladier-Jugroot, C.; Bowron, D. T.; Soper, a. K.; Johnson, M. E.; Head-Gordon, T. Structure and Water Dynamics of Aqueous Peptide Solutions in the Present of Co-Solvents. *Phys. Chem. Chem. Phys.* **2010,** *12*, 382-392.

22. Vagenende, V.; Yap, M. G. S.; Trout, B. L. Mechanisms of Protein Stabilization and Prevention of Protein Aggregation by Glycerol. *Biochem.* **2009,** *48*, 11084-11096.

23. Gekko, K.; Timasheff, S. N. Mechanism of Protein Stabilization by Glycerol: Preferential Hydration in Glycerol-Water Mixtures. *Biochem.* **1981,** *20* (16), 4667-76.

24. Avdulov, N. A.; Chochina, S. V.; Daragan, V. A.; Schroeder, F.; Mayo, K. H.; Wood, W. G. Direct Binding of Ethanol to Bovine Serum Albumin: A Fluorescent and ^{13}C NMR Multiplet Relaxation Study. *Biochem.* **1996,** *35* (1), 340-7.

25. Banerjee, S.; Gosh, R.; Bagchi, B. Structural Transformations, Composition Anomlaies and a dramatic Collapse of Linear Polymer Chains in Dilute Ethanol-Water Mixtures. *J. Phys. Chem. B.* **2012,** *116*, 3713-3722.

26. Calamai, M.; Canale, C.; Relini, A.; Stefani, M.; Chiti, F.; Dobson, C. M. Reversal of Protein Aggregation Provides Evidence for Multiple Aggregated States. *J. Mol. Biol.* **2005,** *346* (2), 603-16.

27. Toal, S.; Amidi, O.; Schweitzer-Stenner, R. Conformational Changes of Trialanine Induced by Direct Interactions between Alanine Residues and Alcohols in Binary Mixtures of Water with Glycerol and Ethanol. *J. Am. Chem. Soc.* **2011,** *133* (32), 12728-12739.

28. Doghaei, A. V.; Housaindokht, M. R.; Bozorgmehr, M. R. Molecular Crowding Effects on Conformation and Stability of G-Quadruplex DNA Structure: Insights from Molecular Dynamics Simulations. *J. Theo. Biol.* **2015,** *2015*, 103-112.

29. Measey, T.; Schweitzer-Stenner, R. Simulation of Amide I' Band Profiles of Trans Polyproline Based on an Excitonic Coupling Model. *Chem. Phys. Lett.* **2005,** *408*, 123-127.

30. Karplus, M. Theoretical Calculation Links NMR Coupling Constant to Molecular Geometry. *J. Chem. Phys.* **1959,** *30*, 11.

31. Wang, A. C.; Bax, A. Determination of the Backbone Dihedral Angles phi in Human Ubiquitin from Reparametrized Empirical Karplus Equations. *J. Am. Chem. Soc.* **1996,** *118*, 2483.

32. Hu, F. H.; Luo, W. B.; Hong, M. Mechanism of Proton Conduction and Gating in Influenca M2 Proton Channels from Solid State NMR. *Sci.* **2010,** *330*, 505-508.

33. Lambermont-Thijs, H. M. L.; van Kuringen, H. P. C.; van der Put, J. P. W.; Schubert, U. S.; Hoogenboom, R. Temperature Induced Solubility Transitions of Various Poly(2-oxazoline)s in Ethanol-Water Solvent Mixtures. *Polym.* **2010,** *2*, 188-199.

34. Bonang, C. C.; Anderson, D. J.; Cameron, S. M.; Kelly, P. B.; Getty, J. D. Ultraviolet Raman Scattering of Simple Alcohols and a Related Diol as a Study of Low lying Rydberg-valence Characteristics. *J. Chem. Phys.* **1993,** *99*, 6245-6252.

35. Jentzen, W.; Unger, E.; Karvounis, G.; Shelnutt, J. A.; Dreybrodt, W.; Schweitzer-Stenner, R. Conformational Properties of Nickel(II) Octaethylporphyrin in Solution. 1. Resonance Excitation Profiles and Temperature Dependence of Structure-Sensitive Raman Lines. *J. Phys. Chem.* **1995,** *100*, 14184-14191.

36. Egashira, K.; Nishi, N. Low-Frequency Raman Spectroscopy of Ethanol−Water Binary Solution: Evidence for Self-Association of Solute and Solvent Molecules. *J. Phys. Chem. B.* **1998,** *102* (21), 4054-4057.

37. Torii, H.; Tatsumi, T.; Kanazawa, T.; Tasumi, M. Effects of Intramolecular Hydrogen-Bonding Interactions on the Amide I Mode of N-Methylacetamide: Matrix Isolation Infrared Studies and ab Initio Molecular Orbital calculations. *J. Phys. Chem. B* **1998,** *102*, 309-314.

38. Wang, Y.; Purello, R.; Georgiou, S.; Spiro, T. G. UVRR Spectroscopy of the Peptide Bond. 2. Carbonyl H-Bond Effects on the Ground- and Excited-State Structures of N-Methylacetamide. *J. Am. Chem. Soc.* **1991,** *113*.

39. Mukherjee, S.; Chowdhury, P.; Gai, F. Infrared Study of the Effect of Hydration on the Amide I Band and Aggregation Properties of Helical Peptides. *J. Phys. Chem. B.* **2007,** *111* (17), 4596-4602.

40. Eker, F.; Cao, X.; Nafie, L.; Schweitzer-Stenner, R. Tripeptides Adopt Stable Structures in Water. A Combined Polarized Visible Raman, FTIR, and VCD Spectroscopy Study. *J. Am. Chem. Soc.* **2002,** *124* (48), 14330-14341.

41. Gerig, J. T. Investigation of Ethanol–Peptide and Water–Peptide Interactions through Intermolecular Nuclear Overhauser Effects and Molecular Dynamics Simulations. *J. Phys. Chem. B.* **2013,** *117* (17), 4880-4892.

42. Ma, S.; Cao, X.; Mak, M.; Sadik, A.; Walkner, C.; Freedman, T. B.; Lednev, I. K.; Dukor, R. K.; Nafie, L. A. Vibrational Circular Dichroism Shows Unusual Sensitivity to Protein Fibril Formation and Development in Solution. *J. Am. Chem. Soc.* **2007,** *129* (41), 12364-12365.

43. Measey, T. J.; Schweitzer-Stenner, R. Vibrational Circular Dichroism as a Probe of Fibrillogenesis: The Origin of the Anomalous Intensity Enhancement of Amyloid-like Fibrils. *J. Am. Chem. Soc.* **2011,** *133*, 1066-1076.

44. Yan, C.; Pochan, D. J. Rheological Propensities of Peptide-Based Hydrogels for Biomedical and Other Applications. *Chem. Soc. Rev.* **2010,** *39*, 3528-3540.

45. Hamley, I. W. Peptide Fibrillization. *Angew. Chem. Int. Ed. Engl.* **2007,** *46* (43), 8128-47.

46. Ruan, L.; Zhang, H.; LLuo, H.; Jingping, L.; Tang, F.; shi, Y.-K.; Zhao, X. Designed Amphiphilic Peptide Forms Stable Nanoweb Slowly Releases Encapsulated Hydrophobic Drug, and Accelerates Animal Hemostasis. *Proc. Natl. Acad. Sci.* **2009,** *106*, 5105-5110.

47. Yokoi, H.; Kinoshita, T. Strategy for Designing Self-Assembling Peptides to Prepare Transparent nanofiber hydrogel at neutral pH. *J. Nanomat.* **2012,** *2012*, 537262.

48. Wang, R.; Liu, X.-Y.; Xiong, J.; Li, J. Real-Time Observation of Fiber Network Formation in Molecular Organel: Supersaturation-Dependent Microstructure and its Related Rheological Property. *J. Phys. Chem. B.* **2006,** *110*, 7275.

49. Reches, M.; Gazit, E. Casting Metal Nanowires within Discrete Self-Assembled Peptide Nanotubes. *Sci.* **2003,** *300*, 625.

50. Ma, M.; Yuang, Y.; Gao, Y. Q.; Zhang, Y.; Gao, P.; Xu, B. Aromatic-Aromatic Interactions Induce the Self-Assembly of Pentapeptide Derivatives in Water To Form Nanofibers and Supramolecular Hydrogels. *J. Am. Chem. Soc.* **2010,** *132*, 2719-2728.

51. Hore, M. J. A.; Hammouda, B.; Li, Y.; Cheng, H. Co-Nonsolvency of Poly(n-isopropylacrylamide) in Deuterated Water/Ethanol Mixtures. *Macromol.* **2013,** *46*, 7894-7901.

52. Jenkins, J. E.; Craeger, M. S.; Lewis, R. V.; Holland, G. P.; Yarger, J. L. Quantitative Correlation Between the Protein Primary Sequences and Secondary Structure in Spider Dragline Silks. *Biomacromol.* **2010,** *11*, 192-200.

53. Measey, T. J.; Schweitzer-Stenner, R. Self-Assembling Alanine-Rich Peptides of Biomedical and Biotechnological Relevance. In *Protein and Peptide Folding, Misfolding and Non-Folding*, Schweitzer-Stenner, R., Ed. Wiley & Sons: Hoboken, 2012; pp 309-350.

54. Schweitzer-Stenner, R.; Hagarman, A.; Toal, S.; Mathieu, D.; Schwalbe, H. Disorder and Order in Unfolded and Disordered Peptides and Proteins: A View Derived from Tripeptide Conformational Analysis. I. Tripeptides with Long and Predominantly Hydrophobic Side Chains. *Proteins* **2013,** *81* (6), 955-67.

55. Sreerama, N.; Woody, R. W. Structural Composition of βI and β2 Proteins. *Protein Sci.* **2003,** *12*, 384-388.

56. Tooke, L.; Duitch, L.; Measey, T. J.; Schweitzer-Stenner, R. Kinetics of Self-Aggregation and Film Formation of Poly-L-Proline at High Temperatures By Circular Dichroism. *Biopolym.* **2010,** *93*, 451-457.

3.8 Appendix

Conformational Analysis of GAG. In an earlier study we reported conformational distributions of GxG peptides in water based on the global analysis of amide I′ band profiles in corresponding IR, polarized Raman and VCD spectra and of a set of different J-coupling constants. In this analysis each conformation was represented by a two-

dimensional Gaussian distribution in the Ramachandran space.[6] For cationic GAG, this analysis yielded a pPII fraction of 0.72 and a β-strand fraction of 0.18. The remaining ten percent of the distribution is shared by various turn structures including a right-handed helical conformation. For the present study we confined our analysis on the available IR and VCD profiles and the corresponding $^3J(H^NH^\alpha)$ coupling constants of GAG in the 50 mol% ethanol/water mixture. The differences between the respective IR and VCD band profiles of GAG in D_2O and this ethanol/water mixture are modest, our analysis revealed that it mainly reflects (slightly different) red shifts of the two amide I′ bands. On the contrary, the two $^3J(H^NH^\alpha)$ constants are rather different. We considered two options. First we kept the (ϕ,ψ) positions and the halfwidths of the pPII and β-distributions in the Ramachandran space constant and solely changed their statistical weight. This led to the pPII scale in Figure 3.4, the results suggest a substantial reduction of the pPII fraction for the considered ternary mixture. These changes have a negligible effect on the amide I′ IR and VCD profiles, as one can read from the satisfactory reproduction of the amide I′ profiles of the ternary mixture displayed in Figure A3.4 (Appendix). This reflects the aforementioned insensitivity of the two profiles for any changes of distributions along the ϕ-coordinate between ca. -120 ^{o} and -65 ^{o}.[54] The earlier analysis of GAG had yielded ϕ-values of -115 ^{o} and -69 ^{o} for β-strand and pPII, respectively. Second, we kept the statistical weight constant and varied the ϕ-coordinate of pPII. This reproduced the experimentally obtained $^3J(H^NH^\alpha)$ constant with ϕ = -79 ^{o}. Changes along ψ lead to changes of both the VCD and the IR profile; they were therefore not considered. Changes of the ϕ-coordinate of the β-strand distribution can be excluded, since it sits very close to the maximum of the respective Karplus curve[8] so that any change would cause a

reduction rather than an increase of $^{3}J(H^{N}H^{\alpha})$. Even though a final assessment of the ethanol-induced structural changes requires some more experiments, we decided to opt for changes of the statistical weight of the distributions as the prime effect for the following reason. A shift of the pPII conformation towards lower ϕ-values would increase the overlap with the β-strand conformation. If true, this would reflect a lowering of the barrier between both conformations. In this case fluctuations at higher temperatures would not 'see' any barrier between pPII and β. Such an effect can be expected to substantially reduce the temperature dependence of the J-coupling constant, contrary to our observations.

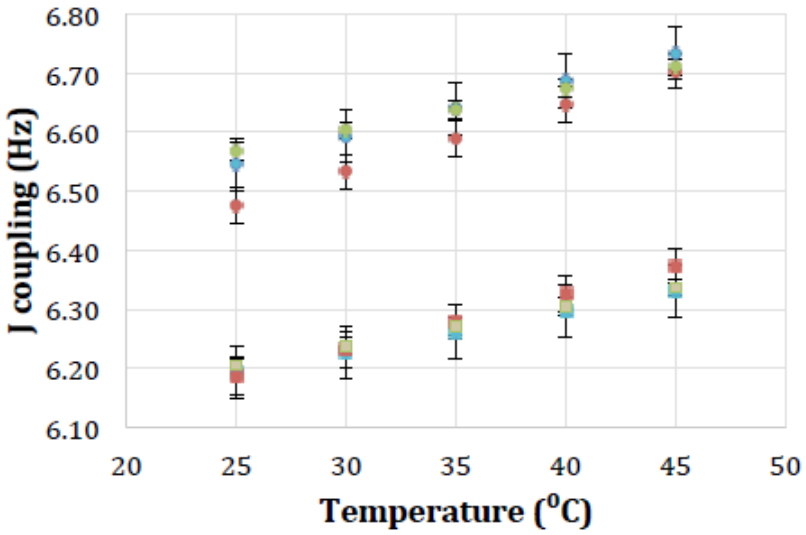

Figure A3.1. Temperature dependent $^{3}J(H^{N}H^{\alpha})$ of the N-terminal amide proton of cationic GAG in ethanol/water mixtures of 0.14 (squares) and 0.48 (circles) mol% ethanol taken at different concentrations of GAG (blue symbols: 50 mM GAG, red symbols: 75 mM GAG, and green symbols: 100 mM GAG). Error bars are shown to indicate that there are no statistical significant differences between $^{3}J(H^{N}H^{\alpha})$ obtained from samples with different concentrations of GAG.

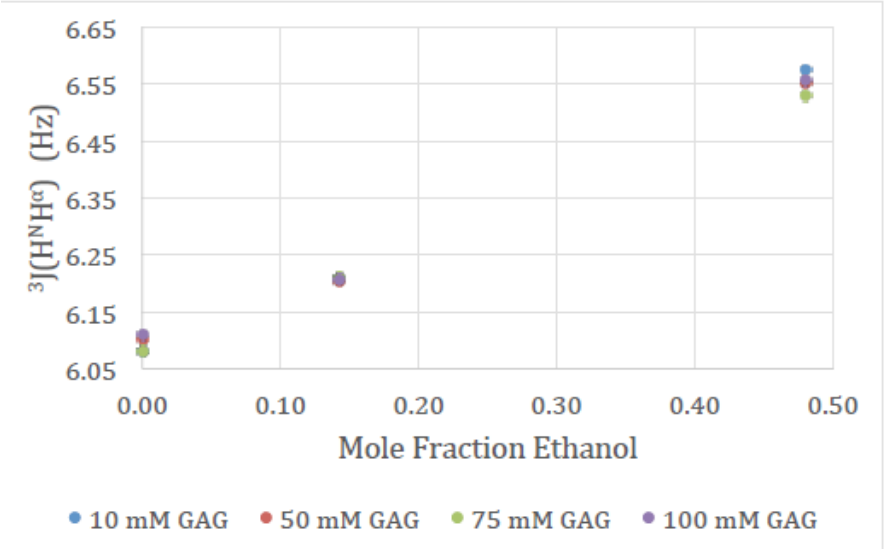

Figure A3.2. $^3J(H^NH^\alpha)$ of the N-terminal amide proton of cationic GAG in water and ethanol/water mixtures with 0.14 and 0.48 mole % ethanol obtained at different concentrations of GAG, as shown in figure legend, at 25 ^oC.

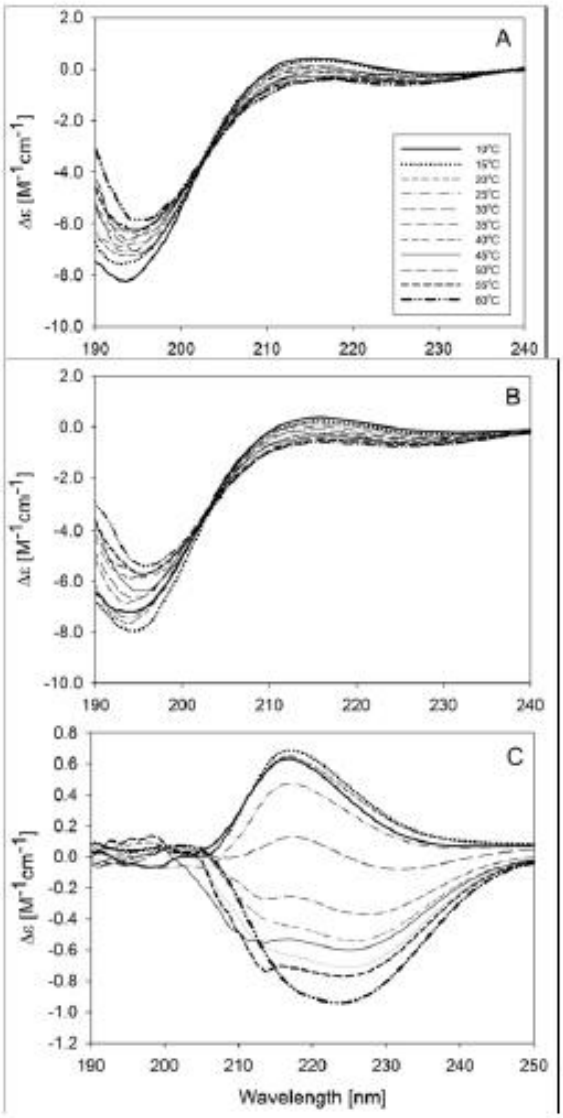

Figure A3.3. UVCD spectra of cationic GAG at concentrations of 5 mM (A) in 55 mol% ethanol, 10 mM (B) in 48 mol% ethanol, and 220 mM (C) in 55 mol% ethanol. Temperatures are indicated by the legend. For the 220 mM solution, the absorbance exceeded the instrumental detection limit at wavelengths below 210 nm. The spectra taken at 5 and 10 mM show the typical signal of a peptide with high pPII content.[55] At high concentration, however, the weak positive maximum at 215 nm is replaced by a negative maximum at 225 nm that qualitatively resembles spectra obtained for poly-L-proline films at high temperatures.[56]

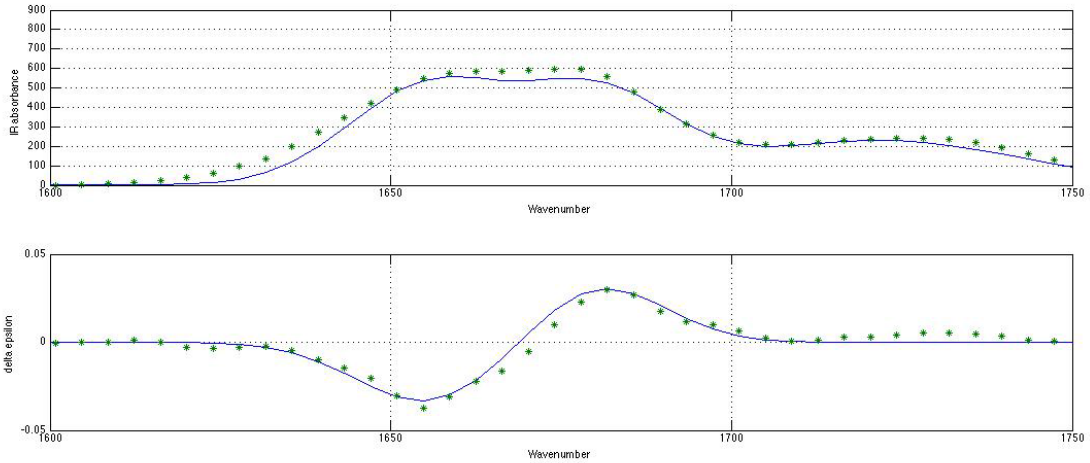

Figure A3.4. Simulation of the amide I′ profiles of cationic GAG in 50 mol% ethanol/water by using the excitonic coupling model described in earlier publications. The solid lines are the result of the simulation. The figure has been directly produced by our Matlab software.

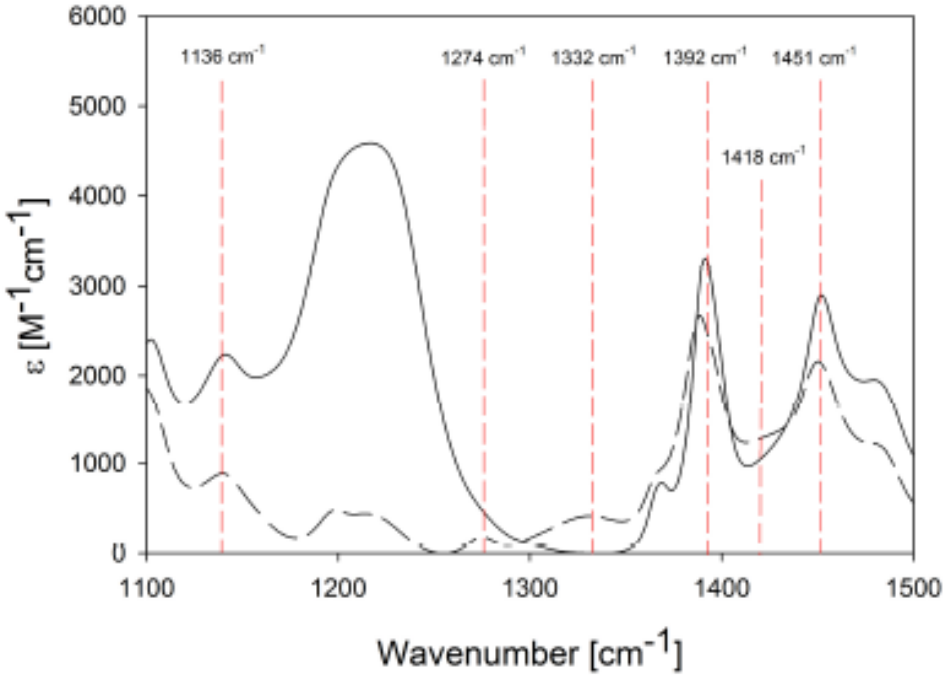

Figure A3.5. IR spectra bands of ethanol bending and stretching modes from 1100 to 1500 cm^{-1} after background subtraction of D_2O using our program Multifit: 17 mol% ethanol (solid line) and 55 mol% ethanol (dashed line).

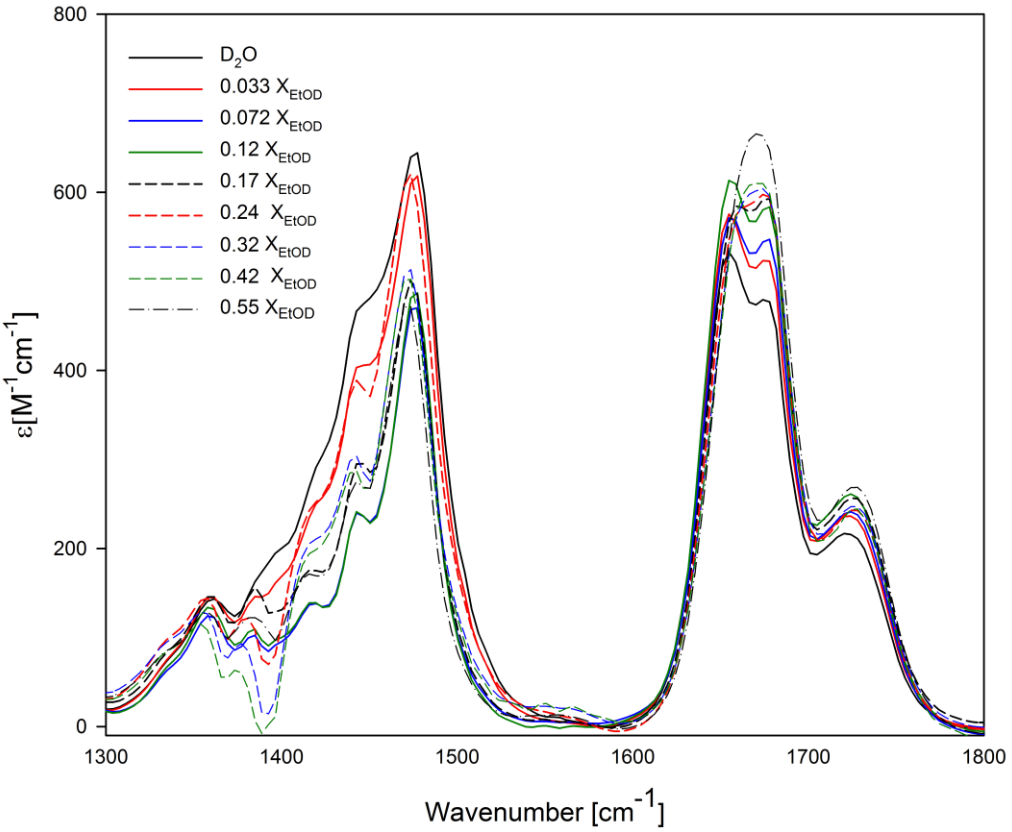

Figure A3.6. IR spectra of the 1300-1800 cm^{-1} region of 200 mM cationic GAG dissolved in the indicated ethanol/water mixture. The numbers reflect the molar fractions of ethanol in the mixture. The bands between 1300 and 1500 cm^{-1} result mostly from CH_2 and CH_3 deformation modes. The most intense band in this region is assignable to a mixture of amide II′ and CH_3 out-plane antisymmetric bending modes. The 1600-1700 cm^{-1} region contains the amide I′ band profile. The band at ca. 1700 cm^{-1} is assignable to the C-terminal C=O stretching mode.

CHAPTER 4. THE INTERPLAY OF AGGREGATION, POLYMERIZATION AND GELATION OF AN UNEXPECTED LOW M OLECULAR WEIGHT GELATOR: GLYCYLALANYLGLYCINE IN ETHANOL/WATER

Reproduced from :
Farrell, S., DiGuiseppi, S., Alvarez, N., & Schweitzer-Stenner, R. The Interplay of Aggregation, Polymerization, Polymerization and Gelation of An Unexpected Low Molecular Weight Gelator: Glycylalanylglycine in Ethanol/Water. Submitted to *Soft Matter*, **2016**.

4.1 Abstract

Hydrogels formed by polypeptides could be much-favored tools for drug delivery because their main ingredients are generally biodegradable. However, the gelation of peptides in aqueous solution generally requires a critical minimum length of the peptide as well as distinct sequences of hydrophilic and hydrophobic residues. The aggregation of short peptides such as tripeptides, which are relatively cheap and offer a high degree of biodegradability, are generally thought to require a high hydrophobicity of their residues. We found that contrary to this expectation cationic glycylalanylglycine in 55 mol% ethanol/45 mol% water forms a hydrogel below a melting temperature of ca. 36^{o} C. The gel phase consists of crystalline fibrils of several 100 μm, which form a sample-spanning network. Rheological data reveal a soft elastic solid gel. We investigated the kinetics of the various processes that lead to the final gel state of the ternary mixture by a unique combination of UV circular dichroism, infrared, vibrational circular dichroism and rheological measurements. A mathematical analysis of our data show that gelation is preceded by the formation of peptide β-sheet like tapes or ribbons, which give rise to a significant enhancement of the amide I′ VCD signal, and the subsequent formation of rather thick and long fibrils. The VCD signals indicate that the tapes exhibit a right-handed helicity at temperatures above 16^{0} C and a left-handed helicity below. The

tapes'/ribbons' helicity change occurs at a temperature where the UVCD data reflect a process with a relatively long nucleation process. The kinetics of gel formation probed by the storage and loss moduli are composed of a fast process that follows tape/ribbon/fibril formation and is clearly identifiable in a movie that shows the gelation process and a slow process that causes an additional gel stabilization. The rheological data indicate that left-handed fibrils observed at low temperatures form a more solid-like structure than their right-handed counterparts formed at higher temperatures. Taken together our data reveal GAG as an unexpected gelator, the formation of which is accomplished by a set of distinguishable kinetic processes.

4.2 Introduction

Peptides belong to a special class of polymers, which can self-aggregate into large-scale structures like fibrils, colloids and nanotubes[1,2,3.] This propensity of peptides has both a problematic and beneficial aspect. On one side, the oligomerization and perhaps also the fibrillization of β-amyloid peptides, glutamine as well as alanine-rich peptide/protein sequences are the probable cause of many neurodegenerative diseases.[4,5] On the other side, certain peptides can form hydrogels that serve a variety of biotechnological purposes.[1] In this context, very short and unblocked peptides have become attractive because of their low production costs, biodegradability, and scalability.[6,7,8,9]

Considering our current understanding of peptide self-aggregation and gelation mechanisms, the use of such low molecular weight biomolecules as gelators seems to have its limits. More specifically, the ability for peptides to form large scale fibrils is argued to depend on the percentage of hydrophobic content along the backbone.[10,11,9]

These empirically observed rules are highly restrictive and significantly reduce the range of useful gelating peptides.[12] It is therefore noteworthy that recent findings by DiGuiseppi et al.[13] and Milorey et al.[14] are in complete disagreement with the above empirically observed mechanisms. The former reported that unblocked zwitterionic GHG forms large-scale hydrogels in water at centimolar concentrations. While H is an aromatic residue in its deprotonated state, it does not have such a large propensity for aggregation as e.g. the aromatic residues F, Y and W.[6,10,9,15] The observation of Milorey et al. is even more surprising. They found that cationic GAG in 55 mol% ethanol/45 mol% water forms a rather viscous hydrogel if the peptide concentration exceeds 200 mM. This peptide concentration is rather high, but alanine ranks very low on any hydrophobicity scale.[16,17] Generally, one needs rather long polyalanine chains or the addition of aliphatic groups to support fibrillization.[18,19,20] Even more peculiar than the observed gel formation was the discovery that the underlying network is comprised of unusually long crystalline fibrils of remarkable thickness which extend to lengths on the 10 μm scale. They are clearly visible on images taken with a light microscope.

The present study combined various spectroscopic tools with rheological measurements to identify the underlying mechanism of the GAG gelation process and the respective time scales. Rheology is used to study the stability of the gel at different temperatures. Our data reveal very complex kinetics of the aggregation and gelation processes and a rather unusual dependence on temperature. With regard to the latter it is particularly remarkable that a decrease of the temperature away from the gelation point leads to major structural reorganizations which involve a change of the helicity of the

fibrils below 20^0 C. To our best knowledge, such a phenomenon has not yet been observed.

4.3 Experimental

Materials. A solvent mixture of 55 mol% ethanol (200 proof, Pharmco-Aaper)/45 mol% deionized water was first prepared. For the vibrational studies of FTIR, and VCD, deuterated ethanol (99% purity, Sigma Aldrich) and deuterated water (99.9% purity, Sigma Aldrich) were used to avoid interference of the water bending mode with the amide I region (1600-1700cm^{-1}) as described in the text. Solutions of cationic glycylalanylglycine (GAG) (>98% purity, Bachem) were then dissolved in the solvent mixture. The pH of each solution was adjusted to about 1.5-2.0 by adding HCl (ACS grade, Ricca Chemical Company).

Methods

Ultra-Violet Electronic Circular Dichroism (UVCD). Spectra were measured on a Jasco J-180 spectropolarimeter (model J-810-150S) purged with nitrogen. The temperatures were controlled using a Peltier controller (model PTC-423S). The sample was loaded into a 100-μm cell from International Crystal Laboratories. UVCD spectra were recorded between 190 and 250 nm and background corrected. They were measured using a scan speed of 500 nm/min, a data pitch of 0.05 nm, a bandwidth of 5 nm, and a response time of 1.0 s. Five accumulations were obtained and averaged for each time interval, and all spectra were corrected using appropriate background subtraction. For measurements incubated directly at temperature, the controller was set and the sample allowed to equilibrate for two minutes prior to first measurement at five minutes after preparation. For quenching measurements, the sample was loaded and the controller was

held at 50^{o} C for one minute then moved to the desired temperature, and the first reading was taken at ten minutes after preparation. Scans of spectra were taken at five or ten minute intervals for a total run time of 180 minutes. Raw data retrieved in ellipticity were converted to molar dichroism using the Beer-Lambert Law relation with the known path length and concentration of the sample.

Fourier Transform Infrared Spectroscopy (FTIR). As described above, vibrational spectroscopy studies required the use of deuterated solvents. Spectra were measured on a BioTools ChiralIR and were loaded in a 59.5-μm CaF_2 Biocell from BioTools. Spectra with a resolution of 8 cm^{-1} and scan speed of 83 scans per minute were collected in Grams/IR 7.00 (Thermo Galactic) from 1300-1800 cm^{-1}. A total of 75 scans were collected every five minutes for one hour to observe kinetics at small time intervals. Data at three temperatures (10^{o} C, 16^{o} C, and 23^{o} C) were collected and maintained at respective temperatures by a BioTools water-cooled temperature controller for the respective runs. The IR spectra were not background corrected to observe changes of solvent bands, and were decomposed into spectral bands using our Multifit program.[21]

Vibrational Circular Dichroism (VCD). Samples for VCD experiments were prepared separately and run with the same instrument, software, and loading cell as FTIR. Two minute scans were collected every five minutes for one hour with a resolution of 8 cm^{-1} and scan speed of 83 scans/minute from 1300-1800 cm^{-1}. Spectra were recorded at 10^{o}, 16^{o}, and 23^{o} C, maintained by a BioTools water-cooled temperature controller.

Rheology. Measurements were made on a DHR-3 (TA instruments) using an 8mm top plate and a 25-mm bottom plate. Temperature control was achieved using the electrically heated plates (EHP) accessory. A solvent trap was created using safflower oil

to surround the sample and prevent solvent evaporation. Samples were prepared 24 hours in advance and loaded onto a 25-mm plate. An amplitude sweep was run to determine the linear regime of the sample from 0.01 to 1.0% strain, a strain of 0.3% was chosen for the small amplitude oscillatory shear measurements. A gap less than 1 mm was chosen for the frequency sweep. The frequency sweep was carried out from 0.001 to 100 rad/second, allowed to hold for one minute, then reversed from 100 to 0.001 radians/second. The entire sweep was repeated seven times, and the data were averaged together. The kinetics of gelation was probed using the same instrument via a time sweep at a chosen amplitude and frequency. The peptide samples were loaded onto an 8-mm parallel plate without the use of a solvent trap immediately following preparation. For all measurements we used an optimized strain of 0.3%, an angular frequency of 5 radians/second, a data pitch of 5 seconds/point, and a gap of less than 1 mm. The storage and loss moduli were recorded as a function of time over a period of 4800 seconds at 10^{o}, 16^{o}, and 23^{o} C with a nitrogen cooling system for temperatures below room temperature.

4.4 Results and Discussion

In spite of GAG's lack of all the "necessary" characteristics, GAG forms a hydrogel in 55 mol% ethanol/45 mol% water if the peptide concentration exceeds 200 mM at room temperature. Milorey et al. documented this directly by an image from a bright field microscope and indirectly with the enhancement of the amide I′ VCD, which is generally indicative of fibril formation. The formation of rather long crystalline fibrils and rods is documented in a short movie that can be downloaded from the RSC website. It covers a time of 60 minutes after incubation at room temperature. In the initial phase, the images reveal a rather homogeneous spherulitic domain, which are present only three

minutes after preparation (*vide infra*). Over time it converts into a fibrillar sample-spanning network. From microscopy imaging, this fibrillation process appears to be completed in about 15 minutes. Two thick, black lines become visible around 14 and 17 minutes, and they eventually combine. They are believed to be either the solvent layers separating or the ethanol beginning to evaporate due to the time spent in a non-closed system.

The goal of the investigations described in this section is to shed light on the dynamics of the processes that lead to the unexpected gelation of GAG in 55 mol% ethanol/45 mol% water. To this end we used spectroscopic techniques to probe the structural reorganization of the peptide and rheology to explore the kinetics of the gelation process itself. This section is organized as follows. First, we describe how UVCD spectroscopy was employed to probe the gel state of a ternary GAG/ethanol/water mixture. Peptide UVCD spectra measured in the far UV region generally reflect the secondary structure,[22] i.e. the conformation of the peptide backbone. However, in the case of aggregation, inter-strand and possibly even inter-sheet transition dipole coupling affects the CD signal. It therefore directly probes the formation and subsequent changes of some kind of tertiary structure (we consider fibrils as tertiary structure). By means of the UVCD spectrum as a function of temperature, the gelation temperature will be obtained. In a second step, we probed the underlying kinetics of the gelation process by measuring the dichroism at a distinct wavelength as a function of time at various temperatures below the gel point. The third step involved the recording of the UV absorption at 221 nm as a function of time. Changes of the absorptivity in this region reflect changes of the sample's turbidity, which is an indicator of large-scale

aggregation.[23] In a fourth step, we investigated how quenching affects the gelation kinetics. Here, we heated the peptide-solvent sample up to a temperature above the gel point from which we quenched the sample to different temperatures in the gel phase. We expected these experiments to inform us about the character of the gelation process. In a fifth step, we measured both the IR and the VCD spectrum of GAG as a function of time after incubation at different temperatures below the gel point. In particular the amide I′ band(s) in these spectra can be used for an assessment of the secondary structure as well as long-range fibrillization, if the latter involves helical twists.[24,25,26,27] Sixth, we characterized the sample rheologically at different temperatures by means of a frequency sweep to determine the storage and loss moduli as well as by kinetic experiments, where we monitored the changes of these moduli after incubation at different temperatures as a function of time. We compare the different kinetic traces obtained with the above described techniques and apply different models for quantitative assessment.

UVCD spectra. Figure 4.1 shows the far UV ECD spectrum of 220 mM GAG in 55 mol% ethanol/45 mol% water measured at different temperatures between 200 and 250 nm in a temperature range from 10^{o} and 60^{o} C. The concentration is too high to allow for a spectral recording below 200 nm. At low temperatures, the spectrum shows a positive maximum at ca 216 nm, which is much more pronounced than it is in the spectrum of cationic GAG in water.[14]

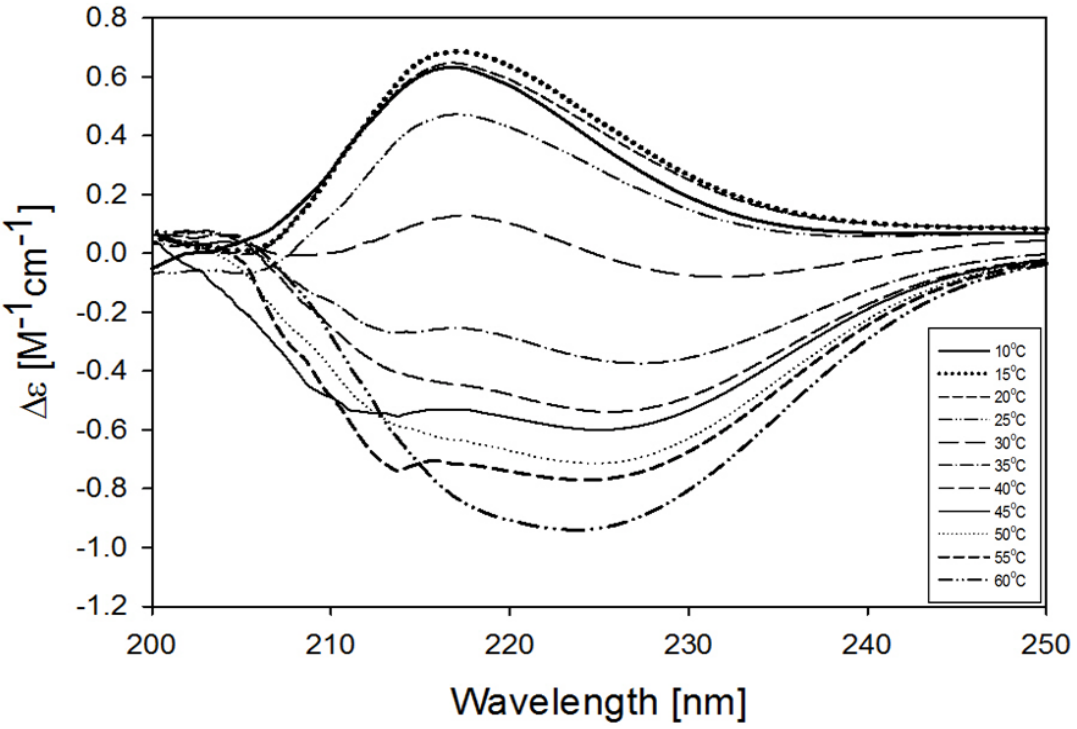

Figure 4.1. UV circular dichroism spectra of 220 mM GAG in 55 mol% ethanol/45 mol% H_2O measured at the indicated temperatures. Data below 200nm could not be recorded due to the high concentration of peptide. The dichroism values are expressed as differences between molar absorptivities of right- and left-handed circular polarized light.

With increasing temperature the positive maximum converts to a negative maximum at ca 225 nm, which is more reminiscent of what one observes for GAG in pure water even though it appears somewhat redshifted. In Figure 4.2, the Δε-value at 221 nm (denoted as $\Delta\varepsilon_{221}$) is plotted as a function of temperature. The corresponding value obtained from the spectra of a 100 mM sample is shown for comparison.

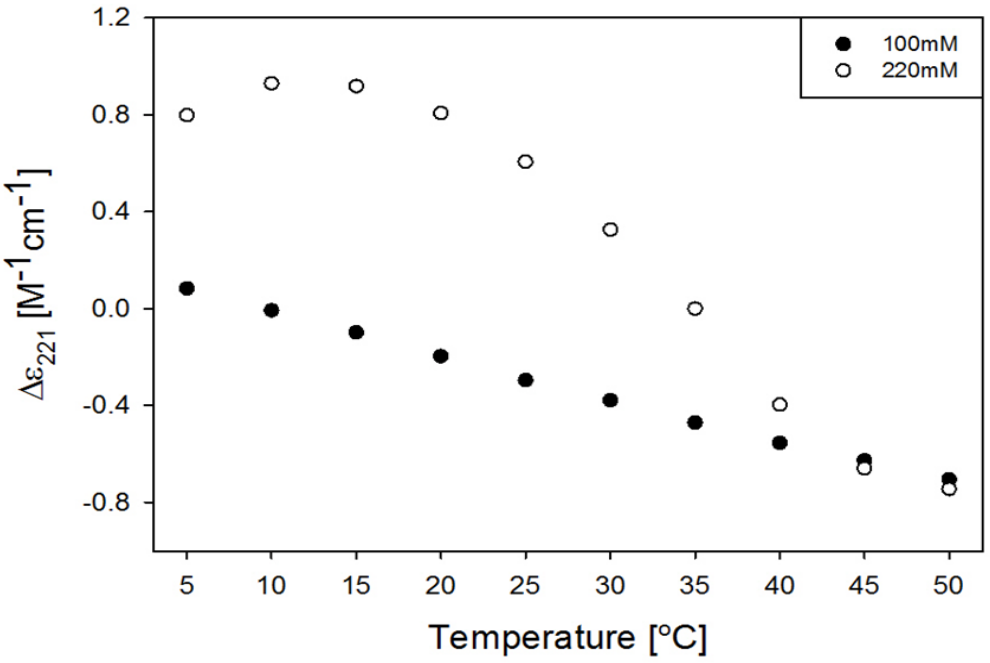

Figure 4.2. Circular dichroism of 100 and 220 mM GAG in 55 mol% ethanol/45 mol% H_2O measured at 221nm plotted as a function of temperature.

This concentration lies below the gel point along the concentration axis. As a consequence, $\Delta\varepsilon_{221}$ decreases nearly linearly with temperature as observed for a large number of different tripeptides in aqueous solution.[28] For the 220 mM GAG sample, however, $\Delta\varepsilon_{221}(T)$ is highly non-linear. The values lie substantially above the $\Delta\varepsilon_{221}$ values of the 100-mM sample below 40^0 C but approach the latter at higher temperatures. At this point, we interpret the differences between the $\Delta\varepsilon_{221}$-values of the 220 mM and 100mM sample as indicating different degrees of gelation/peptide aggregation in the former sample. From these data, we estimated a melting/gelation temperature of ca. 36^0C.

UVCD: Time dependence of secondary/tertiary structure. Figure 4.3 shows $\Delta\varepsilon_{221}$ of the 220 mM GAG sample as a function of time for different temperatures. For these

experiments the protein was incubated at the indicated temperatures. These kinetic traces probe some yet unspecified changes of the secondary and tertiary structure due to peptide aggregation. The solid lines result from fits which are described in more detail below. Two observations are noteworthy. First, the amplitude of the kinetic trace increases with decreasing temperature. This implies a concomitant increasing departure from the behavior in the sol phase (*vide supra*, Figure 4.1). Second, the rate of the relaxation process probed by $\Delta\varepsilon_{221}$ indicates a non-continuous dependence on temperature in that the kinetic trace displays a sigmoidal character in a very narrow temperature region between 15^{o} and 17^{o} C. The thus indicated occurrence of a nucleation time will guide the theoretical modeling below.

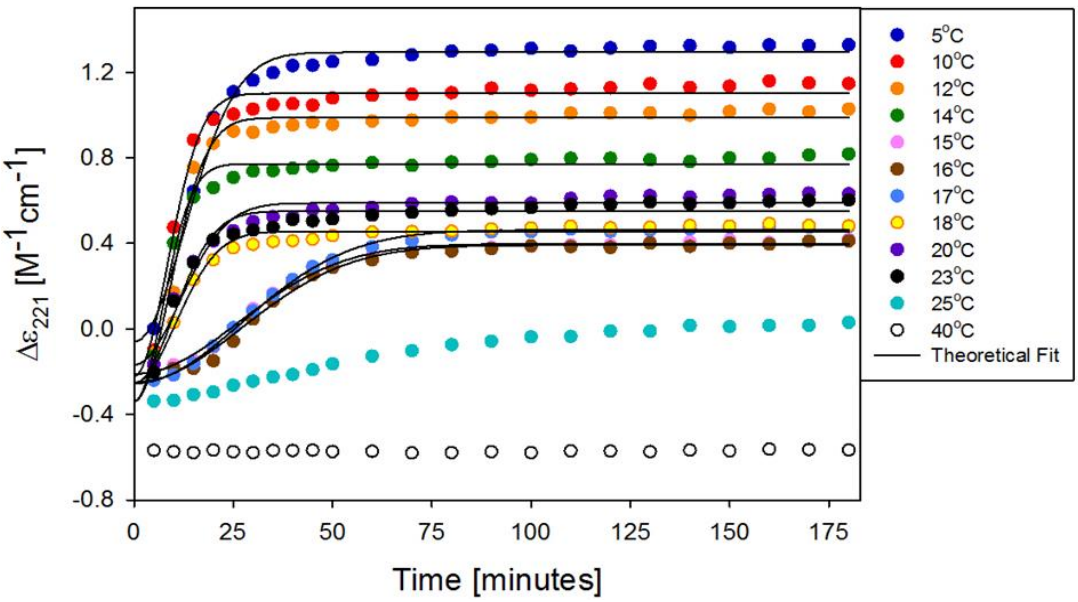

Figure 4.3. Circular dichroism of 220 mM GAG in 55 mol% ethanol/45 mol% H_2O monitored at 221 nm and the indicated temperatures as a function of time. For each of these kinetic measurements the sample was incubated directed at indicated temperature. The solid lines are the fits resulting from the model described in the text, eq. (6).

Figure 4.4 shows the results of our quenching experiments. The solid lines resulted from a fitting procedure to be described below. Here, we incubated the peptide at room temperature and heated the sample up to a temperature of 50^{o} C, well above the gelation temperature (*vide supra*). We allowed the sample to sit at this temperature for one minute and subsequently decreased the sample temperature to the indicated values.

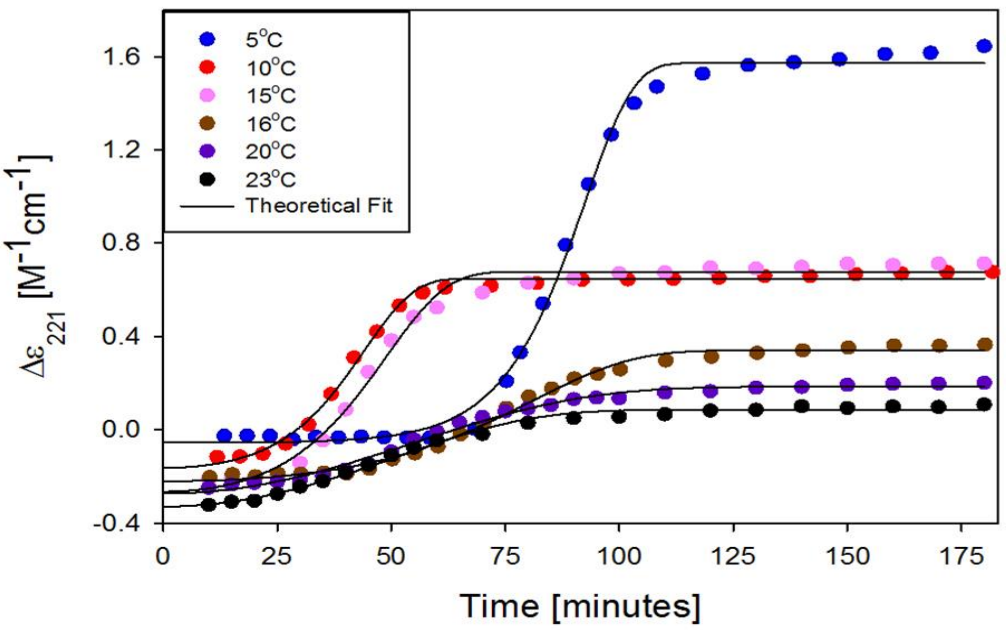

Figure 4.4. Circular dichroism of 220 mM GAG in 55 mol% ethanol/45 mol% H_2O monitored at 221 nm and the indicated temperatures as a function of time. For each of these kinetic measurements the sample was first held at 50^{o} C for one minute and subsequently cooled to the indicated temperatures. The solid lines are the fits resulting from the model described in the text, eq. (6).

The recorded kinetic traces can be categorized as follows. The kinetic data recorded at 16^{o}, 20^{o} and 23^{0} C exhibit a sigmoidal behavior with a low slope. The data taken at 10^{o} and 15^{o} C show a steeper sigmoidal curve in conjunction with a lag phase of 20 minutes. At 5^{0} C, the lag phase increases to approximately 60 minutes. Only the traces recorded at

5^0 C and 16^0 C reach approximately the level of the corresponding traces in Figure 4.3. These data clearly reveal that heating the sample to temperatures well above the gel point eliminates most of the aggregates and therefore creates a situation that is different from that produced by direct incubation of the peptide when pre-aggregation already took place during the loading time of our experiments. Altogether, the observations suggest that the aggregation process that eventually leads to the sample's gelation goes through a nucleation phase.

Turbidity. Absorbance spectra were simultaneously measured as a function of time for experimental conditions reminiscent of those used for the data in Figures 4.3 and 4.4. Changes of the absorptivity at 221 nm, which lies well above the peak wavelength of the $\pi \rightarrow \pi^*$ transitions of the peptide backbone are predominantly an indicator of changing turbidity. These experiments served two purposes. First, we were aimed at probing the occurrence of large-scale aggregations which are a prerequisite for gelation. Second, we can use the data to estimate the influence of turbidity changes on the obtained dichroism values by utilizing textbook relations between absorptivity and ellipticity.[29] Figure 4.5a shows the traces for the samples for which data were recorded after direct incubation at the indicated temperatures. We can again discern three types of data sets. At T=15^o, 16^o, 17^0, and 25^o C the changes are rather modest. Some intermediate level changes were found to occur at 5^o, 18^o, 20^o and 23^o, while rather significant changes were observed at 10^o, 12^o and 14^o C. This highly discontinuous behavior (with respect to T) is rather surprising and defies an easy explanation. Interestingly, however, none of the traces

exhibits a lag phase. This observation suggests that aggregation itself might precede the process monitored by the above CD-data.

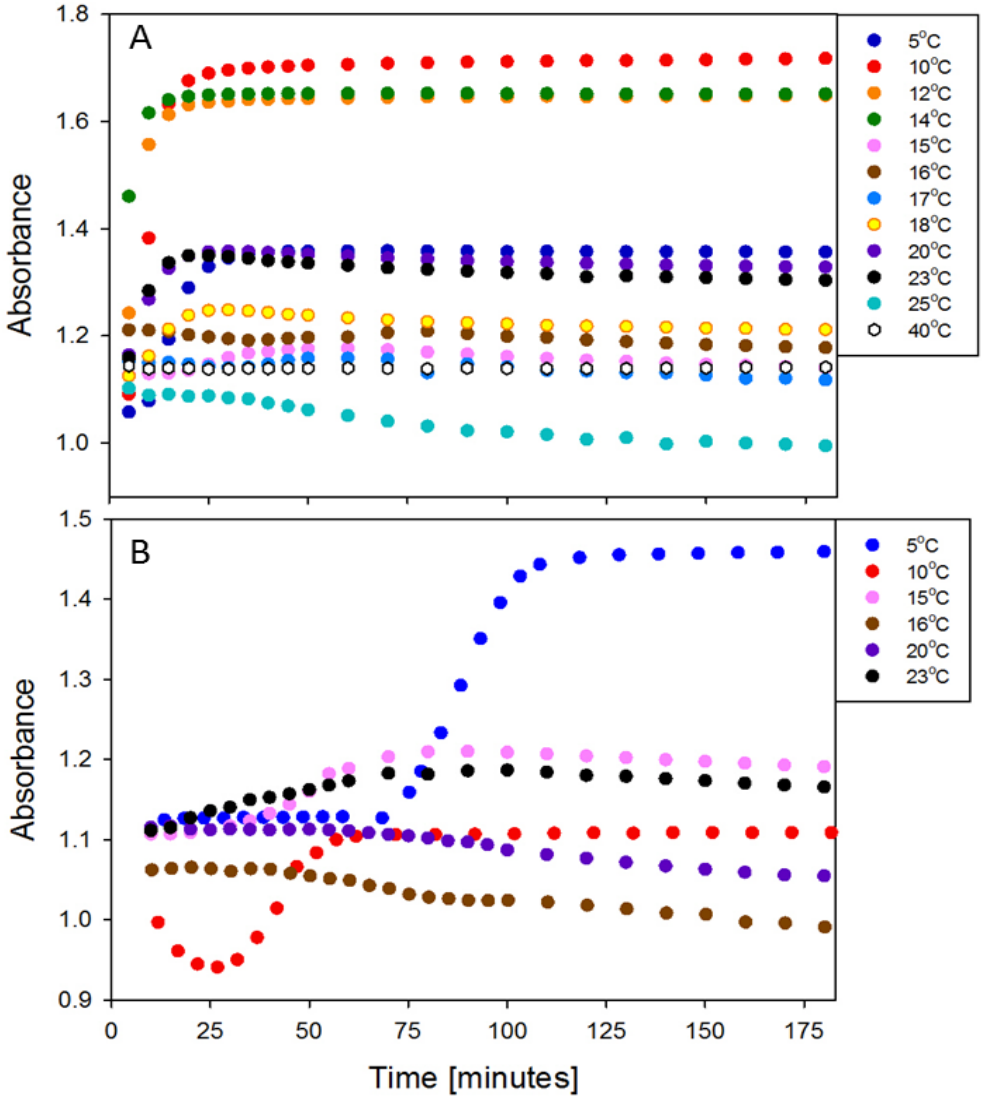

Figure 4.5. Absorbance of 220 mM GAG in 55 mol% ethanol/45 mol% H_2O monitored at 221 nm over time for a) directly incubating at the indicated temperatures and b) quenching from 50° C to indicated temperature.

Figure 4.5b shows changes of the 221 nm absorptivity measured after quenching samples from 50° C to the indicated temperatures. Interesting changes were only

observed for quenching temperatures of 5^o and 10^o C. For the former, the kinetic trace is clearly sigmoidal and displays a lag time comparable with what is shown in Figure 4.4 for $\Delta\varepsilon_{221}$. This clearly suggests that no large scale aggregation is occurring during the lag time. For 10^o C, the amplitude is much less pronounced. The data measured at 25^o C indicate somewhat of a minimum of the kinetic trace which precedes a clearly sigmoidal behavior. If one identifies the time corresponding to the minimum with the lag time, the data again correspond to what we observed for $\Delta\varepsilon_{221}$ at this temperature.

One might wonder whether the change of baseline absorption, which was used above as an indicator of turbidity has an effect on the $\Delta\varepsilon_{221}$-values derived from our CD measurements. In the Appendix, we show that these effects are minimal and the observed changes of $\Delta\varepsilon$ are therefore assignable to structural changes (Figure A4.1, Appendix).

IR and VCD spectroscopy. We measured the FTIR spectrum of 220 mM GAG in 55 mol% d-ethanol/45 mol% D_2O as a function of time at 10^o, 16^o and 23^o C in the range between 1300 and 1800 cm^{-1}. The use of deuterated solvents was necessary to avoid an overlap of the HOH water bending mode with amide I, which leads to vibrational mixing between both modes.[30,31] The corresponding spectra and the solvent spectrum measured at 10^o C are shown in Figure 4.6.

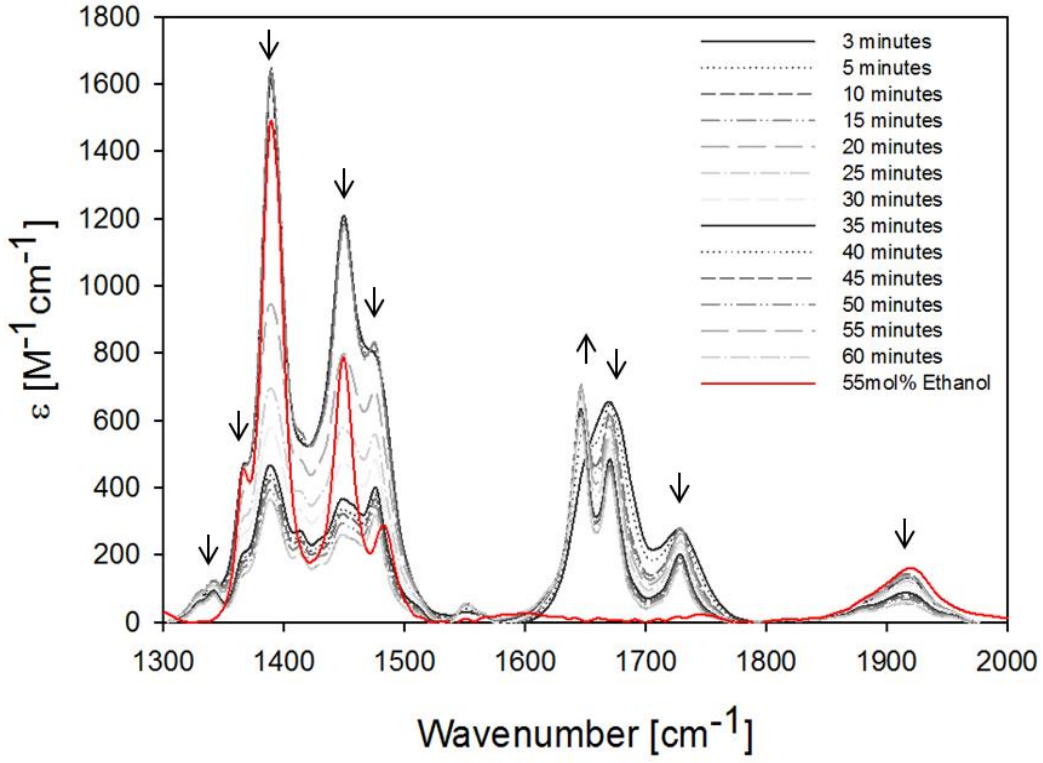

Figure 4.6. FTIR spectra of 220mM GAG in 55 mol% d-ethanol/45 mol% D_2O measured at 10^o C. The red line depicts the spectrum of the solvent mixture without peptide.

The region between 1300 and 1500 cm^{-1} is rather crowded due to the overlap of bands assignable to CH_3-bending and CH-bending modes of the solvent and the peptide.[32] The band at 1449 cm^{-1} is assignable to amide II′, which is vibrationally mixed with CH_3 antisymmetric bending modes.[33] The band(s) between 1600 and 1700 cm^{-1} are all assignable to amide I′, whereas the band at 1729 cm^{-1} must be attributed to the C=O stretching vibration of the protonated C-terminal.[25] We decomposed all spectra self-consistently into its spectral components by using our program Multifit.[21] Spectral parameters are listed in Table A4.1 (Appendix). Two observations are noteworthy. First, the intensities of all bands in the 1350-1500 cm^{-1} region decrease over time with the

solvent bands being more affected than the peptide bands. This suggests a major reorganization of the ethanol co-solvent. This trend is not reproduced in the amide I′ region, which demonstrates that the above effect is not due to precipitation. The amide I′ band shows a change of a different kind. A broad band at ca 1669 cm^{-1} which is characteristic for GAG in the utilized ethanol-water mixture[14] is replaced by two comparatively narrow bands at 1646 cm^{-1} (AI_1') and 1670 cm^{-1} (AI_2'). With increasing time, the low wavenumber band gains intensity while the intensity of the higher wavenumber component decreases.

Figure 4.7 shows the integrated intensities of the AI_1' and AI_2' as a function of time for all three investigated temperatures. While the overall intensity gains of AI_1' are comparable with the intensity losses of AI_2', the latter occur on a significantly slower time scale than the former. The solid lines result from fits to be described below. Interestingly, AI_1' indicates a much faster response than AI_2'. It seems that the underlying kinetics is purely exponential; there is no indication of a sigmoidal character.

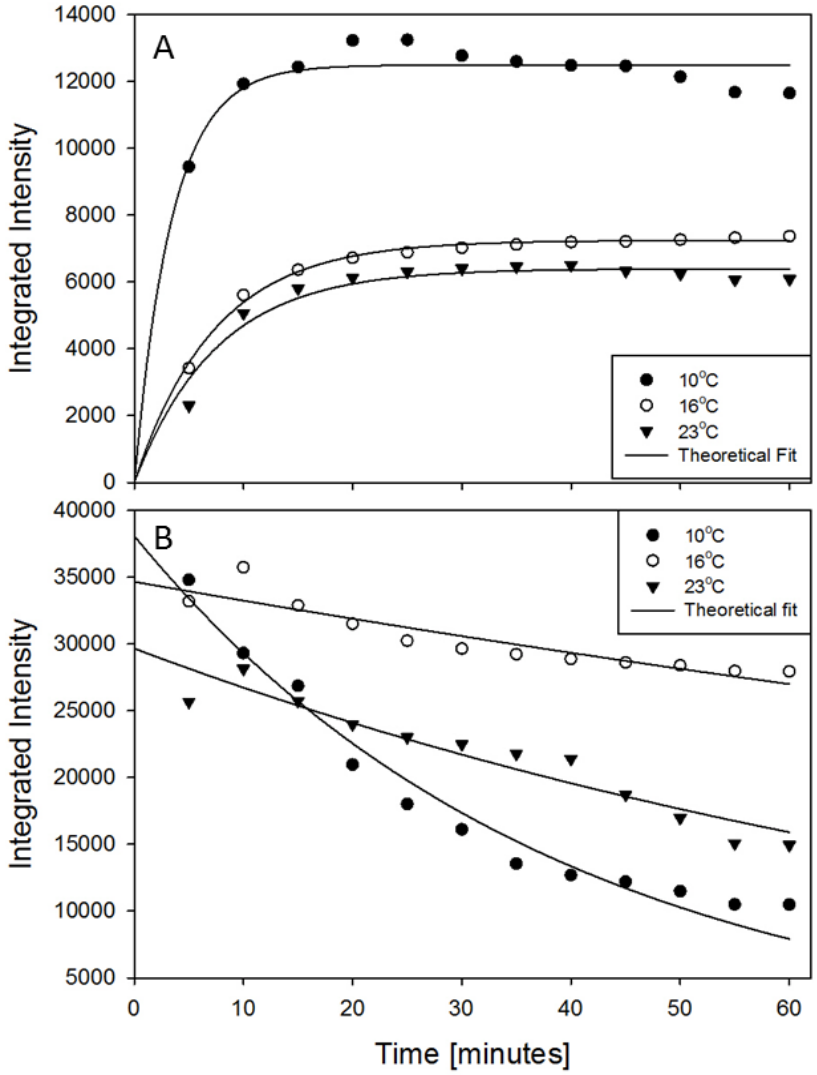

Figure 4.7. Integrated intensities of AI_1' and AI_2' plotted as a function of time for the indicated temperatures. The respective values were obtained from a spectral decomposition into Voigtian and Gaussian bands with our program Multifit. The solid lines are the fits resulting from the model described in the text, eq. (7).

The amide I mode is the most sensitive indicator of structural changes in the IR spectrum (in the following we use the notation amide I for general characteristics of amide I modes and the prime (′) sign if we refer to actual spectra of the peptide in D_2O).[24] In the case of peptide aggregation, excitonic coupling between amide I modes of different peptide groups leads to a delocalization of excited vibrational states and thus to

the redistribution of intensities and significant wavenumber shifts.[34,35,36] We will use the concepts of excitonic coupling below in order to propose the structural development underlying the time dependence of amide I′. Another even more sensitive tool is the VCD signal associated with amide I′. In its original polyproline II (pPII) dominated statistical coil state the amide I′ VCD of GAG is a pronounced negative couplet with a positive maximum of ca 0.015 and a negative maximum of ca. 0.025 $M^{-1}cm^{-1}$.[37] Figure 4.8 shows the VCD spectrum of GAG in 55 mol% d-ethanol/45 mol% D_2O recorded at different times after incubation at 10^o, 16^o and 23^o C. These data provide some very important information about the temporal development of the sample.

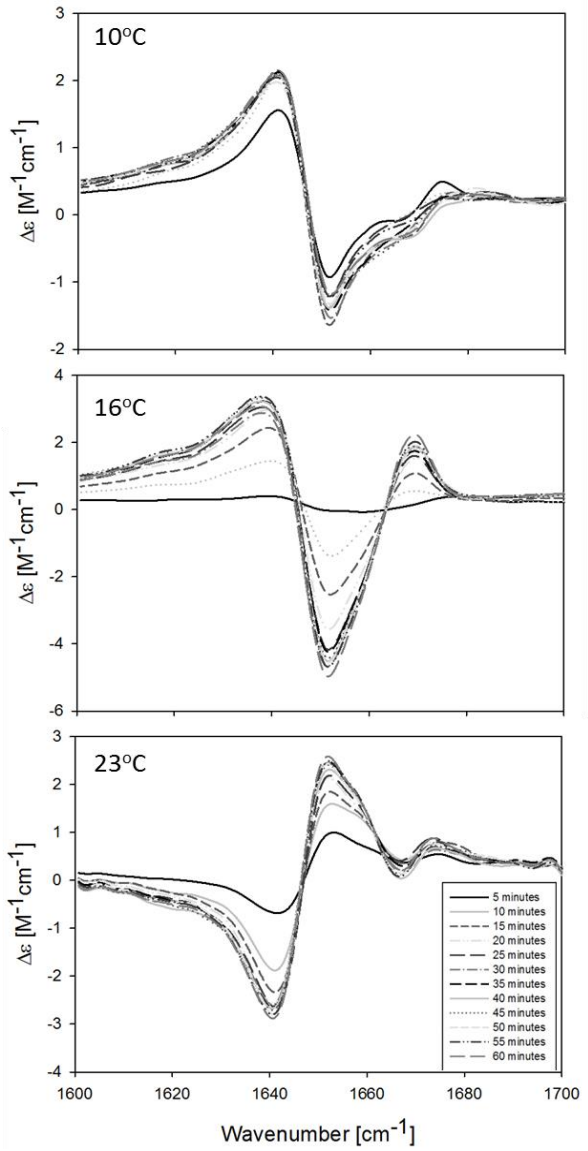

Figure 4.8. VCD spectra of 220mM GAG in 55 mol% d-ethanol/45 mol% D_2O measured at different times after incubation at the indicated temperatures.

Even at the initial state, the VCD signals are enhanced by a factor of ca. 50 compared with the original GAG signal. With increasing time the signal triples. This enhancement exceeds that of an alanine-based heptamer earlier reported by Measey et al.[27, 38] Such a VCD enhancement was first reported for lysozyme and insulin aggregates by Nafie and coworkers.[26,39] Measey and Schweitzer-Stenner assigned it to the helical twist of a

parallel β-sheet,[27] but alternative explanations were explored by others.[40,41] Whatever the correct interpretation is, all analyses thus far agree in suggesting that a large enhancement of the amide I′ in VCD reflects the formation of long twisted fibrils.

One might argue that part of the VCD amplification reflect some anisotropy of the sample caused by an alignment of the very long crystalline fibrils observed by Milorey et al.[14] In order to check for this possibility, we varied the orientation of the sample in the spectrometer. As shown in Figure A4.2 (Appendix), this did not change the VCD in a significant way. Thus, we can conclude that the obtained VCD enhancement of amide I′ solely reflects the growth of long and twisted fibrils. It is rather surprising that a short peptide like GAG can form such peculiar supramolecular structures.

A direct comparison of the VCD spectra taken at the above temperatures provides even more interesting insights. First, all spectra actually depict a superposition of two couplets, which are individually associated with the two IR-bands. This shows that each of these bands is composed of sub-bands assignable to different excitonic states of the peptide polymer.[35,34,36] At 23^{o} C, the AI_1' couplet is clearly dominant, but it should be emphasized that even the minor AI_2' component shows considerable enhancement compared with a normal amide I′ VCD signal. At 16^{0} C something really surprising happens. The VCD of AI_1' has changed its sign, it is now a positive couplet. It overlaps with the increased negative maximum of the still negative couplet of $AI_2^{'}$, thus producing a rather pronounced negative signal. At 10^{o} C, the spectrum is dominated by a positive couplet at AI_1', the still negative signal at AI_2' is much weaker. These data reveal that the peptide fibrils probed by AI_1' undergo a change of their helicity at ca. 16^{o} C. A similar change of fibril helicity has once been obtained for insulin, where it is being caused by

lowering the pH of the already acidic sample below 2.5.[39] It is reasonable to assume that it is this change of helicity, which is associated with the longer lag time probed by our CD data.

The difference between the peak values of the positive and the negative maximum of the amide I′ VCD ($\Delta\Delta\varepsilon$) is plotted as a function of time in Figure A4.3 (Appendix). The changes seem to coincide with those of the amide I′ intensities in Figure 4.7. This observation suggests that the spectral changes in the amide I′ region of the FTIR spectrum coincide with the fibril formation probed by the VCD enhancement.

Rheology. The rheology of the peptide solutions were measured via small amplitude oscillatory shear in the linear viscoelastic regime. The storage modulus G’ and the loss modulus G’’ as a function of frequency were determined under controlled strain. Figure 4.9 shows G’ > G’’, which is indicative of a soft elastic solid or gel. Power law fits to the data reveal exponents for storage and elastic moduli of 0.066 and 0.062 respectively. Both moduli show a very shallow increase with frequency and very similar power-law scaling, signifying that the phase angle δ is nearly constant with frequency. This steady state result, which is measured several hours after mixing, can be used to determine the kinetics of formation by monitoring G’ and G’’ as a function of time for a given frequency just after forming the peptide solution.

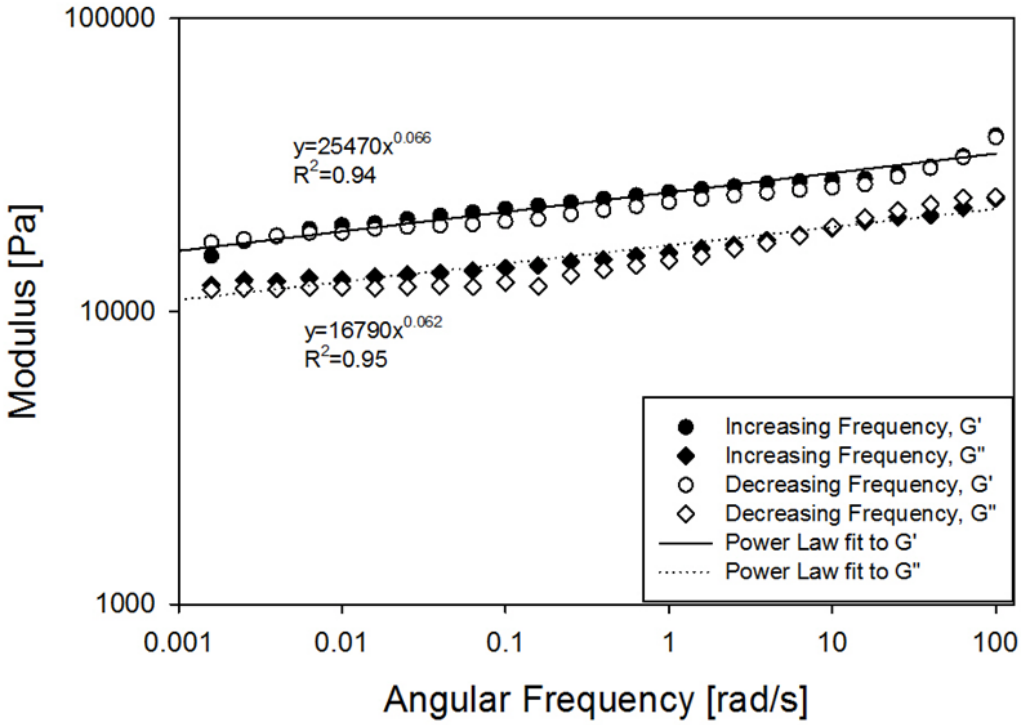

Figure 4.9. Rheological frequency sweep of storage G' and loss G" moduli at 23^{o} C shown for the hydrogel after development for 24 hours. One cycle of the sweep involved increasing angular frequency, stabilizing for one minute, then decreasing angular frequency. Seven sweeps were averaged and shown here with fits to power law curves.

Figures 4.10a and 4.10b show the time dependence of G' and G" for three different temperatures (10^{o} C, 16^{0} C and 23^{o} C), respectively. We observe from the kinetic traces that the fastest rate of gel formation (slope of G') is observed in order of increasing temperature.

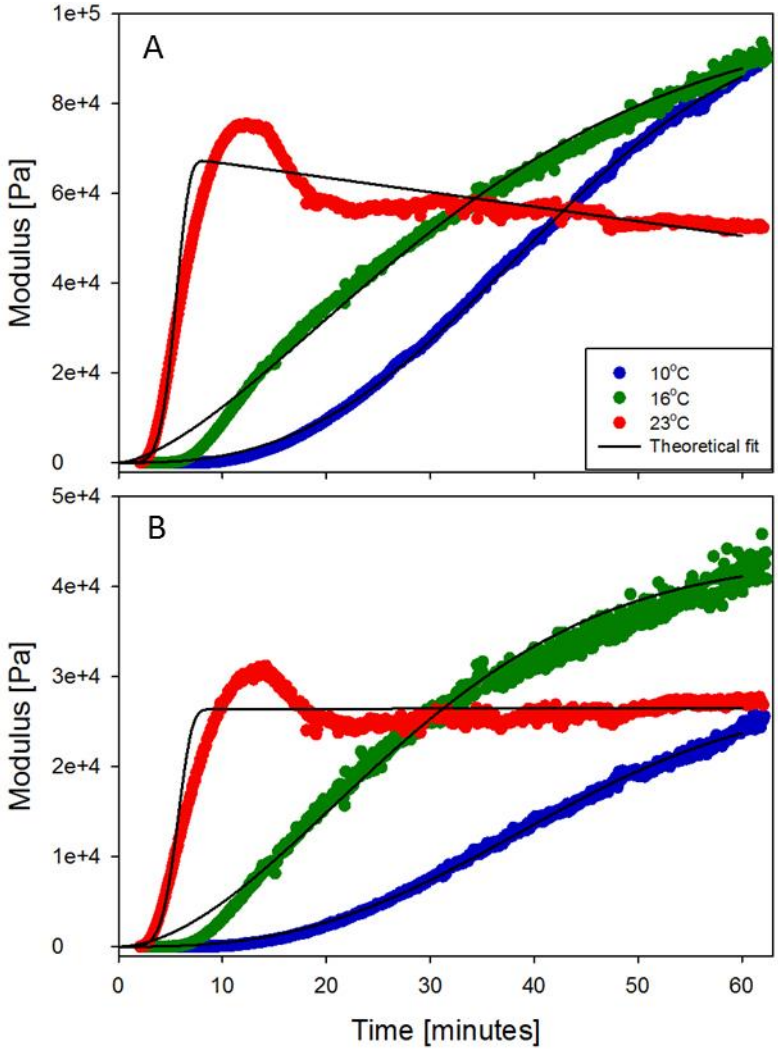

Figure 4.10. Gelation kinetics of 220mM GAG in 55 mol% ethanol/45 mol% H_2O monitored at the indicated temperatures by measuring a) the storage modulus G' and b) the loss modulus G". The solid lines are the fits resulting from the model described in the text, eq. (8).

There is a curious overshoot that occurs at 23° C, which is not observed in the other traces. A lag-time before noticeable aggregation kinetics is observed for 10° C and 16° C. The time at which the storage modulus is greater than the loss modulus indicates the onset of a connected gel network. The times at which the moduli coincide in this manner are 8, 5, and 3 minutes for 10°, 16°, and 23° C respectively.

Kinetic analysis of $\Delta\varepsilon_{221}(t)$. There is no unifying model that we could use to analyze the kinetic data gathered in this study. The $\Delta\varepsilon_{221}(t)$ data exhibit a lag time and a sigmoidal shape at temperatures between 15^o and 17^o C. This is generally indicative of a nucleation process which precedes polymerization. Taking this into account, we opted to use the model developed by Knowles et al. to explain the self-aggregation of insulin and β-lactoglobulin.[42] It is based on the following reaction equation for the time dependence of the concentrations of filaments of length j, where j denotes the number of units (peptides in our case):

$$f_j(t) = 2m(t) \cdot k_+\left[f_{j-1}(t) - f_j(t)\right] - k_-\left[(j-1)f_j(t) + 2 \cdot \sum_{i=j+1}^{\infty} f_i(t)\right] + k_n m(t)^{n_c}\delta_{j,n_c} \qquad (1)$$

where *m(t)* is the peptide concentration, k_+ is the rate constant for a process which adds a peptide to a polymer with *j* peptides, and k_- is the rate constant for the inverse process (i.e. a polymer can break at any of its *j* linkages). The last term in eq. (1) describes the formation of growth nuclei of the order n_c. δ_{jk} is the Kronecker symbol which identifies n_c with *j*. The equation accounts for the occurrence of homogeneous nucleation (association of monomers into oligomers) and inhomogeneous nucleation, which involves the formation of fragments. The latter seeds the formation of new fibrils. Eq. (1) does not describe gelation, such a formalism would have to account for the formation of physical contacts between fibrils (network formation).[43,44] Knowles et al. found an analytical solution for eq.(1), which expresses the mass concentration of filaments as a function of time.[42] If we assume that $\Delta\varepsilon_{221}(t)$ scales linearly with the mass concentration of filaments, their solution can be written in the following way:

$$\Delta\varepsilon_{221}(t) = A[1 - \exp\left(-\left(B_+ + \frac{C}{2}\right)e^{\kappa t} + \left(B_- - \frac{C}{2}\right)B_- e^{-\kappa t} + C\right] + \Delta\varepsilon^o_{221}(t) \qquad (2)$$

A is a constant that is proportional to the total peptide concentration, m_{tot}. The coefficients $B_\pm$ are defined as follows:

$$B_\pm = \frac{k_+}{\kappa}P(0) \pm \frac{M(0)}{2m_{tot}} \qquad (3)$$

where *P(0)* and *M(0)* are the initial number and mass concentrations of the filaments. Here we assume that $B_\pm = 0$. For the coefficient C we can write:

$$C = k_n m_{tot}^{n_c - 1} k_-^{-1} \qquad (4)$$

The rate constant κ in eq. (2) can be written as:

$$\kappa = \sqrt{2m_{tot}k_+k_-} \qquad (5)$$

If one expresses the total peptide concentration in units of Molar, a large number for n_C reduces *C* significantly. We can now simplify equation (2) as follows:

$$\Delta\varepsilon_{221}(t) = A[1 - \exp\{C \cdot (1 - \cosh(\kappa t))\}] + \Delta\varepsilon^o_{221} \qquad (6)$$

The hyperbolic cosine term can account for a sigmoidal behavior since it decreases slowly close to t = 0 and much more rapidly over time. For $t > \tau$, it becomes very large and as a consequence the exponential term vanishes.

We fit eq. (6) to the $\Delta\varepsilon_{221}$ kinetic traces shown in Figures 4.3 and 4.4. The resulting best fit is given by the solid lines in Figures 4.3 and 4.4. The fitting parameters are listed in Tables 4.1 and 4.2.

Table 4.1. Parameters obtained from fitting eq. (6) to the UVCD kinetic data in Figure 4.3.

T [^{o}C]	A	κ [min^{-1}]	C	$\Delta\varepsilon_{221}^{0}$ [M^{-1}cm^{-1}]	χ_R^2
5	1.35	$1.5\cdot10^{-3}$	$2.59\cdot10^{3}$	-0.060	1.27
10	1.32	$2.3\cdot10^{-3}$	$2.63\cdot10^{3}$	-0.22	0.87
12	1.33	$2.1\cdot10^{-3}$	$2.70\cdot10^{3}$	-0.34	0.81
14	1.11	$2.6\cdot10^{-3}$	$2.79\cdot10^{3}$	-0.34	0.57
15	0.61	$0.90\cdot10^{-3}$	$1.81\cdot10^{3}$	-0.21	0.11
16	0.64	$0.92\cdot10^{-3}$	$1.64\cdot10^{3}$	-0.25	0.20
17	0.72	$0.91\cdot10^{-3}$	$1.64\cdot10^{3}$	-0.25	0.06
18	0.71	$2.1\cdot10^{-3}$	$1.95\cdot10^{3}$	-0.25	0.37
20	0.76	$2.0\cdot10^{-3}$	$1.88\cdot10^{3}$	-0.17	0.77
23	0.81	$2.3\cdot10^{-3}$	$1.91\cdot10^{3}$	-0.26	0.95

Table 4.2. Parameters obtained from fitting eq. (6) to the UVCD kinetics data in Figure 4.4.

T [^{o}C]	A	κ [min^{-1}]	C	$\Delta\varepsilon_{221}^{0}$ [M^{-1}cm^{-1}]	χ_R^2
5	1.63	$9.3\cdot10^{-2}$	$3.44\cdot10^{-4}$	-0.054	0.81
10	0.81	$9.1\cdot10^{-2}$	0.036	-0.16	0.19
15	0.94	$7.5\cdot10^{-2}$	0.051	-0.26	0.57
16	0.56	$4.6\cdot10^{-2}$	0.050	-0.22	0.15
20	0.46	$2.3\cdot10^{-2}$	0.69	-0.27	0.12
23	0.42	$3.1\cdot10^{-2}$	0.46	-0.33	0.09

The reduced chi-squared values indicate very satisfactory and statistically reliable fits. Figure A5.5 (Appendix) shows the temperature dependence of the fitting parameters A, κ and C obtained from the fits to the data, which we measured after incubating the peptide at different temperatures. All parameters show minima in the narrow 15^o-16^o region, which coincides with the occurrence of the lag times indicated by the respective kinetic data. Thus, the relaxation constant κ does clearly show a non-Arrhenius behavior. From our fits to the quenching experiments, we obtain that the relaxation constant decreases with increasing temperature in a highly non-linear way, which could be characterized as anti-Arrhenius behavior. The C-value is very small for temperatures below 20^o C. Overall, the temperature dependence of the kinetic data strongly suggests that outside of the transition region between 15^o C and 17^o C the structural changes probed by $\Delta\varepsilon_{221}$ do not encounter a significant activation barrier.

According to eq. (5) the observed decrease of κ at ca. 16^o C could reflect a decrease of k_+ and or k_-. However, a decrease of the latter would cause a concomitant increase of the parameter C (eq. (4)), which is the opposite of what we observe. Hence, we conclude that the changes of κ predominantly reflect changes of the forward constant k_+. In this case, the simultaneous decrease of C must reflect a decrease of k_n and/or an increase of n_c.

Kinetic analysis of IR data. We fit the kinetics probed by AI_1' and AI_2' with the following simple exponential equations:

$$I_{AI_1} = I_{AI_{1,\infty}} \cdot (1 - \exp(-\kappa_1' t)) + I_{AI_{1,0}}$$

$$I_{AI_2} = I_{AI_{2,\infty}} \cdot \exp(-\kappa_2' t) + I_{AI_{2,0}} \qquad (7)$$

where we denoted the relaxation constants as κ_1' and κ_2' in order to distinguish them from the relaxation constant in eq. (6). The meaning of the amplitudes and intensity constants is self-explanatory. Eq.(7) was satisfactorily fit to the data in Figure 4.7, and the parameters can be found in Table 4.3. Based on the obtained values for the relaxation constants κ_1' and κ_2' the decay of AI_2' is an order of magnitude much slower than the increase of AI_1', but itself is slightly faster than the relaxation probed by $\Delta\varepsilon_{221}$ data.

Table 4.3. Parameters obtained from fitting eq. (7) to the integrated intensities of the FTIR kinetic data in Figure 4.7.

T [^{o}C]	A_{IR} [AI_1', 1646 cm^{-1}]	κ'_1 [min^{-1}]	t_c[min]	A_{IR} [AI_2', 1670 cm^{-1}]	κ'_2 [min^{-1}]
10	$1.25\cdot10^4$	0.29	10	$3.81\cdot10^4$	$2.6\cdot10^{-2}$
16	$7.25\cdot10^3$	0.14	103	$3.47\cdot10^4$	$4.2\cdot10^{-3}$
23	$6.40\cdot10^3$	0.13	18	$2.97\cdot10^4$	$1.0\cdot10^{-2}$

We did not separately fit the kinetic traces of the corresponding VCD data, since the respective changes occur on the same time scale as those of the corresponding IR data (Figure A4.3, Appendix). Moreover, the $\Delta\Delta\varepsilon$ data recorded at 10^{o}C indicate some non-continuous behavior which we decided not to analyze for this thesis. A more detailed study of the fibrils' chirality and its changes will be subject of future research.

Kinetics analysis of rheology data. While the above introduced polymerization model of Knowles et al. works fine for the kinetics probed by our CD data, we do not consider it an appropriate choice for our rheological data for two reasons. First, the Knowles et al. model does not account for cross-linking by means of intersecting fibrils, which is a pre-requisite for gelation. Second, it is unclear whether G' and G'' are as simply related to concentration as is ellipticity. We therefore decided to employ the more heuristic model that Gao et al.[45] used to fit the time dependence of the dynamic structure function of thermoreversible colloidal gels. For our purpose their algorithm can be written as:

$$G = G_o[1 - a \cdot \exp(-\kappa_1'' t) - (1 - a \cdot \exp\left(-(\kappa_2'' t)^{\beta}\right)] \cdot (1 - \kappa_3'' t) \quad (8)$$

G_o, a, and β are constants, which can be expected to depend on temperature. The constants κ_1'' and κ_2'' represent different relaxation processes, the former being exponential and the latter anomalous. A linear term with a third relaxation constant κ_3'' term has been added to the formalism of Gao et al.[45] Using this formalism yielded nearly perfect fits to the data recorded at 10° and 16° C, for which we assumed $\kappa_3'' = 0$ (Table 4.4).

Table 4.4. Parameters obtained from fitting eq. (8) to the rheology kinetics data in Figure 4.10.
A. Storage modulus

T [°C]	A_{rheol}	a	β	κ_1 [min^{-1}]	κ_2 [min^{-1}]	κ_3 [min^{-1}]
10	$9.72 \cdot 10^4$	-	2.72	$9.8 \cdot 10^{-4}$	0.022	0
16	$1.03 \cdot 10^5$	0.030	1.54	$2.8 \cdot 10^{-4}$	0.027	0
23	$7.61 \cdot 10^4$	0.080*	5.69	$8.0 \cdot 10^{-4}$*	0.17	$4.7 \cdot 10^{-3}$

B. Loss modulus

T [^{o}C]	A_{rheol}	a	β	κ_1 [min^{-1}]	κ_2 [min^{-1}]	κ_3 [min^{-1}]
10	$2.70 \cdot 10^4$	-	2.72	$9.8 \cdot 10^{-4}$*	0.022	0
16	$4.71 \cdot 10^4$	0.090	1.82	$7.0 \cdot 10^{-4}$	0.031	0
23	$2.90 \cdot 10^4$	0.090	5.59	$8.4 \cdot 10^{-4}$	0.17	0

* Constrained values

Only for the G' data measured at 23^{o}C was it necessary to consider this third relaxation. The fits to both the G' and the G'' data measured at 23^{o}C exhibit some deviation from the experimental data, owing to the existence of a maximum which is formed during the initial phase of the gelation process. We feel that we do not have enough information at present to allow for a further development of our theoretical approach.

Comparison of relaxation processes. If one were to naively compare the relaxation rates obtained from the different kinetics, the following hierarchy for 10^0 and 23^o C results: $\kappa_1'(AI_1') > \kappa_2''(rheology) > \kappa_2'(AI_2') \geq \kappa(\Delta\varepsilon_{221}) > \kappa_1''(rheology)$. The same hierarchy stands for 16^o C except that the process probed by $\Delta\varepsilon_{221}$ precedes the decay of AI_2'. However, this analysis is incorrect, since we have not taken into account the fact that the relaxation time constant is within a hyperbolic cosine in eq. (6). Instead of comparing $\kappa(\Delta\varepsilon_{221})$ directly, we instead assess the time period of the processes probed by the kinetic traces of $\Delta\varepsilon_{221}$. To this end, we calculated the derivative of the argument of the exponential function in eq. (2) and found it to depend linearly on time. Thus, we found

that below a certain critical time, $t_c(\Delta\varepsilon_{221})$, the processes probed by $\Delta\varepsilon_{221}$ are slower than those measured by AI_1' absorption and VCD enhancement, while they are faster for $t>t_c(\Delta\varepsilon_{221})$. The critical time can be obtained from the argument of the exponential function in eq. (6) as the time at which its derivative equals $\kappa_1'(AI_1')$. For corresponding kinetics measured at 10^o, 16^o and 23^o C this yields 10, 103 and 18 minutes, respectively (listed also in Table 4.3). Hence, the real hierarchy of the observed processes is $\kappa_1'(AI_1') > \kappa(\Delta\varepsilon_{221}) > \kappa_2''(rheology) > \kappa_2'(AI_2') > \kappa_1''(rheology)$ below and $(\Delta\varepsilon_{221}) > \kappa_1'(AI_1') > \kappa_2''(rheology) > \kappa_2'(AI_2') > \kappa_1''(rheology)$ above the respective threshold values.

To interpret this correctly, we have first to clarify the meaning of the different relaxation constants. Changes of the far UV electronic circular dichroism generally reflect changes of the secondary and tertiary structure (if aggregation is again counted as tertiary structure formation). The spectral changes shown in Figure 4.1 are not indicative of a classical β-sheet formation, for which one would observe a pronounced negative maximum in the 210-220 nm region. Note this was observed for temperatures above the gel point where the β-strand conformation of the alanine residue becomes predominantly populated.[14] Instead, we observe that at all temperatures the CD spectra switch from a negative to a positive maximum in the above spectral region. For a monomeric peptide, this is indicative of an increasing population of polyproline II conformations.[46] However, in the present context we consider it more likely that electronic coupling between peptide groups in the observed very thick fibrils (*vide infra* and the online available movie) lead to the observed spectral changes. The rationale for this view follows from the sequence of processes, which are deduced from our experimental data below.

The coincidence between the increase of AI_1' and its VCD signal suggests that they both monitor the formation of rather long twisted tapes or ribbons (cf. a detailed discussion below), which eventually aggregate into rather thick fibrils as seen in the corresponding movie (available as web enhanced object on the ACS web site) and in the microscopic image reported by Milorey et al.[14] We posit that our CD data (i.e. $\Delta\varepsilon_{221}(t)$) probe this process. The rather non-linear character of its effective time constant indicates that the fibril formation process is cooperative, i.e. it proceeds slowly at low concentrations of tapes and ribbons and increasingly fast at higher concentrations. Interestingly, the gelation process itself as probed by G'(t) and G''(t) proceeds nearly on the same time scale as the tape/ribbon formation at 23^0 C while a clear delay between aggregation/fibrillization and gelation occurs at 16^o and 10^o C. The tape/ribbon formation probed by AI_1' is followed by a slower process reflected by the partial decay of AI_2'. We assign this band a subpopulation of short tapes and fibrils, which might serve as building blocks for a secondary nucleation[42] and for further crosslinking of fibrils to stabilize the gel supporting network. The slowest process as derived from the kinetics of G' and G'' (reflected by κ_2") and might reflect a further stabilization of the gel phase.

It is obvious that the fibrillization process that leads to the gelation of the GAG in 55 mol% ethanol/45 mol% water is different from what is reported for most of the self-aggregating peptides.[3] The positions of the two amide I′ bands and corresponding UVCD spectra seem to rule out the formation of β-sheet structures, which are even formed by rather short peptides.[47,8] Generally, one expects the corresponding amide I′ wavenumber for β-sheet fibrils to be below 1630 cm^{-1}.[35, 48,38] On the other side it is noticeable that at least AI_1' is significantly redshifted compared with the position in the liquid phase of the

solvent. The latter is indicative of a predominantly non-aqueous environment of the C-terminal carbonyl group.[14,49] Therefore, the AI_1' data might indeed reflect the formation of a β-sheet-like structure. To test this hypothesis we utilized an earlier algorithm reported by Measey and Schweitzer-Stenner[27] to calculate the amide I′ IR and VCD spectrum of a parallel β-sheet dimer sketched in Figure 4.11.

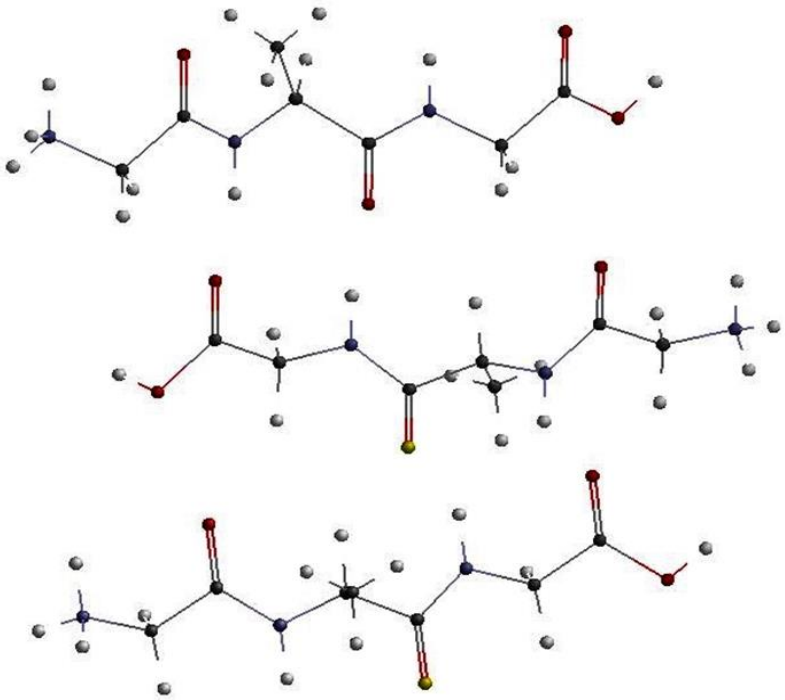

Figure 4.11. A representative parallel β-sheet structure formed by three cationic GAG peptides which would allow excitonic coupling between the C-terminal amide I′ vibrations.

We opted for a parallel structure since Measey and Schweitzer-Stenner showed that the VCD amplification is much less pronounced for an antiparallel structure. For the spectral simulation we assumed amide I′ wavenumbers of 1665 and 1675 cm^{-1}, which would lead

to the broad amide I′ band observed for the peptide in the liquid phase. Figure 4.12 shows the calculated amide I spectra for a sheet of 100 peptides. The assumed helical twist angle was ± 2^o per peptide where the plus and minus sign correspond to a left- and right-handed helical structure. For both cases the amide I′ band appears at 1641 cm^{-1}, which is very close to the observed wavenumber position of AI_1'. The magnitude of the VCD enhancement (ca. 3.8 $M^{-1}cm^{-1}$ per residue) is already close to what we experimentally observed. The positive and negative couplets reflect a left- and right-handed helical twist.

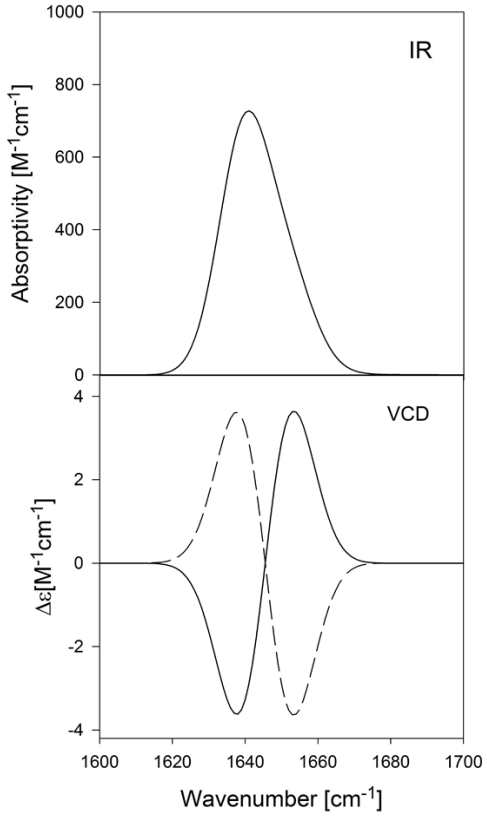

Figure 4.12. Simulation of the IR and VCD band profiles of amide I by assuming a sheet of 100 parallel oriented strands with two peptide groups, representing the GAG peptide. The solid and dashed line in the lower panel represent simulations assuming a right-handed and left handed helical twist of ± 2^0 per strand. The theory for the simulation has been reported in reference[27].

We cautiously propose that the observed enhancement of AI_1' which is not explainable by conformational changes might indicate the formation of polarons, which arise from anharmonic coupling between, e.g., amide I and low wavenumber phonons in a rather periodic structure.[50] The crystalline form of the observed fibrils and the reduced halfwidth of the amide I′ bands both indicate the existence of such a structure. Originally it had been thought that this type of coupling leads to a localization (trapping) of amide I excitation,[50] which would be inconsistent with the observed VCD enhancement. However, as shown by Hamm and Edler,[51] such a 'trapping model' is too simplistic, since it ignores the translational invariance of a periodic structure.

In spite of the good agreement between simulation and experiment we have to consider this structural model as hypothetical at the present stage. The word of caution is underscored by our difficulty to account for the behavior of AI_2'. Apparently, based on the observation of a lesser but significant VCD enhancement this band must be assigned to some type of fibril structure. However, the band is on the high energy side of the amide I′ band in the spectrum of the liquid state which suggests the absence of any downshifting. We wonder whether an out-of-register formation of sheets occurs, in which the alanine residues of adjacent residues point in opposite directions. Fibrils formed this way could serve as a linker by connecting alanine side chains of different regular fibers. However, further investigations, which should also include measurements of the respective Raman spectra, are necessary for a less ambiguous assignment of $AI_2^{'}$ and the relaxation process probed by the respective kinetic trace.

Interpretation of rheological data. While spectroscopy data shows the relative rates of formation of aggregates, the rheology probes the overall connectivity of these structures. Snapshot images are shown in Figure 4.13.

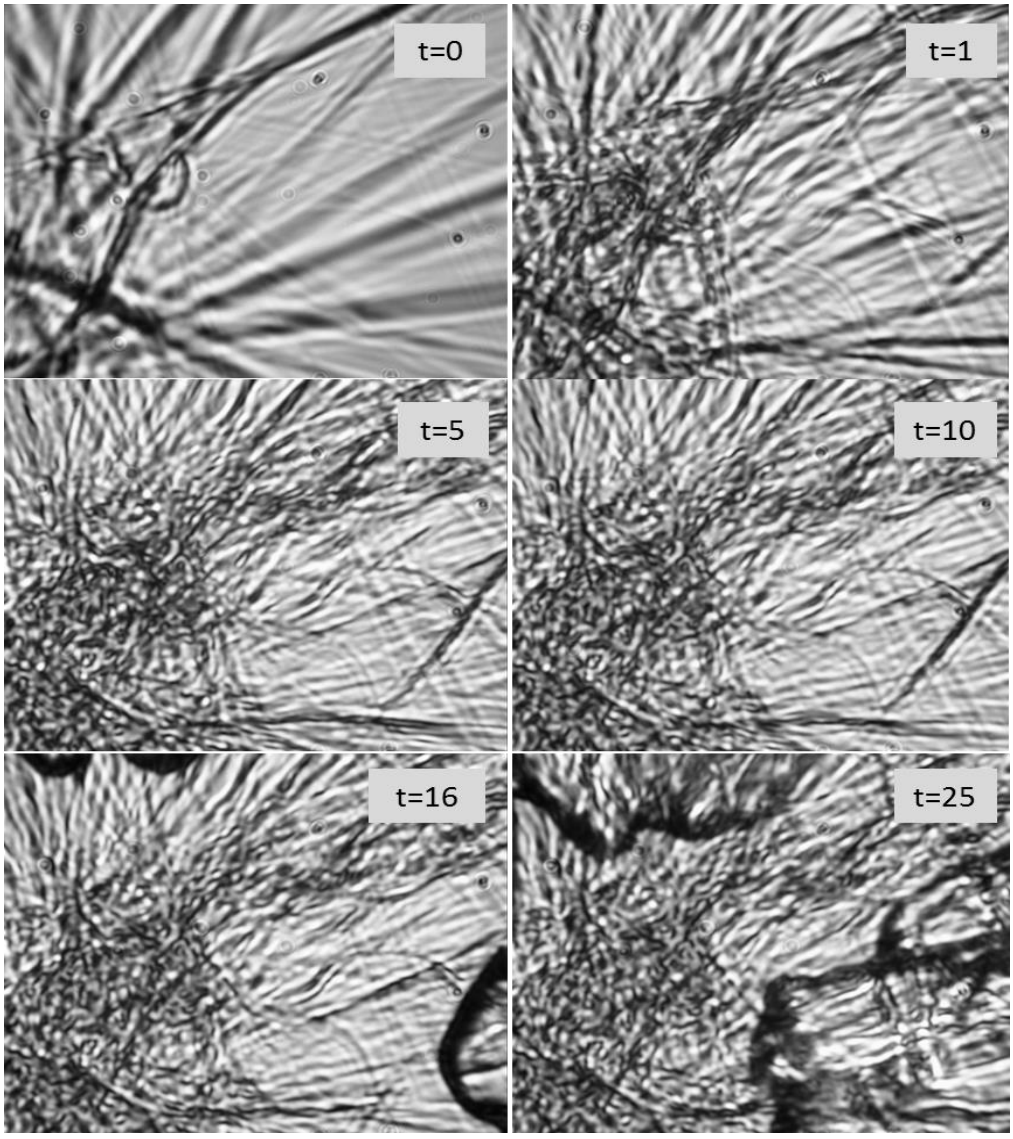

Figure 4.13. Snapshot images taken from the movie of cationic GAG in 55 mol% ethanol/45 mol% water at the respective time in minutes after mixing indicated in each panel. The first image (t = 0) was taken 3 minutes after loading the sample.

Initially at t = 0, there is a foundation of large fibrils set as a framework for the gel. For the next several minutes, fibrils appear to cross and overlay to form an increasingly connected fibril network. It is likely that the changes of $\Delta\varepsilon_{221}$ are reflecting this process, which leads to the elastic and storage moduli increase and gel strengthening for 23^{o} C depicted in Figure 4.10 for the first ten minutes. At t = 16 minutes, a dark substance penetrates into the corners of the image, and then finally continues to create layers of spanning gel. This coincides with the abrupt relaxation of the elastic and storage moduli after ten minutes and the steady relaxation after 20 minutes in rheology kinetics. At lower temperatures, the rheology moduli exhibit lagging nucleation times and do not reach stabilization within the measurement time frame. From these observations it is clear that fibril formation promotes a strengthening of the gel, followed by further fibril entanglement and crossing. This agrees well with the determined time constants of the relaxation processes.

Finally, we emphasize an apparent correlation between the strength of the hydrogel (as expressed by moduli G' and G") and the helicity of the fibrils. Our kinetic data suggest much higher G' and G'' values for the left-handed helical fibrils formed at low temperatures than for the right-handed fibrils observed between between 16^{o} C and the gel temperature. The tan δ value in the saturation region is also slightly higher at low temperatures (1.8 at 10^{0} C versus 1.6 at 23^{o} C).

4.5 Conclusions

The various processes of aggregation, fibrillization, and gelation of cationic GAG in 55 mol% ethanol/45 mol% water were investigated by various spectroscopies and rheological measurements. Significant structural changes were observed in vibrational

spectroscopy measurements, such as in FTIR where a single broad amide I′ band transformed into two narrow bands. The appearance of AI_1' intensity coincided with extreme enhancements of the VCD amide I′ signal, and can therefore be considered another indication of fibril formation. A change in helicity was observed at 16^o C from VCD measurements, which corresponded to temperatures where a nucleation time was noticeable in the UVCD data. The fibril formation involves the stacking of rather long sheets due to hydrophobic interactions between alanine side chains, which leads to the formation of twisted tapes and ribbons.[52] The overall gelation process and network connection occurred more rapidly with increasing temperature, which closely follows the formation of tapes, ribbons and fibrils. At low temperatures we observe a lag time between tape formation and fibrillization on one side and gelation on the other side. We wonder whether this might be due to changed helicity of the tapes/ribbons as documented by the VCD signal. If this notion was true we would have established a relationship between the helicity of tapes or even fibrils and their capability to form a sample spanning network. A movie of cationic GAG in 55 mol% ethanol/45 mol% water showed a correlation to the rheology kinetics, and pictured an extensive network of gigantic fibrils and interaction of peptide and solvent during this remarkable gelation process. The compared relaxation rates for the various kinetic processes provided insight on the changes of the cationic peptide solution over time on both local and macroscopic levels.

4.6 Acknowledgements

We like to thank Prof. Frank Ferrone from the Department of Physics of Drexel University for a very useful discussion of our data and for suggesting checking for

changes of turbidity and applying a model to our CD-based kinetics which takes into account homogeneous and inhomogeneous polymerization. We also like to thank Zachary Hinton from the Department of Chemical and Biological Engineering of Drexel University for his assistance with taking the rheology video.

4.7 References

1. Yan, C.; Pochan, D. J. Rheological Propensities of Peptide-Based Hydrogels for Biomedical and Other Applications. *Chem. Soc. Rev.* **2010,** *39*, 3528-3540.

2. Rajagopal, K.; Schneider, J. P. Self-Assembling Peptides and Proteins for Nanotechnological Applications. *Curr. Op. Struct. Biol.* **2004,** *14*, 480.

3. Hamley, I. W. Peptide Fibrillization. *Angew. Chem. Int. Ed. Engl.* **2007,** *46* (43), 8128-47.

4. Murphy, R. M. Peptide Aggregation in Neurodegenerative Disease. *Annu. Rev. Biomed. Eng.* **2002,** *4*, 155-74.

5. Toriumi, K.; Oma, Y.; Kino, Y.; Futai, E.; Sasagawa, N.; Ishiura, S. Expression of Polyalanine Stretches Induces Mitochondrial Dysfunction. *J. Neurosci. Res.* **2008,** *86* (7), 1529-1537.

6. Gazit, E. Self Assembly of Short Aromatic Peptide into Amyloid Fibrils and Related Nanostructures. *Prion* **2007,** *1*, 32-35.

7. Reches, M.; Gazit, E. Casting Metal Nanowires within Discrete Self-Assembled Peptide Nanotubes. *Sci.* **2003,** *300*, 625.

8. Reches, M.; Porat, Y.; Gazit, E. Amyloid Fibril Formation by Pentapeptide and Tetrapeptide Fragments of Human Calcitonin. *J. Biol. Chem.* **2002,** *277*, 35475-35480.

9. Frederix, P. W.; Scott, G. G.; Abul-Haija, Y. M.; Kalafatovic, D.; Pappas, C. G.; Javid, N.; Hunt, N. T.; Ulijn, R. V.; Tuttle, T. Exploring the Sequence Space for (Tri-)Peptide Self-Assembly to Design and Discover New Hydrogels. *Nat. Chem.* **2015,** *7* (1), 30-7.

10. Kim, W.; Hecht, M. H. Generic Hydrophobic Residues Are Sufficient to Promote Aggregation of the Alzheimer's Abeta42 Peptide. *Proc. Natl. Acad. Sci. U SA.* **2006,** *103* (43), 15824-9.

11. West, M. W.; Wang, W.; Patterson, J.; Mancias, J. D.; Beasley, J. R.; Hecht, M. H. *De Novo* Amyloid Proteins From Designed Combinatorial Libraries. *Proc. Natl. Acad. Sci. USA* **1999,** *96*, 11211-11216.

12. Hirst, A. R.; Coates, I. A.; Boucheteau, T. R.; Miravet, J. F.; Escuder, B.; Castelletto, V.; Hamley, I. W.; Smith, D. K. Low-Molecular-Weight Gelators: Elucidating the Principles of Gelation Based on Gelator Solubility and a Cooperative Self-Assembly Model. *J. Am. Chem. Soc.* **2008,** *130* (28), 9113-21.

13. DiGuiseppi, D.; Schweitzer-Stenner, R. Probing Conformational Propensities of Histidine in Different Protonation States of the Unblocked Glycyl-Histidyl-Glycine Peptide By Vibrational and NMR Spectroscopy. *J. Raman Spectrosc.* **2016,** *in press*.

14. Milorey, B.; Farrell, S.; Toal, S. E.; Schweitzer-Stenner, R. Demixing of Water and Ethanol Causes Conformational Redistribution and Gelation of the Cationic GAG Tripeptide. *Chem. Commun. (Camb.)* **2015,** *51* (92), 16498-501.

15. Ma, M.; Yuang, Y.; Gao, Y. Q.; Zhang, Y.; Gao, P.; Xu, B. Aromatic-Aromatic Interactions Induce the Self-Assembly of Pentapeptide Derivatives in Water To Form Nanofibers and Supramolecular Hydrogels. *J. Am. Chem. Soc.* **2010,** *132*, 2719-2728.

16. Kyte, J.; Doolittle, R. F. A Simple Method for Displaying the Hydropathic Character of a Protein. *J. Mol. Biol.* **1982,** *157* (1), 105-32.

17. (a) Fauchere, J.-L.; Pliska, V. E. Hydrophobic Parameters π of Amino Acid Side Chains from the Partitioning of N-Acetyl-Amino Acid Amides. *Eur. J. Med. Chem.* **1983,** *18*, 369-375; (b) Takano, K.; Yutani, K. Hydrophobic Parameters Pi of Amino Acid Side Chains from the Partitioning of N-Acetyl-Amino Acid Amides. *Protein. Eng.* **2001,** *14*, 525-528.

18. Measey, T. J.; Schweitzer-Stenner, R. Self-Assembling Alanine-Rich Peptides of Biomedical and Biotechnological Relevance. In *Protein and Peptide Folding, Misfolding and Non-Folding*, Schweitzer-Stenner, R., Ed. Wiley & Sons: Hoboken, 2012; pp 309-350.

19. Blondelle, S. E.; Forood, B.; Houghten, R. A.; PerezPaya, E. Polyalanine-Based Peptides as Models for Self-Associated Beta-Pleated-Sheet Complexes. *Biochem.* **1997,** *36* (27), 8393-8400.

20. Giri, K.; Bhattacharyya, N. P.; Basak, S. pH-Dependent Self-Assembly of Polyalanine Peptides. *Biophys. J.* **2007,** *92* (1), 293-302.

21. Jentzen, W.; Unger, E.; Karvounis, G.; Shelnutt, J. A.; Dreybrodt, W.; Schweitzer-Stenner, R. Conformational Properties of Nickel(II) Octaethylporphyrin in Solution. 1. Resonance Excitation Profiles and Temperature Dependence of Structure-Sensitive Raman Lines. *J. Phys. Chem.* **1995,** *100*, 14184-14191.

22. Sreerama, N.; Woody, R. W. Structural Composition of βI and β2 Proteins. *Protein Sci.* **2003,** *12*, 384-388.

23. Wood, S. J.; Maleef, B.; Hart, T.; Wetzel, R. Physical, Morphological and Functional Differences between pH 5.8 and 7.4 Aggregates of the Alzheimer's Amyloid Peptide Aβ. *J. Mol. Biol.* **1996,** *256* (5), 870-877.

24. Bandekar, J.; Krimm, S. Normal Mode Spectrum of the Parallel-Chain β-Sheet. *Biopolym.* **1988,** *27*, 909-921.

25. Schweitzer-Stenner, R. Advances in Vibrational Spectroscopy as a Sensitive Probe of Peptide and Protein Structure. A Critical Review *Vibr. Spectrosc.* **2006,** *42*, 98-117.

26. Ma, S.; Cao, X.; Mak, M.; Sadik, A.; Walkner, C.; Freedman, T. B.; Lednev, I. K.; Dukor, R. K.; Nafie, L. A. Vibrational Circular Dichroism Shows Unusual Sensitivity to Protein Fibril Formation and Development in Solution. *J. Am. Chem. Soc.* **2007,** *129*, 12364-12365.

27. Measey, T. J.; Schweitzer-Stenner, R. Vibrational Circular Dichroism as a Probe of Fibrillogenesis: The Origin of the Anomalous Intensity Enhancement of Amyloid-like Fibrils. *J. Am. Chem. Soc.* **2011,** *133*, 1066-1076.

28. Toal, S. E.; Verbaro, D. J.; Schweitzer-Stenner, R. Role of Enthalpy-Entropy Compensation Interactions in Determining the Conformational Propensities of Amino Acid Residues in Unfolded Peptides. *J. Phys. Chem. B.* **2014,** *118* (5), 1309-18.

29. Schweitzer-Stenner, R.; Soffer, J. B. Optical Spectroscopy. In *Biophysical Techniques for Structural Characterization of Macromolecules,* Dyson, H. J., Ed. Oxford Academic Press: Oxford, 2012; Vol. 1, pp 533-591.

30. Sieler, G.; Schweitzer-Stenner, R. The Amide I Mode of Peptides in Aqueous Solution Involves Vibrational Coupling Between The Peptide Group and Water Molecules of The Hydration Shell. *J. Am. Chem. Soc.* **1997,** *119*, 1720.

31. Chen, X. G.; Schweitzer-Stenner, R.; Asher, S. A.; Mirkin, N. G.; Krimm, S. Vibrational Assignments of trans-N-Methylacetamide and Some of Its Deuterated Isotopomers from Band Decomposition of IR, Visible, and Resonance Raman Spectra. *J. Phys. Chem.* **1995,** *99*, 3074-3083.

32. (a) Bonang, C. C.; Anderson, D. J.; Cameron, S. M.; Kelly, P. B.; Getty, J. D. Ultraviolet Raman Scattering of Simple Alcohols and a Related Diol as a Study of Low Lying Rydberg-Valence Characteristics. *J. Chem. Phys.* **1993,** *99*, 6245-6252; (b) Schweitzer-Stenner, R.; Eker, F.; Huang, Q.; Griebenow, K.; Mroz, P. A.; Kozlowski, P. M. Structure Analysis of Dipeptides in Water by Exploring and Utilizing the Structural Sensitivity of Amide III by Polarized Visible Raman, FTIR-Spectroscopy and DFT Based Normal Coordinate Analysis. *J. Phys. Chem. B.* **2002,** *106*, 4294-4304.

33. Lee, S.-H.; Krimm, S. An Ab-Initio Based Vibrational Analysis of α-Poly(L-Alanine). *Biopolym.* **1998,** *46*, 283-317.

34. Kubelka, J.; Keiderling, T. A. Differentiation of β-Sheet-Forming Structures: Ab Initio-Based Simulations of IR Absorption and Vibrational CD for Model Peptide and Protein β-Sheets *J. Am. Chem. Soc.* **2001,** *123*, 12048-12058.

35. Lee, C.; Cho, M. Local Amide I Mode Frequencies and Coupling Constants in Multiple-Stranded Antiparallel β-Sheet Polypeptides. *J. Phys. Chem. B.* **2004,** *108,* 20397-20407.

36. Schweitzer-Stenner, R. Simulated IR, Isotropic and Anisotropic Raman, and Vibrational Circular Dichroism Amide I Band Profiles of Stacked β-Sheets. *J. Phys. Chem. B.* **2012,** *116*, 4141-4153.

37. Hagarman, A.; Measey, T. J.; Mathieu, D.; Schwalbe, H.; Schweitzer-Stenner, R. Intrinsic Propensities of Amino Acid Residues in GxG Peptides Inferred from Amide I' Band Profiles and NMR Scalar Coupling Constants. *J. Am. Chem. Soc.* **2010,** *132* (2), 540-51.

38. Measey, T. J.; Smith, K. B.; Decatur, S. M.; Zhao, L.; Yang, G.; Schweitzer-Stenner, R. Self-Aggregation of a Polyalanine Octamer Promoted by Its C-Terminal Tyrosine and Probed by a Strongly Enhanced Vibrational Circular Dichroism Signal. *J. Am. Chem. Soc.* **2009,** *131*, 18218-18219.

39. Kurouski, D.; Lombardi, R. A.; Dukor, R. K.; Lednev, I. K.; Nafie, L. A. Direct Observation and pH Control of Reversed Supramolecular Chirality in Insulin Fibrils by Vibrational Circular Dichroism. *Chem. Commun. (Camb.)* **2010,** *46* (38), 7154-6.

40. Welch, W. R. W.; Keiderling, T. A.; Kubelka, J. Structural Analyses of Experimental 13C Edited Amide I′ IR and VCD for Peptide β-Sheet Aggregates and Fibrils Using DFT-Based Spectral Simulations. *J. Phys. Chem. B.* **2013,** *117*, 10359-10369.

41. Welch, W. R. W.; Kubelka, J.; Keiderling, T. A. Infrared, Vibrational Circular Dichroism, and Raman Spectral Simulations for β-Sheet Structures with Various Isotopic Labels, Interstrand, and Stacking Arrangements Using Density Functional Theory. *J. Phys. Chem. B.* **2013,** *117*, 10343-10358.

42. Knowles, T. P. J.; Waudby, C. A.; Devlin, G. L.; Cohen, S. I. A.; Aguzzi, A.; Vendruscolo, M.; Terentjev, E. M.; Welland, M. E.; Dobson, C.M. An Analytical Solution to the Kinetics of Breakable Filament Assembly. *Sci.* **2009,** *326*, 1533-1537.

43. Cahn, J. W. Phase Seperation by Spinodal Decomposition in Isotropic Systems. *J. Chem. Phys.* **1965,** *42*, 93-99.

44. MacKintosh, F. C.; Käs, J.; Janmey, P. A. Elasticity of Semiflexible Biopolymer Networks. *Phys. Rev. Lett.* **1995,** *75*, 4425-4428.

45. Gao, Y. Q.; Kim, J.; Helgeson, M. E. Microdynamics and Arrest of Coarsening During Spinodal Decomposition in Thermoreversible Colloidal Gels. *Soft Matt.* **2015,** *11*, 6360-6370.

46. Woody, R. W. Circular Dichroism Spectrum of Peptides in the Poly(Pro)II Conformation. *J. Am. Chem. Soc.* **2009,** *131*, 8234-8245.

47. Motta, A.; Reches, M.; Pappalardo, L.; Andreotti, G.; Gazit, E. The Preferred Conformation of the Tripeptide Ala-Phe-Ala in Water Is an Inverse g-turn: Implications for Protein Folding and Drug Design. *Biochem.* **2005,** *144*, 14170-14178.

48. Measey, T. J.; Schweitzer-Stenner, R.; Sa, V.; Kornev, K. Anomalous Conformational Instability and hydrogel Formation of a Cationic Class of Self-Assembling Oligopeptides. *Macromol.* **2010,** *43*, 7800-7806.

49. Wang, Y.; Purello, R.; Georgiou, S.; Spiro, T. G. UVRR Spectroscopy of the Peptide Bond. 2. Carbonyl H-Bond Effects on the Ground- and Excited-State Structures of N-Methylacetamide. *J. Am. Chem. Soc.* **1991,** *113*.

50. Careri, G.; Buontempo, U.; Galluzzi, F.; Scott, A. C.; Gratton, E.; Shyamsunder, E. Spectroscopic Evidence for Davidov-Like Solitons. *Phys. Rev. B.* **1984,** *30*, 4689-4702.

51. Hamm, P.; Edler, J. Quantum Vibrational Polarons: Crystalline Acetanilide Revisited. *J. Chem. Phys.* **2006,** *73*, 094302-1 - 094302-12.

52. Aggeli, A.; Nyrkova, I. A.; Bell, M.; Harding, R.; Carrick, L.; McLeish, T. C. B.; Semenov, A. N.; Boden, N. Hierachical Self-Assembly of Chiral Rod-Like Molecules as a Model for Peptide β-Sheet Tapes, Ribbons, Fibrils and Fibers. *Proc. Natl. Acad. Sci. USA.* **2001,** *98*, 11857-11862.

4.8 Appendix

Calculation of effects of turbulence on dichroism

In this paragraph we estimate the influence of turbidity on the measured dichroism values of our UVCD spectra. Turbidity can increase the overall absorptivity and thus upshift the baseline of the absorption spectra. The ellipticity θ of the transmitted light is proportional to the difference ΔA between the absorptivity of right- and left-handed circular polarized light:

$$\theta = \frac{180^\circ \ln(10)}{4\pi} \Delta A \qquad \text{(A1)}$$

Ellipticity is converted into molar dichroism Δε by using the Beer-Lambert relationship and the well-established relationship between molar ellipticity and molar dichroism:[1]

$$\Delta\varepsilon = \frac{180° \ln(10)}{4\pi * b * c * 32980} * \Delta A \qquad \text{(A2)}$$

where b is the pathlength of the cuvette and c the molar concentration of the peptide. The variation δΔA caused by the turbidity of the sample can be calculated as (α-1)·ΔA, where α is the factor by which the absorptivity is increased from values observed for a transparent sample. Propagation of error therefore yields:

$$\delta\Delta\varepsilon = \frac{180° \ln(10)}{4\pi * b * c * 32980} * \delta\Delta A = \frac{180° \ln(10)}{4\pi * b * c * 32980} * (\alpha - 1)\Delta A \qquad \text{(A3)}$$

The absorbance of a 55 mol% solution of ethanol and water without peptide at 221nm was used as the reference for calculation of α. The plotted results are shown in Figure A4.1 (Appendix).

Table A4.1: Spectral parameters obtained from decomposing the FTIR spectrum shown in Figure 6 using the program Multifit.

A. Integrated Intensities in arbitrary units

	Time [min]	3	5	10	15	20	25	30	35	40	45	50	55	60
1329cm^{-1}	10°C	23047	6637	7667	6417	3076	2154	1805	1467	1392	1442	1332	1296	1301
	16°C	2250	2193	2308	1889	1750	1738	1714	1671	1640	1656	1651	1595	1606
	23°C	1553	2284	3053	2884	2699	2574	2463	2294	2246	1909	1766	1631	1806
1341cm^{-1}	10°C	692	357	332	311	369	249	255	266	277	286	287	293	294
	16°C	659	567	559	572	542	567	572	553	548	558	557	555	550
	23°C	3103	2471	2478	1922	1728	1650	1528	1286	1234	1215	1108	923	794

1364cm^{-1}	10°C	6057	3985	3820	3575	2335	1483	1208	915	843	850	738	625	624
	16°C	3725	3521	3349	3193	3013	2989	2974	2909	2876	2883	2889	2841	2831
	23°C	2226	2074	2045	2093	2107	2081	2036	1951	1925	1565	1420	1263	1252
1389cm^{-1}	10°C	34095	30211	30454	31182	25244	24018	21180	17741	16463	15567	14634	13427	13408
	16°C	35834	36404	36181	36581	37480	37230	37371	37862	37968	37482	37595	37622	37925
	23°C	15862	16119	15651	16291	16903	17062	17291	17729	17823	13281	11040	9072	8909
1418cm^{-1}	10°C	0	42528	43665	41318	24175	14537	11253	7987	7351	6974	6312	5564	5628
	16°C	26090	25101	25750	25365	24698	24875	24874	24708	24591	24868	24935	24581	24577
	23°C	27455	26844	26380	25265	24622	24172	23573	22155	21872	18972	17172	15148	15126
1449cm^{-1}	10°C	24614	15824	15150	14892	11436	9159	7729	6234	5803	5665	5178	4571	4574
	16°C	26655	26625	26086	25915	25889	26098	25962	25811	25824	25301	25520	25689	25694
	23°C	11438	11538	13541	14517	15252	15471	15626	15636	15609	10578	7946	5536	4926
1476cm^{-1}	10°C	24473	20778	20665	22156	19554	15256	12607	9736	8601	8219	7380	6550	6468
	16°C	21883	21151	20376	19711	19358	19534	19417	19357	19256	19813	19317	19129	19113
	23°C	19305	19362	18541	18083	17928	17808	17541	16946	16826	14150	12593	11109	12097
1511cm^{-1}	10°C	2949	198	11	18	133	444	396	341	338	299	300	281	290
	16°C	2261	1630	1322	1256	1127	1252	1221	1208	1170	1082	1186	1026	1111
	23°C	2086	2053	1358	1223	1172	1046	911	807	756	668	649	590	432
1551cm^{-1}	10°C	944	2337	1205	1080	838	745	724	666	639	606	562	543	533
	16°C	335	611	1143	1017	857	997	976	955	905	889	943	728	845
	23°C	537	446	1366	1259	1182	1042	929	834	790	691	675	633	594

1564cm^{-1}	10°C	13318	809	4313	3333	385	336	362	500	591	601	753	895	949
	16°C	1184	664	215	237	256	251	251	259	258	260	251	246	254
	23°C	1274	1605	231	302	317	327	329	317	311	308	309	333	326
1627cm^{-1}	10°C	6227	2796	3218	3224	1483	1655	1923	2319	2539	2637	2994	3377	3462
	16°C	530	665	746	1325	1639	1746	1882	1981	2049	2092	2156	2170	2242
	23°C	1224	1510	1311	1675	1893	2023	2119	2184	2231	2403	2536	2688	2726
1646cm^{-1}	10°C	5390	9450	11934	12438	13230	13248	12773	12600	12482	12466	12147	11677	11655
	16°C	2571	3420	5609	6364	6720	6880	7023	7120	7194	7214	7272	7328	7372
	23°C	2199	2298	5067	5803	6130	6305	6405	6458	6503	6328	6240	6066	6088
1670cm^{-1}	10°C	52087	34807	29328	26868	20961	18010	16115	13545	12691	12198	11490	10504	10489
	16°C	32501	33195	35741	32900	31511	30241	29658	29234	28877	28619	28393	27989	27944
	23°C	25673	25671	28143	25739	23995	23016	22494	21778	21399	18728	16973	15072	14948
1729cm^{-1}	10°C	23944	14505	13495	13246	10384	9289	8399	7193	6668	6395	5893	5241	5214
	16°C	17782	16697	12964	12243	11969	11434	11271	11167	11058	11039	10970	10831	10821
	23°C	16621	17160	10993	9957	9588	9371	9259	9101	9022	8234	7663	6982	6995
1817cm^{-1}	10°C	10227	8178	9745	6851	527	517	414	373	357	402	430	768	795
	16°C	159	153	133	211	229	269	277	286	297	295	298	323	312
	23°C	106	173	337	387	414	434	436	446	462	526	510	428	464
1879cm^{-1}	10°C	529	1988	1363	1292	2471	2269	2042	1790	1670	1619	1455	1309	1275
	16°C	3803	3475	4985	3411	3427	3801	3828	3842	3859	3801	3789	3926	3881
	23°C	1357	2513	4069	3688	3692	3626	3511	3463	3454	2178	1794	1673	1650

1917cm^{-1}	10°C	8679	10095	10166	10879	11979	10808	9467	7439	6816	6640	6107	5369	5367
	16°C	12565	12911	13006	12504	12353	12107	11986	11962	11877	11898	11815	11617	11710
	23°C	13020	12222	12595	12207	11763	11543	11430	11276	11207	10115	9270	8111	8277

B. Lorentzian or Gaussian Primary Halfwidths, denoted (L)/(G)

	Time [min]	3	5	10	15	20	25	30	35	40	45	50	55	60
1329cm^{-1} (G)	10°C	76.7	45.4	45.8	42.3	33.7	28.6	26.8	25.3	25.0	25.8	25.3	25.9	25.9
	16°C	41.3	39.2	36.2	31.6	29.9	29.6	29.0	28.4	27.9	28.1	27.9	27.4	27.3
	23°C	81.3	61.5	62.5	51.7	46.3	44.1	42.0	38.9	38.0	37.8	37.5	36.6	37.7
1341cm^{-1} (G)	10°C	17.5	16.0	11.3	9.9	10.7	7.9	8.0	8.2	8.4	8.6	8.6	8.8	8.8
	16°C	21.7	19.5	15.9	14.7	13.9	13.9	13.7	13.3	13.1	13.1	13.0	13.1	12.8
	23°C	42.2	37.9	35.5	30.0	27.5	26.6	25.6	23.3	22.7	23.4	22.8	21.4	20.5
1364cm^{-1} (G)	10°C	14.8	12.6	12.2	11.8	11.2	10.6	10.6	10.8	10.9	11.2	11.1	11.1	11.1
	16°C	13.8	13.5	13.2	13.0	12.7	12.6	12.6	12.5	12.5	12.5	12.5	12.4	12.4
	23°C	12.1	11.6	11.4	11.4	11.4	11.3	11.2	11.3	11.2	11.4	11.7	12.1	12.1
1389cm^{-1} (L)	10°C	3.7	4.4	4.2	5.2	10.5	19.2	21.4	23.6	23.6	22.4	23.3	23.7	23.6
	16°C	11.2	11.8	11.7	11.9	12.6	12.7	12.7	13.0	13.1	12.9	12.8	12.9	13.1
	23°C	3.3	3.9	0.7	1.6	2.8	3.1	3.7	6.5	7.0	6.4	6.3	7.0	6.6
1418cm^{-1} (G)	10°C	69.6	69.6	69.6	69.6	69.6	69.6	69.6	69.6	69.6	69.6	69.6	69.6	69.6
	16°C	69.6	69.6	69.6	69.6	69.6	69.6	69.6	69.6	69.6	69.6	69.6	69.6	69.6
	23°C	67.9	67.9	67.9	67.9	67.9	67.9	67.9	67.9	67.9	67.9	67.9	67.9	67.9
1449cm^{-1} (L)	10°C	22.7	19.2	18.5	18.3	20.4	21.4	21.7	22.2	22.2	22.5	22.4	22.1	22.0
	16°C	14.8	15.5	15.7	15.8	15.9	16.2	16.2	16.0	16.1	15.5	15.7	16.0	16.1
	23°C	0.8	5.2	12.2	15.1	17.1	17.9	18.5	19.9	20.0	18.1	15.7	11.2	8.6
1476cm^{-1}	10°C	3.7	5.0	8.7	12.6	14.9	13.5	12.8	11.8	10.1	10.0	8.6	8.2	7.7

(L)	16°C	4.9	4.2	1.4	0.7	0.7	0.7	0.7	0.7	0.7	2.0	0.7	0.7	0.7
	23°C	4.8	4.4	4.8	4.9	5.1	5.6	5.7	5.8	5.8	6.7	7.1	8.4	13.6
1511cm^{-1} (G)	10°C	63.2	14.5	7.0	6.2	10.0	12.4	11.9	11.4	11.4	10.8	10.9	10.9	11.0
	16°C	44.2	35.4	22.7	21.4	20.5	20.9	20.6	20.4	20.2	19.6	20.0	19.2	19.6
	23°C	39.8	38.7	24.5	22.6	22.0	21.0	19.7	18.8	18.1	18.4	18.7	18.8	17.0
1551cm^{-1} (G)	10°C	30.3	35.9	22.3	19.8	15.1	13.6	13.6	13.8	13.7	13.2	12.8	12.8	12.6
	16°C	23.3	25.4	28.9	25.3	21.9	23.6	22.9	22.3	21.2	20.7	21.6	16.8	19.5
	23°C	28.3	22.9	28.8	25.6	23.6	20.9	18.4	16.2	15.2	13.7	13.9	13.8	13.1
1564cm^{-1} (G)	10°C	76.0	42.3	62.8	60.1	17.5	14.8	15.8	21.3	24.4	24.5	28.8	32.4	33.5
	16°C	37.6	31.7	23.3	22.6	20.7	22.8	22.2	21.9	20.8	20.1	20.9	15.3	18.7
	23°C	43.3	45.4	24.2	24.6	23.6	21.2	18.1	15.5	14.5	13.9	14.6	16.1	15.5
1627cm^{-1} (G)	10°C	77.9	126.8	45.7	41.6	31.0	31.7	33.3	37.3	39.3	40.3	42.8	44.9	45.4
	16°C	33.7	23.0	20.3	23.3	24.4	24.7	25.1	25.4	25.6	25.6	25.8	25.9	26.0
	23°C	36.4	30.2	23.3	23.9	24.3	24.7	24.9	25.1	25.3	26.3	27.1	28.2	28.3
1646cm^{-1} (L)	10°C	3.6	11.6	11.6	10.9	11.7	12.1	12.1	12.8	12.9	13.0	12.7	12.3	12.2
	16°C	0.7	0.7	0.7	0.7	0.7	0.7	0.7	0.7	0.7	0.7	0.7	0.7	0.7
	23°C	24.5	18.2	17.1	16.8	16.7	16.7	16.7	16.7	16.7	16.7	16.7	16.7	16.7
1670cm^{-1} (L)	10°C	43.5	34.9	30.6	28.6	24.9	23.0	21.7	19.7	18.8	18.3	17.6	16.6	16.5
	16°C	12.8	18.3	36.1	33.9	32.9	31.9	31.5	31.2	30.9	30.7	30.5	30.2	30.1
	23°C	3.5	6.4	34.0	33.5	31.8	30.8	30.3	29.7	29.3	27.8	26.6	25.3	25.1
1729cm^{-1}	10°C	48.3	35.2	30.7	29.8	26.1	25.3	24.4	23.3	22.6	22.2	21.5	20.7	20.6

(L)	16°C	41.9	40.4	34.6	32.8	32.1	31.1	30.8	30.6	30.4	30.3	30.2	29.8	29.9
	23°C	40.9	42.5	32.2	29.7	28.7	28.2	27.8	27.6	27.4	26.9	26.6	26.0	26.0
1817cm^{-1} (G)	10°C	170.9	324.8	233.8	166.9	44.0	45.3	43.4	44.6	45.2	47.9	51.2	66.7	68.1
	16°C	22.7	23.2	22.2	27.4	28.4	30.0	30.5	30.9	31.3	31.4	31.6	31.8	32.0
	23°C	18.3	23.3	30.3	33.0	34.1	34.8	35.0	35.5	35.9	36.7	36.4	34.7	36.2
1879cm^{-1} (L)	10°C	0.7	41.4	32.3	29.3	43.2	42.2	40.3	38.5	37.9	37.7	36.8	35.4	34.9
	16°C	70.0	69.1	95.8	67.2	65.8	66.9	66.1	65.8	65.2	65.0	64.2	63.8	64.1
	23°C	0.7	65.1	73.5	65.0	61.2	58.6	56.3	54.9	54.1	14.3	0.7	0.7	0.7
1917cm^{-1} (L)	10°C	41.5	45.5	45.1	46.5	50.6	50.9	50.0	48.3	48.3	49.0	50.1	51.8	52.0
	16°C	56.0	57.4	58.8	55.8	55.2	54.0	53.4	53.3	53.0	53.1	52.7	51.9	52.3
	23°C	60.2	56.6	57.5	55.1	52.9	51.7	51.1	50.8	50.5	49.7	49.4	48.0	48.9
1955cm^{-1} (G)	10°C	348.2	300.4	271.5	211.6	12.8	12.8	13.0	12.8	12.8	12.7	12.5	12.6	12.5
	16°C	25.0	25.0	25.0	25.0	25.0	25.0	25.0	25.0	25.0	25.0	25.0	25.0	25.0
	23°C	25.0	25.0	25.0	25.0	25.0	25.0	25.0	25.0	25.0	25.0	25.0	25.0	25.0

C. Gaussian halfwidths of Voigtian profiles

	Time [min]	3	5	10	15	20	25	30	35	40	45	50	55	60
1389cm^{-1}	10°C	18.6	17.1	17.6	17.2	20.1	16.8	15.7	12.9	12.2	13.0	11.5	9.5	9.4
	16°C	12.3	11.8	12.3	11.9	11.1	11.4	11.4	10.8	10.7	11.2	11.1	11.1	10.8
	23°C	25.6	26.1	28.1	28.0	27.6	27.6	27.4	26.2	26.0	26.7	26.2	25.3	25.4
1449cm^{-1}	10°C	-	-	-	-	-	-	-	-	-	-	-	-	-
	16°C	13.3	12.3	11.5	11.3	11.1	10.8	10.8	11.0	11.0	11.4	11.2	10.9	10.8
	23°C	26.0	23.1	18.9	17.0	15.5	14.8	14.3	13.5	13.4	14.7	15.7	17.9	19.0
1476cm^{-1}	10°C	28.2	25.8	21.3	17.8	14.7	13.4	12.8	11.8	12.3	12.0	12.4	11.9	12.3
	16°C	28.9	29.0	30.2	30.2	30.0	30.0	30.0	30.0	29.9	29.3	29.9	29.8	29.8
	23°C	31.2	32.3	31.0	30.7	30.5	30.2	30.1	29.9	29.9	29.5	29.1	28.0	25.0
1646cm^{-1}	10°C	22.2	11.9	8.6	8.9	8.4	7.9	7.8	6.7	6.5	6.3	6.4	6.7	6.7
	16°C	25.0	19.6	17.2	16.8	16.7	16.8	16.8	16.8	16.8	16.8	16.8	16.9	16.9
	23°C	-	-	-	-	-	-	-	-	-	-	-	-	-
1670cm^{-1}	10°C	-	-	-	-	-	-	-	-	-	-	-	-	-
	16°C	36.2	31.2	-	-	-	-	-	-	-	-	-	-	-
	23°C	44.5	41.4	9.9	1.8	0.7	0.7	0.7	0.7	0.7	0.7	0.7	0.7	0.7
1879cm^{-1}	10°C	29.0	0.7	0.7	6.3	0.7	0.7	0.7	0.7	0.7	0.7	0.7	3.8	3.4
	16°C	0.7	0.7	0.7	0.7	0.7	0.7	0.7	0.7	0.7	0.7	0.7	0.7	0.7
	23°C	59.8	3.9	0.7	0.7	1.2	3.4	5.6	7.7	8.5	45.2	52.4	52.0	51.7

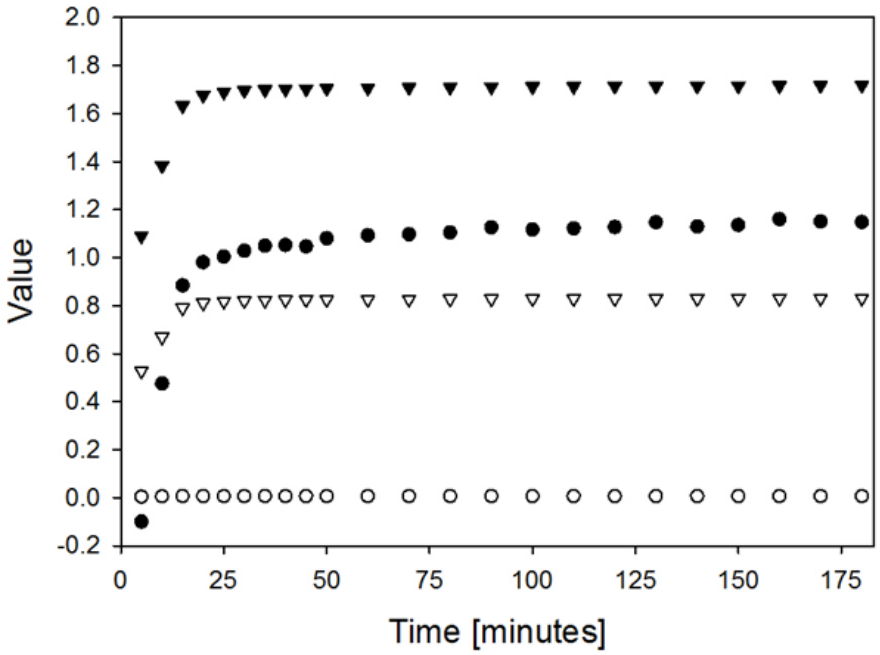

Figure A4.1: Effects of turbidity on molar dichroism calculated using eq. (A3). The figure depicts the dichroism $\Delta\varepsilon_{221}$[$M^{-1}cm^{-1}$] (black circles) of GAG in 55%mol ethanol/45 mol% water at 10^0 C as a function of time, the respective turbidity induced changes $\Delta\Delta\varepsilon_{221}$ [$M^{-1}cm^{-1}$] (white circles), the time dependence of the absorbance A_{221}(black triangles) and the corresponding changes in absorbance ΔA_{221}(white triangles).

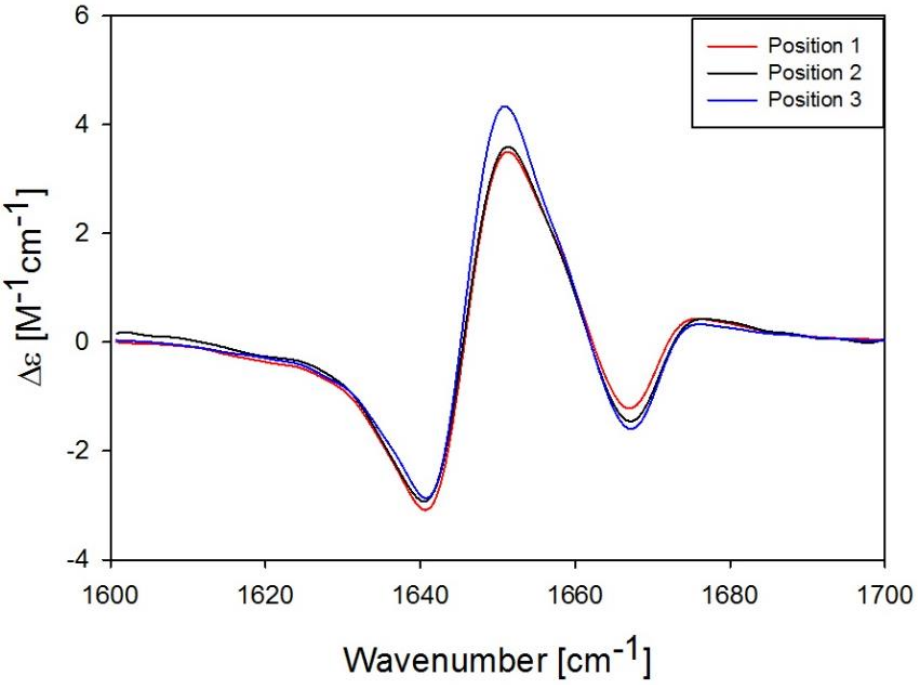

Figure A4.2: VCD scans of the amide I′ region of 220 mM GAG in 55 mol% d-ethanol/45 mol% D_2O for different orientations of the sample, which was rotated 120^o clockwise for each position. The spectra were taken at 23^o C 60 minutes after incubation.

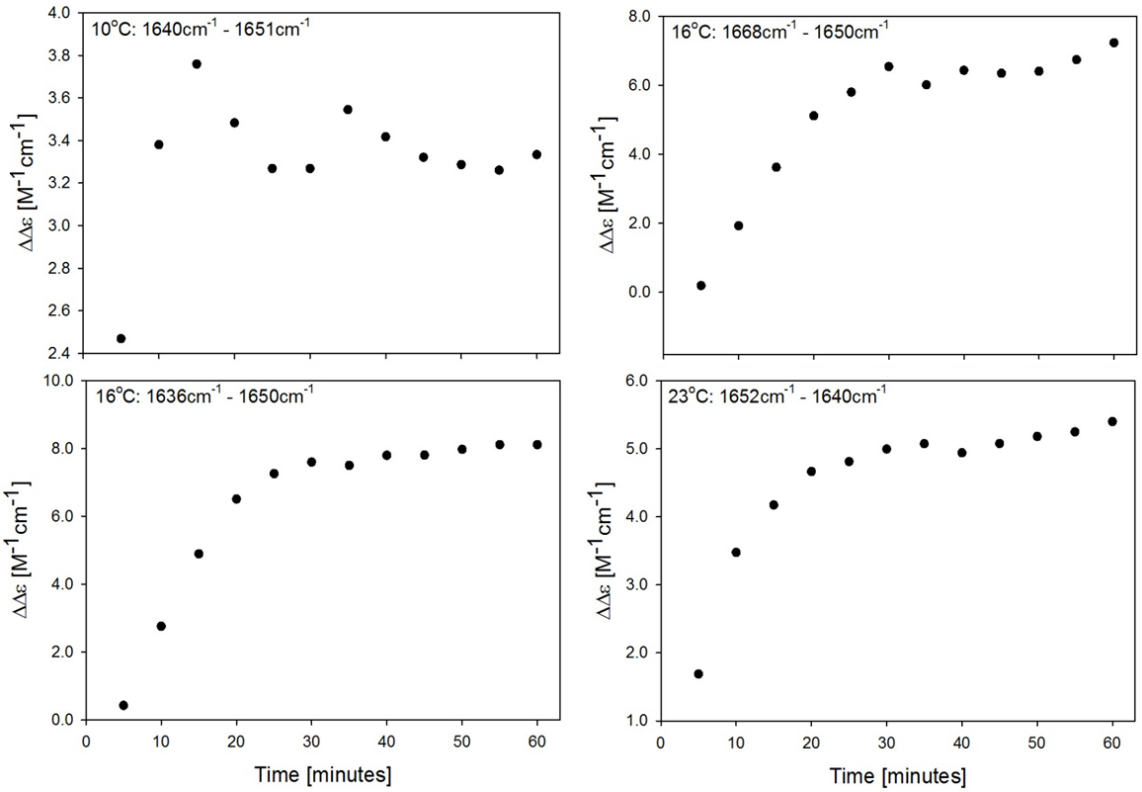

Figure A4.3: $\Delta\Delta\varepsilon$ measured as the differences between the dichroism values of the positive and negative maxima of VCD profile of AI_1' recorded at 10^o, 16^o, and 23^o C. For 16^o C, the respective differences between the negative maximum and both positive maxima are shown.

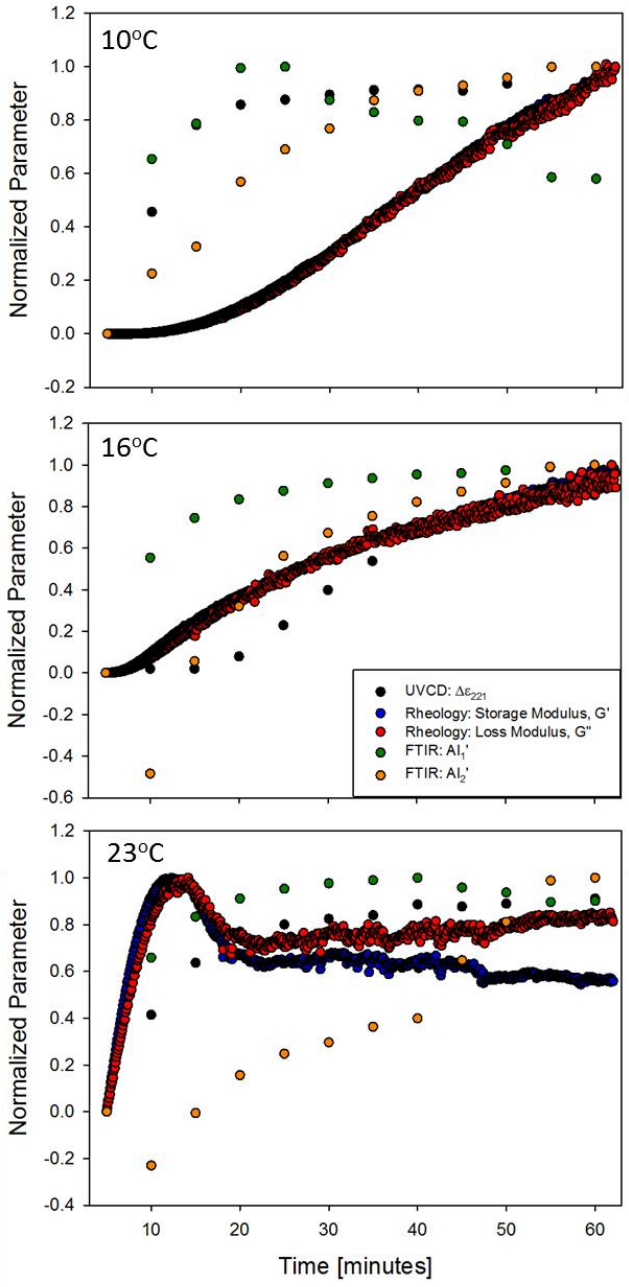

Figure A4.4: Normalized plots of the AI_1' and AI_2' integrated intensities, rheology storage and loss moduli, and UVCD molar dichroism development over time at 10^o, 16^o, and 23^o C. The AI_2' curve was normalized to its lowest value as 1 due to the exponential decreasing nature of the curve to allow for comparison to other methods which increase over time.

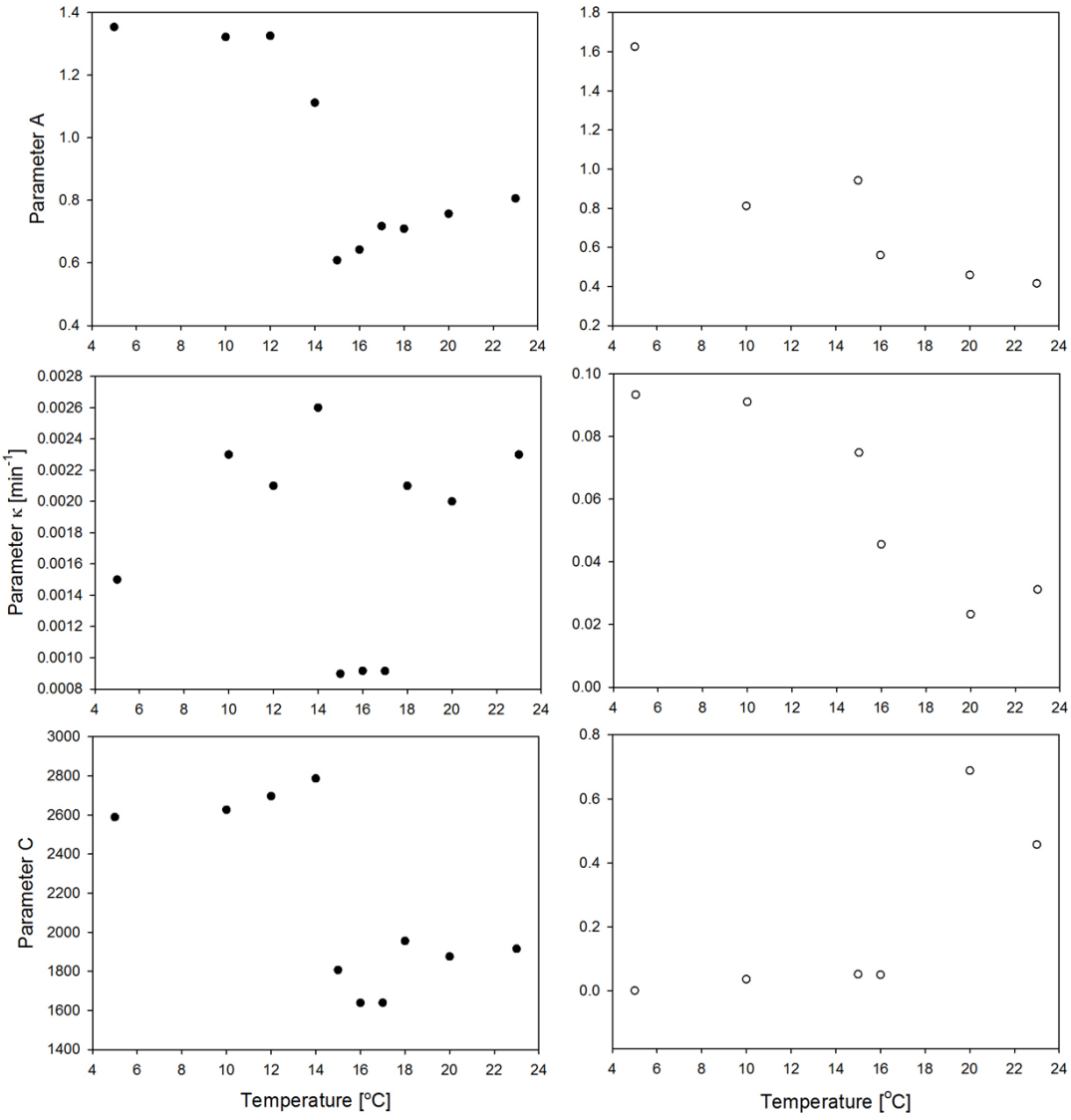

Figure A4.5: Parameters A, κ, and C obtained from the fits of eq. (6) to the data in Figures 3 and 4 plotted as a function of temperature. Measurements taken by going directly to temperature are shown as black circles; those obtained after quenching the sample from 50^{o} C to indicated temperatures are shown as white circles.

4.9 Appendix References

1. Schweitzer-Stenner, R.; Soffer, J. B. Optical Spectroscopy. In *Biophysical Techniques for Structural Characterization of Macromolecules*, Dyson, H. J., Ed. Oxford Academic Press: Oxford, 2012; Vol. 1, pp 533-591.

CHAPTER 5. SUMMARY

The amino acid residue alanine is notorious for exhibiting high propensity for polyproline II conformation in water. The use of a co-solvent system such as ethanol/water mixtures disrupts the stabilization of this conformation, suggesting the alteration of peptide-solvent interactions. These changes promote the aggregation, fibrilization and subsequent gelation of the cationic tripeptide GAG in 55 mol% ethanol/45 mol% water. This is surprising because GAG lacks the typical requirements of known peptide gelators throughout the literature such as hydrophobicity, alignment of alternating charges, and aromaticity. This particular peptide-co-solvent system was extensively studied through the use of vibrational spectroscopies (FTIR, VCD), NMR, electronic spectroscopies (UVCD), microscope imaging (bright-field, AFM) and rheology.

A series of three conformational changes was observed for GAG in ethanol/water mixtures. At 17 mol% ethanol, conformational sampling was shifted from pPII to β-strands. This shift was continued but more pronounced at 40 mol% ethanol. At 55 mol% ethanol and above a peptide concentration of 0.2 M, a hydrogel formed with large crystalline fibrils. FTIR and VCD spectra showed a blueshift of the amide I′ mode with increasing ethanol content, indicating ethanol was penetrating into the hydration shell of the peptide and causing the conformational redistribution. Significant enhancement of the amide I′ in the VCD spectrum with an increase in peptide concentration was attributed to the formation of an extended network of helically twisted fibrils. Through bright-field and atomic force microscopies, the fibrils were determined to be approximately 500 μm

in length, 500 nm in height, and about 7 μm in cross-section. These dimensions were enormous in size compared with other small peptide hydrogel fibrils, commonly on a sub-micrometer scale.

The gelation of cationic GAG in 55 mol% ethanol/45 mol% water was broken down into a set of distinguishable kinetic processes. Using fitting models chosen from the literature, the relaxation time constants of the aggregation, fibrilization and gelation processes were compared. They proceeded in the following order: aggregation into tapes and ribbons, fibrilization as a cooperative process, initial gelation, and subsequent further adjustments of the gelation process, occurring on the order of 10^{-1} min^{-1}, 10^{-2} min^{-1}, 10^{-2} min^{-1}, and 10^{-4} min^{-1} respectively. Understanding the kinetics of these processes has significant application for drug delivery and the introduction of new biomaterials. The tripeptide GAG forming into a viscous hydrogel has potential for advancing drug-release systems due to the combination of its biodegradable and biocompatible nature and its melting temperature of ca. 36^{o} C. Such a simple peptide is not a suspected candidate for gelation, which suggests the vast diversity and functionality of similar gelators yet to be discovered.